NASA CR-134749
ATR-75(7428)-1
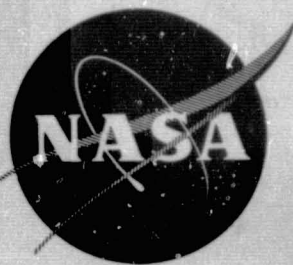
Active Suppression of Pogo on the Space Shuttle

By M. H. LOCK and S. RUBIN

THE AEROSPACE CORPORATION

Prepared for

NATIONAL AERONAUTICS AND SPACE ADMINISTRATION

NASA Lewis Research Center

Contract NAS3-17758

1. Report No. NASA CR-134749	2. Government Accession No.	3. Recipient's Catalog No.
4. Title and Subtitle ACTIVE SUPPRESSION OF POGO ON THE SPACE SHUTTLE		5. Report Date 25 October 1974
		6. Performing Organization Code
7. Author(s) M. H. Lock and S. Rubin		8. Performing Organization Report No. ATR-75(7428)-1
		10. Work Unit No.
9. Performing Organization Name and Address The Aerospace Corporation El Segundo, California 90245		11. Contract or Grant No. NAS 3-17758
		13. Type of Report and Period Covered Contractor Report
12. Sponsoring Agency Name and Address National Aeronautics and Space Administration Washington, D.C. 20546		14. Sponsoring Agency Code

15. Supplementary Notes

16. Abstract

A qualitative analytical study has been made of the use of active pogo suppressors on the Space Shuttle. The study was primarily concerned with suppressor design concepts and the effectiveness of these designs in maintaining the stability of the Shuttle vehicle. Two Aerospace suppressor design concepts were developed by means of a series of parametric stability analyses. These two designs together with two designs provided by NASA were subject to a detailed evaluation. The evaluation considered control effectiveness, performance relative to a passive suppression device, sensitivity of performance to feedback error, suppressor volume flow requirements and suppressor development requirements. The study demonstrated that an active device at the HPOP inlet, involving only the feedback of the HPOP inlet pressure, provides a simple and effective design that is insensitive to error in the feedback signal. The study also indicates that the sizing of an active suppressor will be dependent upon knowledge of the dynamic characteristics of the system.

17. Key Words (Suggested by Author(s)) Pogo Active suppressors Space Shuttle	18. Distribution Statement Unclassified - unlimited		
19. Security Classif. (of this report) Unclassified	20. Security Classif. (of this page) Unclassified	21. No. of Pages 114	22. Price* $3.00

FOREWORD

The work described herein was performed at The Aerospace Corporation under NASA contract NAS-17758. Mr. Carl F. Lorenzo, NASA Lewis Research Center, was Project Manager.

The authors would like to acknowledge the work of Raymond E. Orth in programming the coupled system stability equations used in the study.

CONTENTS

PRECEDING PAGE BLANK NOT FILMED

CONTENTS (Continued)

FIGURES

SUMMARY

A qualitative investigation has been made of the use of active pogo suppressors on the Space Shuttle. The study was primarily concerned with suppressor design concepts and the effectiveness of these concepts in maintaining the stability of the Shuttle vehicle. Topics such as the weight impact of suppressor systems, the hydraulic requirements to operate such systems, the system reliability, and the development requirements for items such as an electronic controller and an electrohydraulic servovalve were not considered.

Two Aerospace suppressor design concepts were developed by means of a series of parametric stability analyses. During these studies, a large number of concepts were eliminated because of their inability to provide acceptable stability. The two selected designs were located at the HPOP (high-pressure oxidizer pump) inlet. One concept was a so-called "optimum" design that was based upon elimination of the oscillatory thrust forces. This design involved feedback of both the relative flow into the HPOP and the pressure at the HPOP inlet. The second design only involved feedback of the pressure at the HPOP inlet. NASA (Lewis) provided two suppressor designs. One design involved feedback of both the HPOP inlet pressure and the engine motion. The other design was a dual-suppressor system comprising a compliant accumulator at the LPOP (low-pressure oxidizer pump) inlet and a pressure feedback device at the HPOP inlet. The intent of the dual system was to reduce the size requirements for the HPOP inlet device.

The four suppressor designs were subjected to a detailed evaluation. All designs were found to eliminate the instabilities predicted for the basic system and to provide performance that was comparable to that of a reference passive device [a 0.057 m^3 (2 ft^3) compliant accumulator]. The Aerospace pressure feedback design and the two NASA designs were found to be insensitive to errors of up to ± 15 percent in the magnitude and ± 45 deg in the phase of the feedback signals. The Aerospace "optimum" design proved to be extremely sensitive to error in the relative flow feedback. Because of this sensitivity and the uncertainty associated with the achievement of satisfactory relative flow (or an equivalent) measurements, this design was deemed to be unsatisfactory. Illustrative volume flow requirements for the suppressors were developed using the modal characteristics of the coupled structural/propulsion system together with assumed levels for the system noise. These volume flow requirements were found to be governed by the fundamental mode response. Relief in the volume flow requirements of the active suppressor by at least a factor of three is possible by addition of an accumulator at the LPOP inlet to satisfy the stability requirement in the fundamental mode. Further relief of up to an order of magnitude is possible by also introducing a shaping function in the feedback to decrease the response of the active suppressor in the fundamental mode.

In conclusion, the study demonstrated that a device at the HPOP inlet, involving only the feedback of the HPOP inlet pressure, provides an effective and simple design that is insensitive to error in the feedback signal. The

study also indicates that the sizing of an active suppressor will be dependent upon knowledge of the dynamic characteristics of the system since the volume flow requirements (and the related hydraulic requirements) are dependent upon such characteristics.

INTRODUCTION

The suppression of pogo instability on the Space Shuttle represents a formidable task because of the complexities introduced by the characteristics of the Shuttle system. The long oxidizer feedline introduces multiple propulsion-system modes into the frequency range of concern; the dual-pump engine design, with a significant length of intermediate ducting, introduces an interpump mode of the propulsion system which is another source of possible instability; and the multibody nature of the vehicle configuration introduces significant coupling of lateral and longitudinal motion in the system modes.

In view of these complexities, it was natural that the use of active suppressors be considered as a means of ensuring that the Shuttle would be free of pogo instability. Such devices would comprise instrumentation for sensing oscillations of the vehicle (pressure, flow, and acceleration in any combination), and a processor for these signals which then activates an electrohydraulic piston-type pulser. This pulser would act as a branch device in a propellant feedline to inject propellant with proper amplitude and phase for the purpose of increasing the pogo stability of the vehicle. In principle the performance of this type of device could be made relatively insensitive to the system dynamics. Interest in the application of active devices had led to the testing of active suppressor designs at both Rockwell International/Rocketdyne Division and NASA (MSFC). The report on the Rocketdyne study (ref. 1) concluded that tests of their suppressor design demonstrated its potential effectiveness. The demonstration was in terms of the attenuation of imposed pressure perturbations over the frequency range from 10 to 30 Hz. The performance in these bench tests provided a preliminary indication of the feasibility of the active suppressor concept. Extension of the evaluation of active suppressors to a flight vehicle configuration was then necessary. The present study represents an initial step in this direction by providing an analytical study of the effectiveness of a variety of active suppressor designs in a simplified dynamic model of the overall Space Shuttle vehicle system.

This study is necessarily of a qualitative nature because of both the simplifications of the dynamic model and the preliminary nature of the employed structural and propulsion system data. On the basis of stability considerations, the study treats the development of useful suppressor design concepts, the effectiveness of such designs, the performance of such designs relative to passive suppressors, and the sensitivity of the designs to feedback error. The suppressor volume flow requirements are examined and the development required to provide the necessary feedback signals is also treated. It should be noted that the study does not treat topics such as the system reliability and the system weight impact. Such topics are germane to the evaluation of active suppressors; however, they involve considerations outside the scope of the present investigation. The plan was for Aerospace to develop two specific active suppressor designs by means of stability considerations and for NASA (Lewis) to provide two additional designs. These

four specific designs would then be subject to a detailed evaluation in the areas previously mentioned.

It should be noted that the present study is a companion study to an investigation of passive suppressors (ref. 2) that was undertaken for NASA (Langley). The general scheme of analysis and numerical procedures was common to both studies and the data employed were identical. This provided a common basis for the evaluation of the relative merits of active versus passive suppressors.

1. ANALYTICAL MODEL FOR STABILITY ANALYSIS

The analytical model employed in the present study is essentially the same as that used in the companion study of passive suppressors (ref. 2). The only difference in the models is that now the flow from the suppression devices is related to a set of feedback variables rather than only to the local pressure at the suppressor inlet.

1.1 Shuttle Propulsion-System/Structural Model

The ascent configuration of the Space Shuttle comprises the orbiter vehicle, an external tank and two solid rocket motors. This configuration is shown schematically in figure 1a. In this figure the main elements of interest in the liquid propulsion system are also indicated. For the purpose of the analysis a simplified single equivalent engine model was employed to represent the three-engine system actually present on the vehicle. The general features of the model are shown in figure 1b together with the model variables, all of which are allowable feedback quantities. The elements of the model comprise a lox tank, a two-segment feedline (one longitudinal section and one lateral section), a low-pressure oxidizer pump (LPOP), a high-pressure oxidizer pump (HPOP), an interpump line, an HPOP discharge line, an injector, and a combustion chamber. The fuel system is believed to be a much less likely contributor to potential pogo instability and was not included in the system model in the interests of simplicity and analytical economy. Also, for simplicity, the motion of the Shuttle vehicle was represented by a single structural mode. As a consequence of this representation, a separate stability analysis was performed for each structural mode selected at the various flight times that were considered. Experience has indicated that the use of a single structural mode model is generally adequate to study the stability of the system. For the exceptional case of close-frequency structural modes with comparable gains, a single equivalent mode was derived by assigning it a structural gain which conservatively accounts for the existence of multiple modes.

Three possible suppressor locations - the LPOP inlet, the LPOP discharge and the HPOP inlet - had been included in the analytical model of the system. However, since the results of both the passive suppressor study (ref. 2) and some preliminary active suppressor analyses had indicated that the LPOP discharge location gave very poor results, only the LPOP inlet and the HPOP inlet locations were treated in the study. The allowable feedback variables are the pressure, volume flow, and structural motion variables at the feedline corner, the LPOP inlet and discharge, and the HPOP inlet and discharge. The pressure in the combustion chamber is another allowable feedback variable.

The detailed equations that govern the behavior of the coupled structural/propulsion system are provided in Appendix A. In these equations the exact solutions for a continuous representation (including resistance) of the

ORBITER
ENGINES
(3)

ORBITER VEHICLE

LOX FEEDLINE

SOLID ROCKET MOTOR

EXTERNAL TANK

LOCATION OF LOX TANK
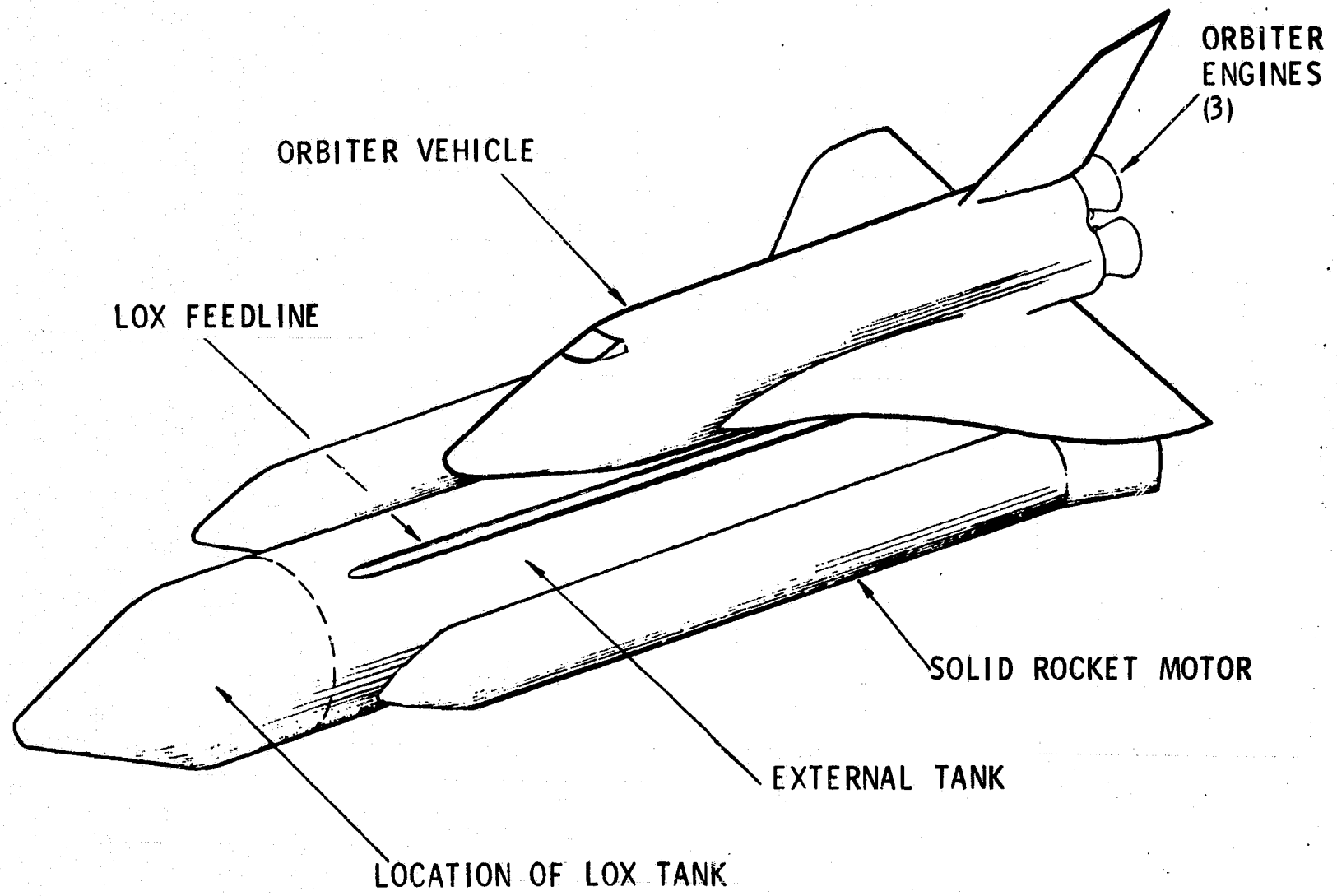
Figure 1a. Shuttle System; Overall Geometry

CHAMBER P_C

STRUCTURAL MOTION

HPOP INLET P_7, Q_7, X_7, Z_7

HPOP DISCHARGE, P_8, Q_8, X_8, Z_8

Q_{a3}

LPOP DISCHARGE P_5, Q_5, X_5, Z_5

Q_{a1}

Q_{a2}

LPOP INLET P_4, Q_4, X_4, Z_4

P ~ PRESSURE

CORNER P_2, Q_2, X_1, Z_1

Q ~ FLOW
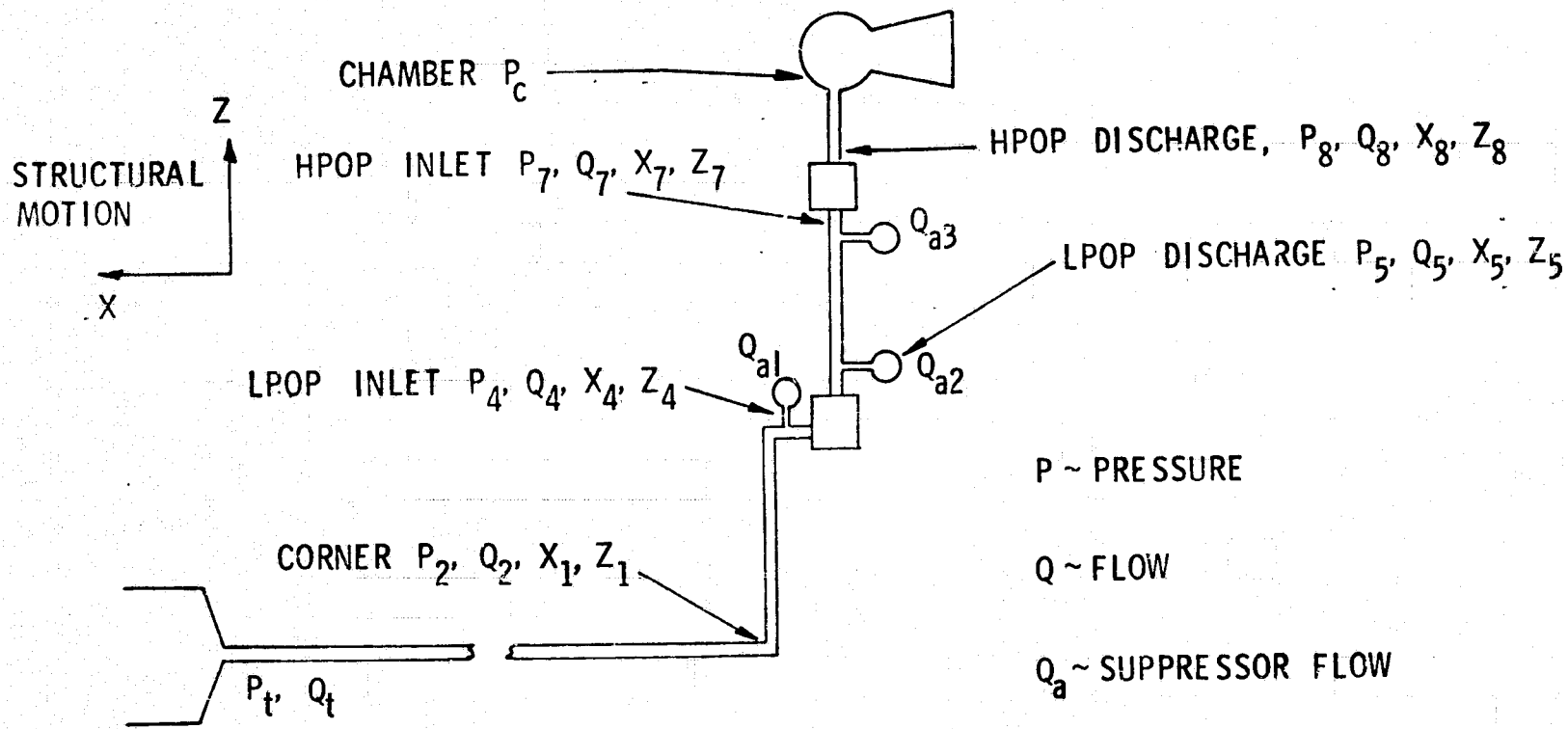
Q_a ~ SUPPRESSOR FLOW

P_t, Q_t

Figure 1b. Shuttle System; Schematic of LOX System
Elements of System Stability Model

feedline flow were employed to develop feedline transmission functions. This was done to assure a good description of the higher organ-pipe modes of the feedline. The flows in the interpump line and discharge line were treated as incompressible since the associated wave transit times were relatively short compared to the structural response times of interest. In the equation for the structural mode, the generalized force contributions that result from fluid resistance and from the convective derivative ($v \, \partial v/\partial x$, where v is the velocity of the flow) in the fluid momentum equation were included. Tank dynamic outflow effects are included on the basis that the structural modes were developed with closed-bottom tanks (ref. 3).

1.2 Computational Procedure

The basic equations governing the coupled structural/propulsion system comprise a 22nd-order system (see Appendix A). For computational efficiency this system was reduced to a 14th-order system for use in the closed-loop stability calculations. The resulting system contained the feedback variables explicitly and had the form

$$\left\{ [V(s)] + [B][E][F(s)] \right\} \hat{H} = 0$$

where the matrix $[V(s)]$ describes the basic coupled structural/propulsion system (i.e., the system in the absence of suppressors); the matrix $[B]$ provides the specification of the suppressor location and feedback variables; the matrix $[E]$ is an error matrix that was introduced to enable evaluation of the sensitivity of the suppressors to errors in the amplitude and phase of the sensed signals; and the matrix $[F(s)]$ describes the processing of the feedback variables. The solution or state vector $\hat{H}$ comprises

$$\hat{H} = \left\{ P_2, P_4, P_5, P_7, P_8, P_c, Q_t, Q_2, Q_3, Q_4, Q_5, Q_7, Q_8, q_n \right\}$$

where P_j and Q_j denote the pressures and flows at various points within the oxidizer system (fig. 1b). The q_n term is the generalized coordinate associated with the nth structural mode; the motion $\vec{x}$ of the vehicle at some point $\vec{r}$ is related to q_n by the following:

$$\vec{x} = q_n e^{st} \phi_n(\vec{r})$$

where $\phi_n(\vec{r})$ is the structural mode shape and s is the Laplace variable.

The matrix equations are completely defined when the propulsion-system parameters and structural-mode data are specified. When this is done, the eigenvalues, s_i, and corresponding eigenvectors, $\hat{H}_i$, of the system can be obtained by satisfaction of the conditions

8

$$\det \left| [V(s_i)] + [B][E][F(s_i)] \right| = 0$$

$$\left| [V(s_i)] + [B][E][F(s_i)] \right| \hat{H}_i = 0$$

Because of the use of the exact feedline solutions, the determinantal equation is a transcendental equation in the Laplace variable. The eigenvalues of the equation were obtained with the use of an iterative root-finding subroutine (ref. 4) that used the input structural frequency, ω_n, and previously calculated propulsion-system eigenvalues as initial estimates.

1.3 Structural-Mode Data

The structural modes employed in the study were taken from data provided by Rockwell International/Space Division. These data comprised the frequencies and mode shapes of the first hundred symmetric vibration modes of the vehicle at five specific flight conditions. Asymmetric mode data were not available for use in the analysis. The employed modes incorporated the primary pitch-longitudinal coupling that results from the vehicle configuration. The absence of yaw motions was not considered to be significant insofar as the present qualitative study was concerned. The lox tank-bottom displacements and pressures were also provided in the modal data. The modal calculations had been made for a vehicle configuration (designated M89B) that was current in early 1973. The Shuttle configuration has subsequently been reduced in size and weight from that design; however, modal data for the new configuration were not available for use in the study. The set of conditions treated by Rockwell is described in the following table together with the associated times of flight and the corresponding maximum and minimum values of the calculated frequencies; the abbreviation SRB that appears in the table denotes the solid-rocket booster.

Condition	Flight Time (sec)	Frequency (Hz)	
		f_1	f_{100}
Liftoff	0	2.18	44.5
Max. Dynamic Pressure	54	2.24	48.9
Before SRB Separation	116^-	2.28	53.3
After SRB Separation	116^+	2.29	62.4
Orbiter End-Burn	480	2.81	103.8

The modal data were examined from the standpoint of the structural gain, G_e, for longitudinal motion of the engine

$$G_e = \phi_e^2/M$$

where ϕ_e is the modal amplitude of the engine in the longitudinal direction and M is the generalized mass of the structural mode. The examination revealed that the higher gains were associated with modal frequencies above 20 Hz. Based upon this feature of the calculated results and the increasing uncertainty of the data for the higher modes, a frequency of 30 Hz was selected as a reasonable upper limit to the frequency range to be considered in the stability analysis. Such a range was considered to be representative for the purpose of the present qualitative study.

For application in the stability analysis, the calculated structural-mode frequencies were allowed to vary through some ±15 percent. This variation was introduced to provide at least some account for changes in vehicle configuration and also uncertainties in the structure/propulsion-system modeling. The variation was expected to cover the worst case conditions in terms of the proximity of structural and propulsion resonances. To account for damping in the vehicle, a critical viscous damping ratio of 0.01 was assigned to each structural mode.

Since the stability analysis is based upon a single equivalent system with three identical engines, it was necessary to develop a relationship between the equivalent engine modal amplitude, ϕ_e, used in the stability calculations and the engine modal amplitudes contained in the provided modal data. The selected relationship was based upon maintaining the same generalized force contribution from the engine thrust and was

$$\phi_e^2 = \frac{1}{3} \sum_{i=1}^{3} \phi_{ei}^2$$

where the ϕ_{ei} are the modal amplitudes of the individual engines. A similar procedure was applied to the tank-bottom pressure excitation $\mathscr{P}_n$ used in the analysis. The relationship between $\mathscr{P}_n$ and the corresponding modal data $\mathscr{P}$ was

$$\mathscr{P}_n = \frac{\mathscr{P}}{3\phi_e} \sum_{i=1}^{3} \phi_{ei}$$

10

1.4 Propulsion-System Parameters

The cross-sectional areas and lengths of the various lines were based upon available Space Shuttle design data. The resistance and inertance of the lines, pumps, engine, and thrust chamber were developed from the basic data given in the SSME Engine Dynamic Model (ref. 5) and from information in a previous pogo study (ref. 3). The estimated values of these parameters are provided in Appendix B. The variation, with time of flight, of the cavitation bubble compliance at the pump inlets and of the pump gains were estimated from available operating data; the compliance estimates were made using the results presented in reference 3 (obtained from the "stay-time" method of ref. 6) and the pump gain from unpublished Titan and Delta vehicle studies. The resulting time variations are shown in figures 2 and 3. The specific values of the compliance and gain parameters that were used in stability analyses at the end-burn, liftoff, and after SRB separation conditions are given in the following table.

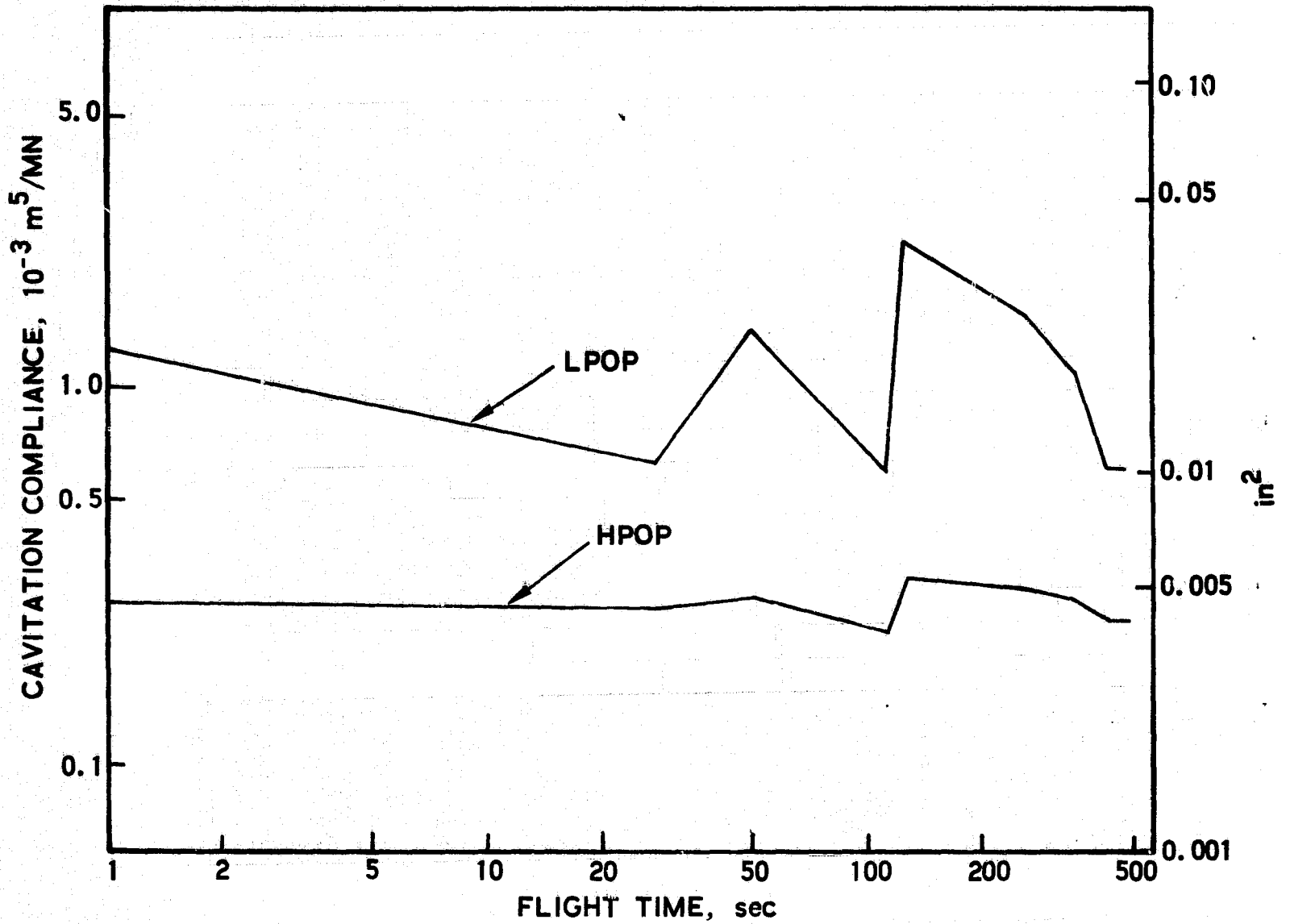| Case Item	Liftoff (t=0)	After SRB Separation (t=116$^+$)	End-Burn (t=480)
LPOP Gain ($m_1 + 1$)	1.625	2.2	1.306
HPOP Gain ($m_2 + 1$)	1.48	1.54	1.42
LPOP Inlet, C_{b1} ($10^{-3}m^5$/MN) (in.^{2})	1.2 (0.0204)	2.3 (0.039)	0.59 (0.01)
HPOP Inlet, C_{b2} ($10^{-3}m^5$/MN) (in.^{2})	0.27 (0.0045)	0.3 (0.0051)	0.24 (0.004)

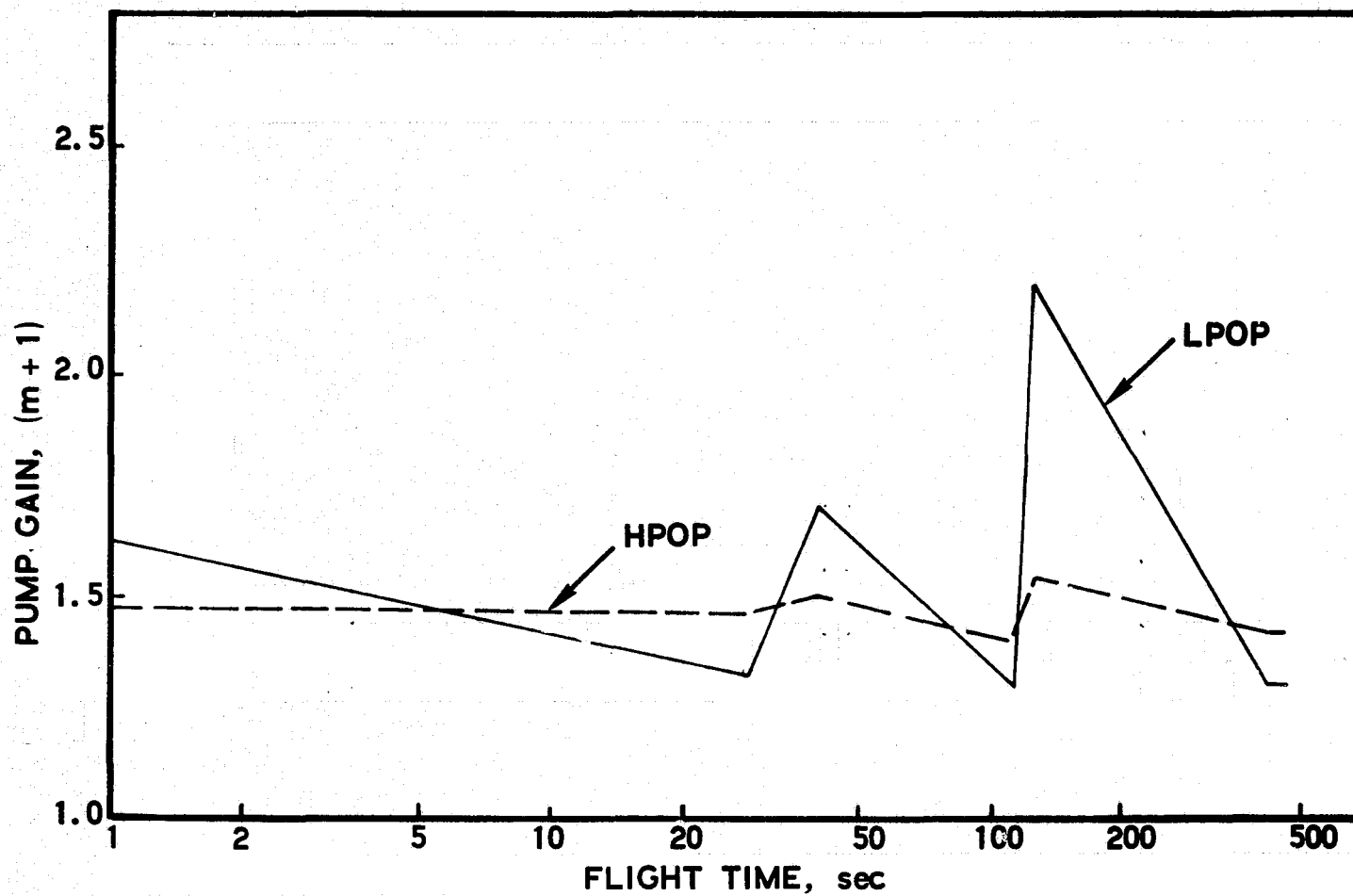Figure 2. Variation of Pump Cavitation Compliances

Figure 3. Variation of Pump Gains

2. STABILITY OF BASIC SYSTEM

The stability results for the basic structural/propulsion system (i.e., the system without suppressors) provide the reference data against which the results for the various suppressor designs can be compared and the effectiveness of the different designs assessed. Since the stability of the basic system was treated extensively in reference 2, the present section provides the main features and results of that work.

2.1 Stability Cases

The stability of the basic system was studied in reference 2 for the following three flight conditions:

1. Orbiter End-Burn

2. Liftoff

3. After Solid-Rocket-Booster (SRB) Separation

The structural modes that were individually studied at these conditions were selected upon the basis of structural gain. The set of modes employed at end-burn are given below together with the associated modal frequencies and structural gains. In the following table, the nomenclature E denotes end-burn while the numbers give the order of the mode.

Mode / Item	E1	E2	E7	E30	E34	E35
f_n (Hz)	2.8	4.7	8.5	22.5	26.8	27.2
G_e (10^{-6}/kg)	1.25	1.14	6.3	57	177	274
(10^{-4} in./lb-sec^2)	(2.2)	(2.0)	(11)	(100)	(310)	(480)

It should be noted that the structural gains assigned to the thirty-fourth and thirty-fifth modes are twice the values given by the modal data. This doubling of the gain was introduced to account for the possibility of destabilizing coupling between the modes. This coupling, which could result from the close modal frequencies (26.8 and 27.2 Hz, respectively), was not describable exactly by the single-mode analysis employed in the stability study. The use of a factor of two was considered to be conservative since the two structural gains were of a comparable magnitude. For completeness a detailed list of the modal amplitudes employed in the calculations is provided in Appendix C.

The corresponding set of modes employed in the analyses at the liftoff condition (denoted by L) are given in the following table. The modal frequencies and structural gains are presented together with the corresponding values of the modal tank-bottom pressure per unit engine acceleration, $\mathscr{P}_n/\phi_e$. The associated model amplitudes are given in Appenidx C.

Item \ Mode	L1	L18	L26	L49	L51	L62
f_n (Hz)	2.2	8.9	12.1	21.9	22.5	27.1
G_e (10^{-6}/kg)	9.1	4.6	11.4	74	8.6	206
(10^{-4} in./lb-sec^2)	(16)	(8)	(20)	(130)	(15)	(360)
$\mathscr{P}_n/\phi_e$ (Ns^2/m^3)	115	5.7	3.0	820	7640	-1.0
(10^{-5} lb-sec^2/in.^{3})	(42)	(2.1)	(1.1)	(300)	(2800)	(-0.4)

The corresponding modal data employed at the after-SRB-separation event (denoted by A) are given in the next table and in Appendix C.

Item \ Mode	A1	A46
f_n (Hz)	2.3	27.0
G_e (10^{-6}/kg)	7.4	194
(10^{-4} in./lb-sec^2)	(13)	(340)
$\mathscr{P}_n/\phi_e$ (Ns^2/m^3)	464	-0.014
(10^{-5} lb-sec^2/in.^{3})	(-170)	(-0.005)

2.2 Propulsion - System Modes

The eigenvalues and eigenvectors of the isolated propulsion system (i.e., stationary structure) were calculated both to provide initial guesses for the root-finding program used in the stability analysis and to identify the

interpump mode of the propulsion system. The modal frequencies and associated critical damping ratios calculated for the orbiter end-burn condition are illustrated in figure 4. The results for the other flight conditions are similar. The interpump mode is noted in the figure and is seen to be relatively highly damped with a frequency of 24.4 Hz (the frequency of this mode at the liftoff and after-SRB-separation conditions was 23.1 and 21.6 Hz, respectively). Physically, this mode is dominated by the motion of the interpump and LPOP fluids between the LPOP inlet cavitation bubble compliance at the upstream end and the HPOP inlet cavitation bubble compliance at the downstream end. The remaining oxidizer system modes can be termed "feedline-type" modes since their frequencies lie within the frequency bands defined by the open-open and open-closed modes of the feedline (fig. 4) and they are dominated by a standing wave behavior in the feedline. The different character of the modes is illustrated in figure 5 where representative fluid pressure amplitude distributions are shown for the interpump mode and the first two feedline-type modes; the in or out phasing, shown crudely, approximates the actual phasing. The appearance of significant amplitudes only within the engine (i.e., beginning with the LPOP) for the interpump mode is clearly seen from this figure.

2.3 Stability Results

The results of the stability analyses performed for the basic system at the three flight events of orbiter end-burn, liftoff, and after SRB separation are presented in figures 6 through 8. The stability curves are given in terms of the system damping ratio ζ versus the assumed value of the structural mode frequency (it will be remembered that the structural mode frequencies are toleranced ±15 percent, about the nominal frequency given in the modal data). The variation of the damping with the assumed structural frequency results from the varying interaction between the structure and the propulsion system. For example, the appearance of two local minima in the damping curves shown in figure 6 is a consequence of the presence of two propulsion system modes in the specified range of frequency. Each minimum represents the most destabilizing interaction between the structural mode and the associated propulsion system mode. On the other hand the appearance of a single minimum (see figure 7 or 8) reflects the interaction between the structural mode and the single propulsion system mode that appears within the specified frequency range. The results reveal the presence of instability at each flight condition. In the case of the end-burn event, the E35 mode was unstable over a limited range of the structural mode frequency (fig. 6). This instability was identified as being due to destabilizing coupling between the structural mode and the interpump mode of the propulsion system. At the liftoff and after-SRB-separation conditions, the fundamental modes (L1 and A1, respectively) were found to be unstable (figs. 7 and 8). The instability at the after-SRB event was the more severe with the calculated damping ratio reaching a negative value of almost -0.009 and the instability persisting over a broader range of the structural frequency; at liftoff the damping ratio went down to about -0.002. In both cases the instabilities were identified as resulting from destabilizing coupling between the structural mode and the first feedline-type mode of the propulsion system.
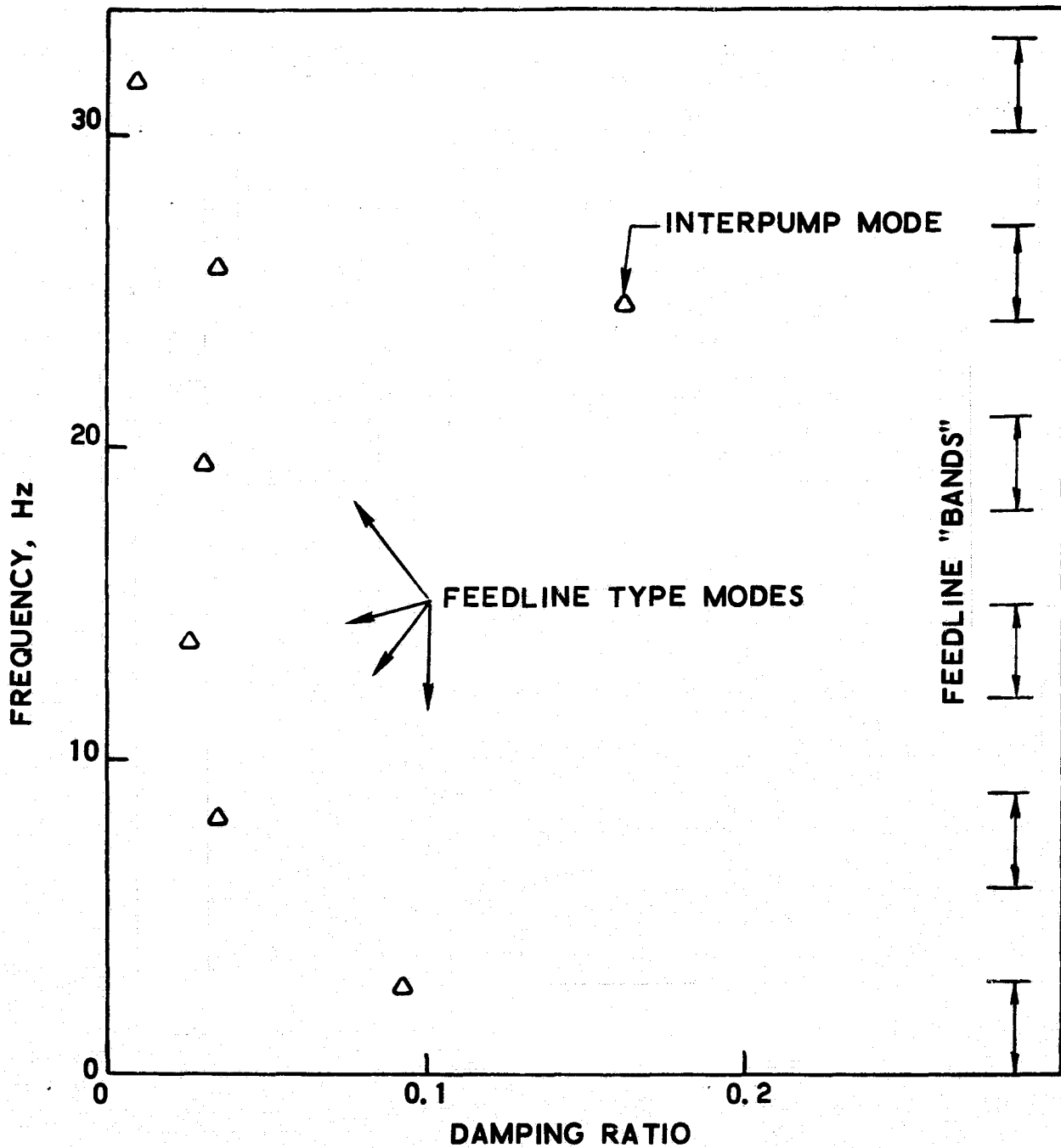
Figure 4. LOX-System Frequencies and Damping
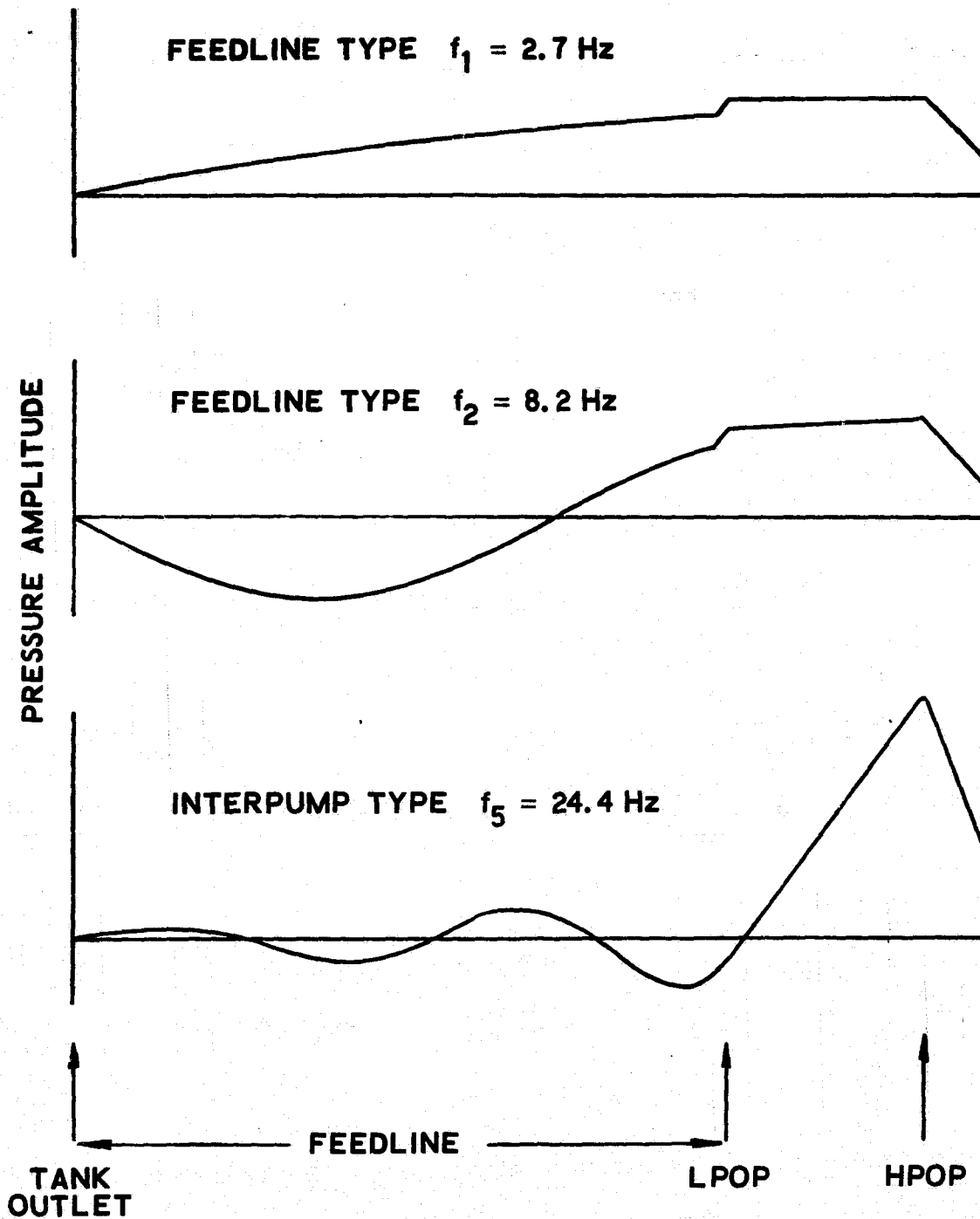Ratios: Orbiter End-Burn
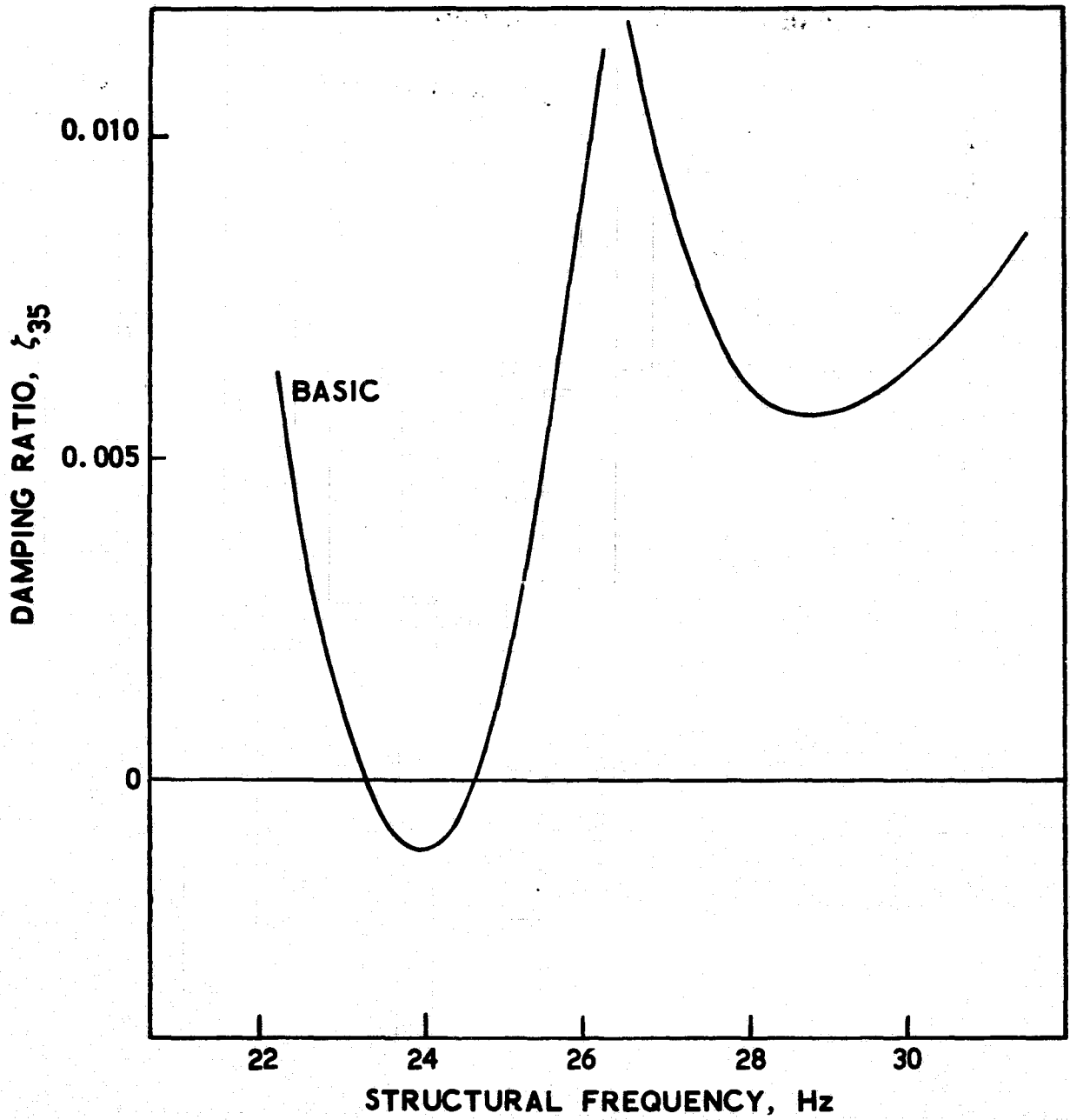
Figure 5. LOX-System Modes: Orbiter End-Burn

19

Figure 6. Stability Results for Basic System:
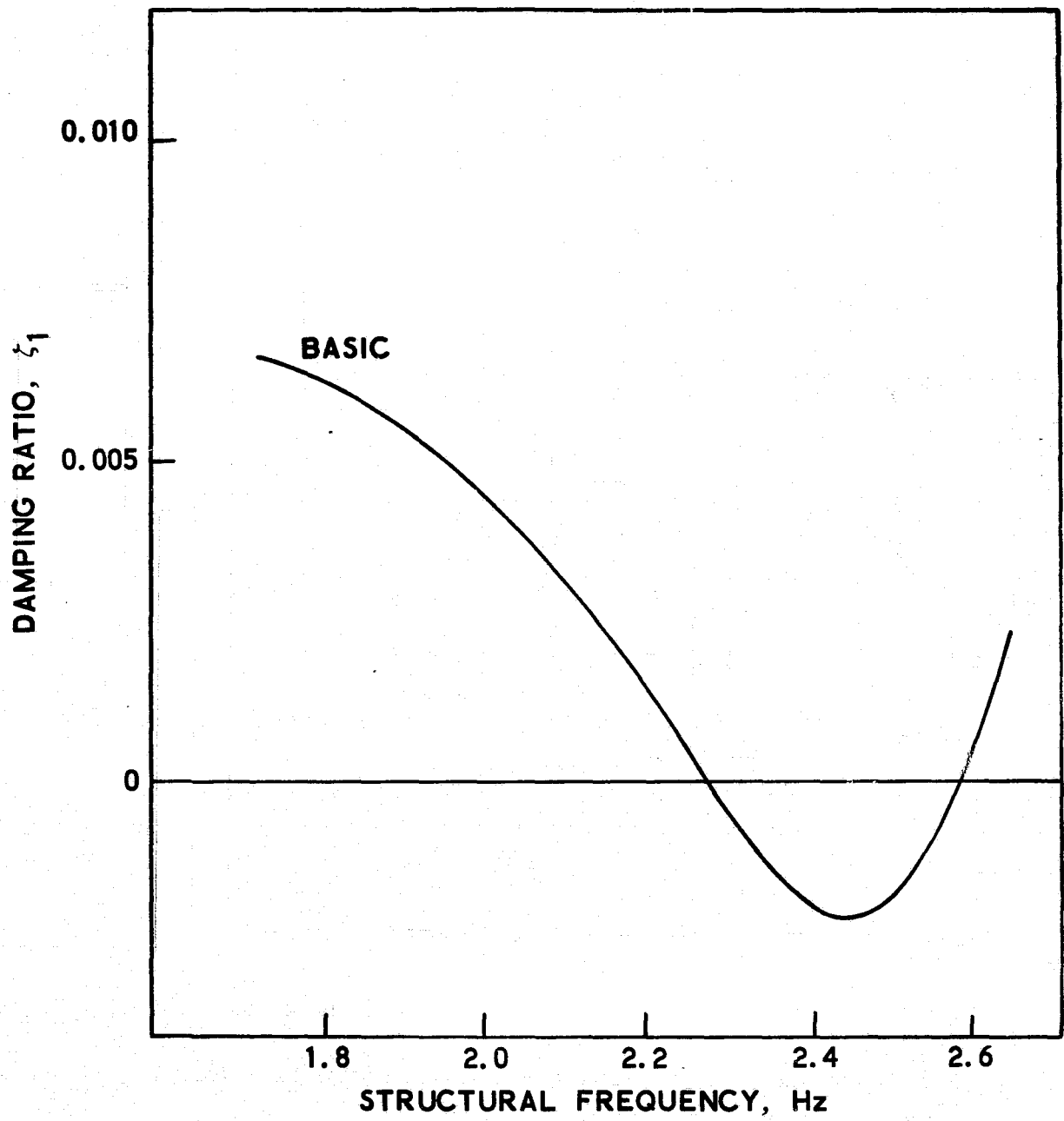Orbiter End-Burn

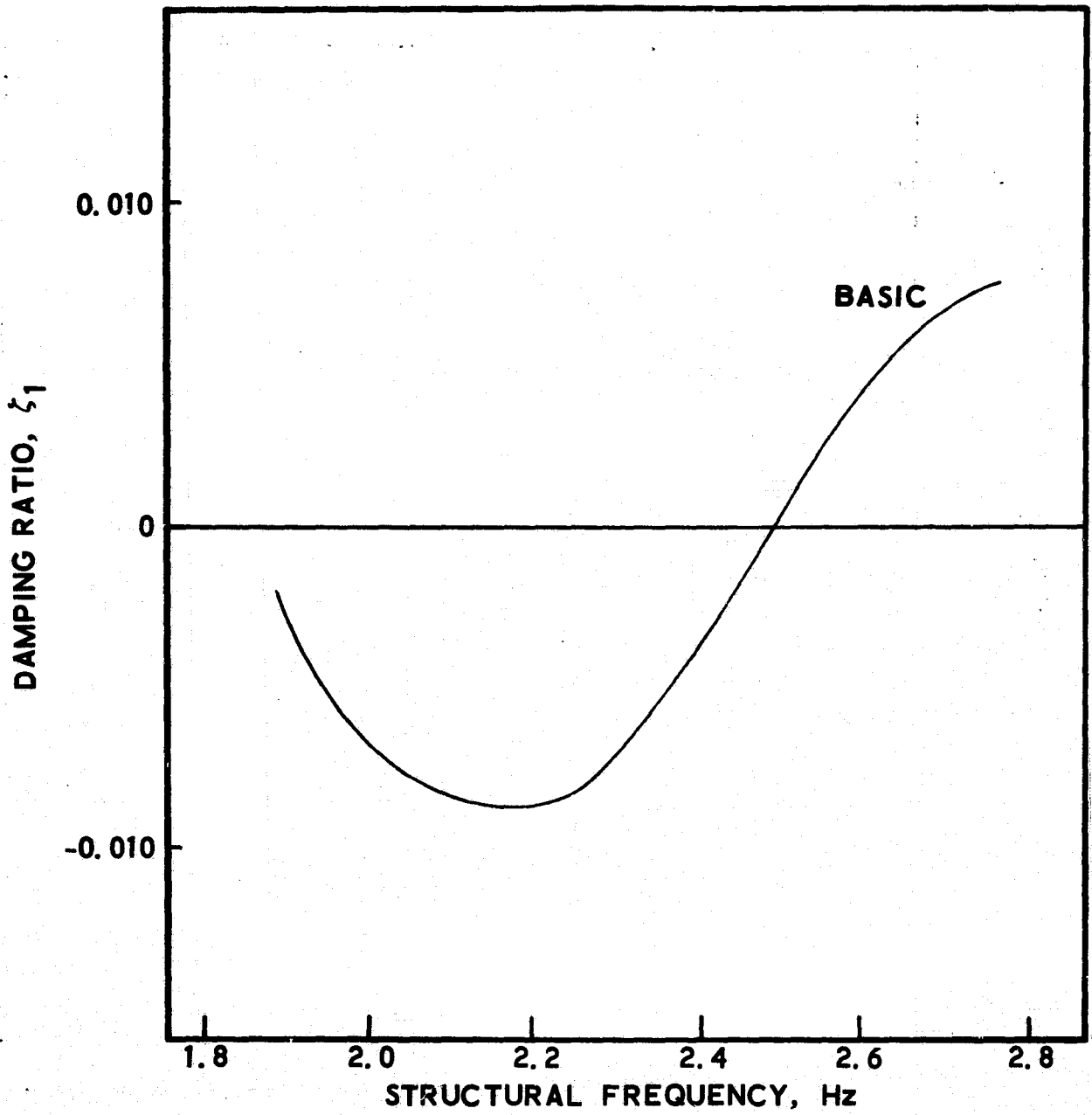Figure 7. Stability Results for Basic System:
Liftoff

21

Figure 8. Stability Results for Basic System:
After SRB Separation

22

3. DEVELOPMENT OF SPECIFIC ACTIVE SUPPRESSOR DESIGNS

The study plan called for two specific suppressor designs to be developed by Aerospace and for two additional designs to be provided by NASA (Lewis). These four designs were then to be subjected to a detailed evaluation. This section deals primarily with the studies undertaken at The Aerospace Corporation to develop its designs. Subsequent to this description, the designs provided by NASA (Lewis) are defined and the basis for their selection is briefly described.

3.1 Aerospace Suppressor Design Studies

The approach employed at Aerospace was to develop a variety of suppressor design concepts on the basis of analysis or physical argument; and then to evaluate the performance of these concepts by means of a limited number of stability analyses for critical flight conditions. Two of the better resulting design concepts were then selected as the specific suppressor designs that would be subject to more detailed examination. The combinations of structural mode and flight event that were used in this design selection procedure were the fundamental mode at the after-SRB-separation event and the high-gain thirty-fifth structural mode at the end-burn condition. These cases were considered appropriate since they represented examples of a severe instability involving a feedline mode and of the instability involving the interpump mode.

3.1.1 Design Concepts

Before describing the details of the various design concepts, the general procedure will be first outlined. The first step was to develop a so-called "optimum" suppressor design. This design was based upon the idea of eliminating the oscillatory thrust forces - the main destabilizing influence acting upon the structural modes of the system. Next, two "limiting case" suppressor designs were developed by means of approximate stability analyses for limiting case conditions. Finally, three simple motion or pressure feedback designs were developed. These latter designs were based upon the idea of introducing dissipative or stabilizing forces into the system.

3.1.1.1 Optimum Design

Stability analyses performed for the basic system indicated that the thrust perturbations were the primary destabilizing component of the generalized force acting upon the structural mode. When these thrust perturbations were removed, any destabilizing influence of the propulsion system became minimal (i.e., the calculated damping ratios were either greater or only slightly less than the assumed structural damping ratios of 0.01). Examination of the equations of motion for the system (Appendix A) indicated

23

that this removal could be effected by use of a suppressor at the HPOP inlet that obeyed the following law:

$$Q_{a3} = (-Q_7 + A_3 \dot{z}_7) + C_{b2} s P_7 \tag{1}$$

where Q_7 denotes the absolute volume flow at the HPOP inlet, P_7 denotes the pressure at the HPOP inlet, $\dot{z}_7$ is the lateral velocity of the engine, A_3 is the area of the interpump line and C_{b2} is the compliance of the cavitation bubble at the HPOP inlet. The term $(Q_7 - A_3 \dot{z}_7)$ represents the relative flow into the HPOP; this is the flow that would be measured by a flowmeter at the HPOP inlet.

In practice it is anticipated that it would be impractical to attempt to follow the variation of the cavitation compliance C_{b2} with flight time. There-fore, it was decided to treat a design that employed a representative value of 2.4×10^{-4} m^5/MN for this parameter (the estimated variation of C_{b2} is quite small and is shown in fig. 2). The resulting design

$$Q_{a3} = (-Q_7 + A_3 \dot{z}_7) + \overline{C}_{b2} s P_7 \tag{2}$$

$$\overline{C}_{b2} = 2.4 \times 10^{-4} \text{ m}^5/\text{MN } (0.1 \text{ in.}^5/\text{lb})$$

was termed the "optimum" design since it was based on the idea of the elimination of the most significant generalized force contribution.

3.1.1.2 Limiting-Case Designs

The complexity of the equations governing the coupled structural/propulsion system precluded the general application of the approximate means of stability analysis identified in reference 7. However, such analyses were possible if certain limiting conditions could be attained at the HPOP by the use of appropriate suppressors at the HPOP inlet. Such limiting conditions were (a) zero discharge flow from the HPOP, (b) zero inlet pressure at the HPOP, and (c) zero inlet flow at the HPOP. The first condition (i.e., zero discharge flow) leads to the elimination of the thrust oscillations and the associated suppressor design is identical to that treated in the previous sec-tion. The suppressor designs associated with the two remaining limiting conditions were

Zero HPOP Inlet Pressure $\qquad Q_{a3} = Q_8 - Q_7 + (A_3 - A_4)\dot{z}_7 \tag{3}$

Zero HPOP Inlet Flow $\qquad Q_{a3} = (-Q_7 + A_3 \dot{z}_7) \tag{4}$

where Q_8 is the discharge flow from the HPOP and A_4 is the area of the discharge line. The feedback in the first case involves the relative flow $(Q_7 - A_3 \dot{z}_7)$ into the HPOP and the relative flow $(Q_8 - A_4 \dot{z}_7)$ out of the HPOP. In the second case, the feedback involves the relative flow into the HPOP. It will be noted that the latter design is essentially the limiting case of the optimum design [eq. (2)] for the condition of zero cavitation compliance at the HPOP inlet.

The imposition of these conditions at the HPOP leads to relatively simple expressions for the engine thrust. For example the application of the zero inlet pressure condition, eq. (3), results in the following equation for the thrust

$$T = A_4 A_T L_e R_c Z_e^{-1} \ddot{z}_7$$

where L_e and Z_e denote the inertance and impedance of the engine; R_c and A_T denote the resistance and the effective area of the thrust chamber, respectively. With simple expressions for the thrust the approximate result, given in reference 7, for the system damping

$$\zeta \approx -\zeta_n - \frac{G_e}{2} \bar{H}_i$$

can be readily evaluated. In this expression ζ_n denotes the structural damping ratio and $\bar{H}_i$ is the imaginary part of the ratio $T/\ddot{x}_e$ where $\ddot{x}_e$ is the engine acceleration. The approximate analyses undertaken in this manner indicated that the suppressors defined by equations (3) and (4) were promising candidates for further examination.

3.1.1.3 Simple Feedback Designs

It was of considerable interest to examine the possibilities offered by simple motion or pressure feedback designs since such systems might be more practically achievable than the optimum and limiting-case designs treated in the preceding sections. The first of these simpler designs was based upon the idea of the addition of a dissipative thrust force to the system. This addition was achieved with the use of a suppressor with a flow rate proportional to the longitudinal velocity $\dot{x}_7$ of the engine

$$Q_a = -K_x \dot{x}_7 \tag{5}$$

when K_x is a positive real-valued constant.

The next suppressor design concept was developed from a detailed examination of the eigenvectors determined from the analysis of the basic system at different unstable conditions. By combining this eigenvector data with the analytical expressions for the oscillatory thrust it was possible to

identify the primary sources of the destabilizing thrust forces and to get a basis for a feedback design that could possibly counter these sources. Writing the oscillatory thrust T as

$$T = A_T R_c \left| \dot{Q}_8 - A_4 \dot{z}_7 \right| \tag{6}$$

it was found that the term $A_4 \dot{z}_7$ was the primary destabilizing factor involved in the interpump mode type of instability. In the case of the fundamental mode instabilities, it was found that the imaginary part of the HPOP discharge flow Q_8 was the main source of instability. Further, the destabilizing character of this flow term was traced to the longitudinal motion of the LPOP: this motion appears as a term $A_1 \dot{x}_4$ in the continuity equation at the LPOP inlet (see detailed equations in Appendix A). On the basis of these findings a suppressor design was selected such that the flow perturbations produced by the $\dot{z}_7$ and $\dot{x}_4$ motions would be cancelled out. This design was

$$Q_a = A_4 \dot{z}_7 - A_1 \dot{x}_4 \tag{7}$$

This design represented another relatively simple motion feedback device. It was also considered desirable to generate a simple pressure feedback design in addition to the motion feedback systems. To develop this design the eigenvector data from the analyses of the basic system were again reviewed. This review indicated that a suppressor with a flow rate proportional to pump inlet pressure

$$Q_a = -K_p P \tag{8}$$

where K_p is a positive real-valued constant, would provide a useful design. This concept is equivalent to a purely resistive accumulator, where $1/K_p$ is the resistance.

3.1.2   Performance of Active Suppressor Concepts

The effectiveness of the various design concepts developed in the preceding section were now determined by conducting stability analyses for the two selected flight cases (i.e., the A1 and E35 cases). In the case of the optimum design and the limiting-case designs the suppressors were considered at the HPOP location only since these designs were specifically developed for that location. In the case of the simple feedback designs the performance was examined for both the HPOP inlet and LPOP inlet locations.

Maintenance of the system damping ratio at a level equal to or greater than 0.005 was established as a goal. That is, the reduction of the 0.01 structural damping ratio due to propulsion system feedback was to be no greater than a factor of two. This goal corresponds to a stability gain margin of 6 db or greater, as defined by equation (2) of the NASA Space Vehicle Design Criteria (ref. 8).

26

3.1.2.1 Optimum Design

The stability curves developed for this design [see eq. (2)] are shown in figure 9 together with the corresponding results for the basic system (i.e., the system without suppressors). As could be anticipated the suppressor is highly effective. In the case of the A1 mode the instability is eliminated. In fact any destabilizing influence of the propulsion system is removed since the calculated damping ratios remain above the input structural damping ratio of 0.01. The interpump mode type of instability in the E35 mode is also eliminated with the minimum calculated damping ratio being maintained above a value of 0.0075 over the specified range of the structural mode frequency.

3.1.2.2 Limiting-Case Designs

The stability curves calculated for the designs associated with the conditions of zero HPOP inlet pressure and zero HPOP inlet flow [see eqs. (3) and (4), respectively] are shown in figure 10. The general features of the curves were quite similar to those obtained for the optimum design (fig. 10). The stability curves were essentially identical in the case of the A1 mode. For the case of the E35 mode the designs were not as effective as the optimum design but still maintained damping ratios in excess of 0.006 (fig. 10b).

3.1.2.3 Simple Feedback Design

An initial estimate of the coefficient K_x in the suppressor design

$$Q_a = -K_x \dot{x}_7$$

was made from the results of the stability analyses for the basic system. This estimate was a value of 0.0013 m^2 (20 in.^{2}). The damping ratios obtained for the A1 and E35 modes with this design at the HPOP inlet are shown in figures 11a and 11b. From the figures it is seen that the fundamental mode instability remains but the interpump mode instability has been eliminated. The coefficient was then increased to a value of 0.0039 m^2 (60 in.^{2}) and stability curves again generated for the two modes. In this instance, the fundamental mode instability was eliminated (fig. 11c) but the performance of the design for the interpump mode instability became questionable (fig. 11d). The coefficient K_x was again increased, this time to a value of 0.0077 m^2 (120 in.^{2}), and damping ratios calculated for the two stability cases. Now it was found that the feedline mode instability was eliminated but the interpump mode instability was present. Finally, damping ratios were calculated for a design located at the LPOP inlet with the coefficient K_x equal to 0.0039 m^2 (60 in.^{2}). In this case, the feedline-mode instability was eliminated but the interpump mode instability remained.

The first set of stability calculations for the second simple feedback design
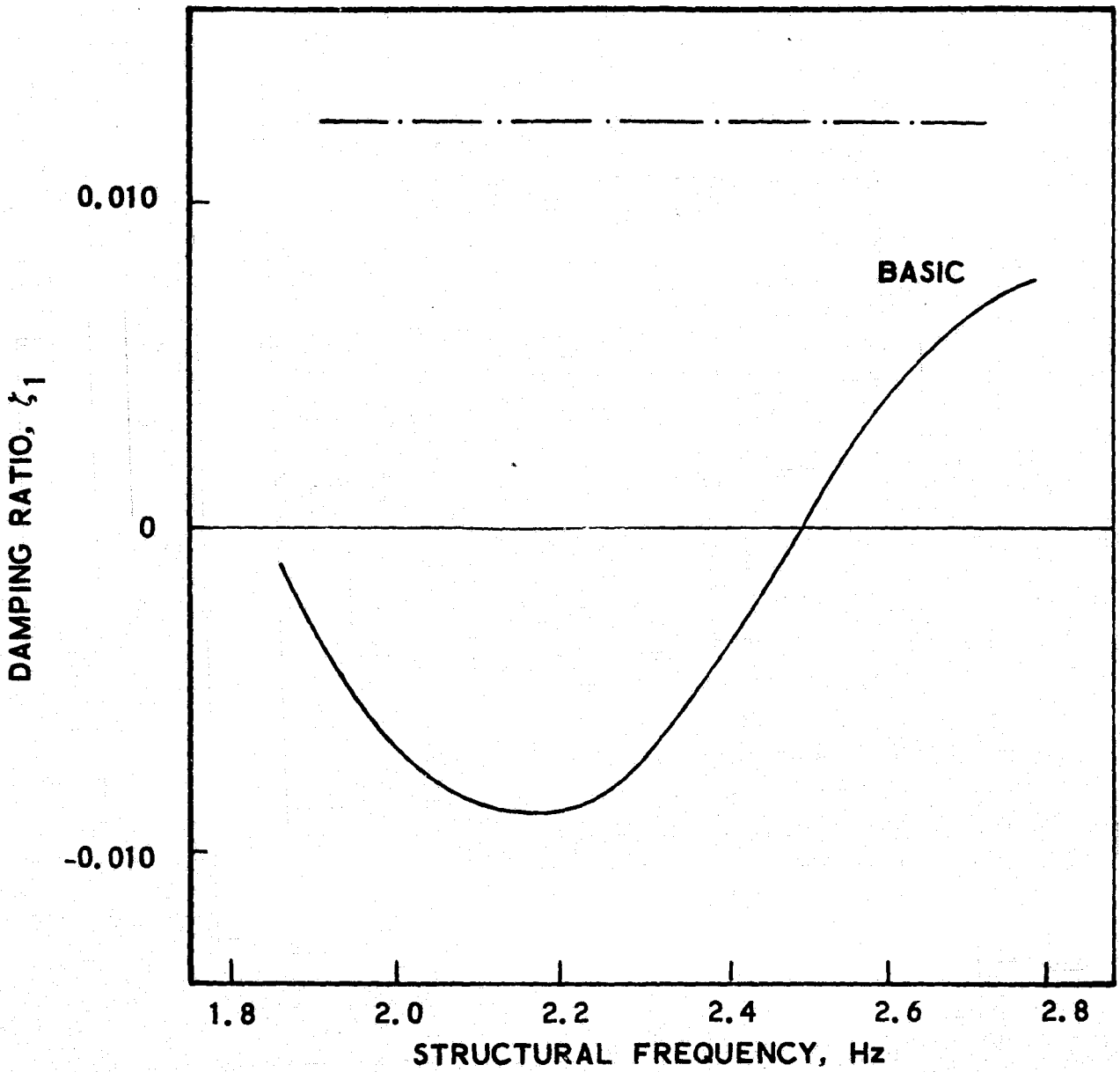
$$Q_a = A_4 \dot{z}_7 + A_1 \dot{x}_4$$

Figure 9a. Stability Results with Aerospace Optimum
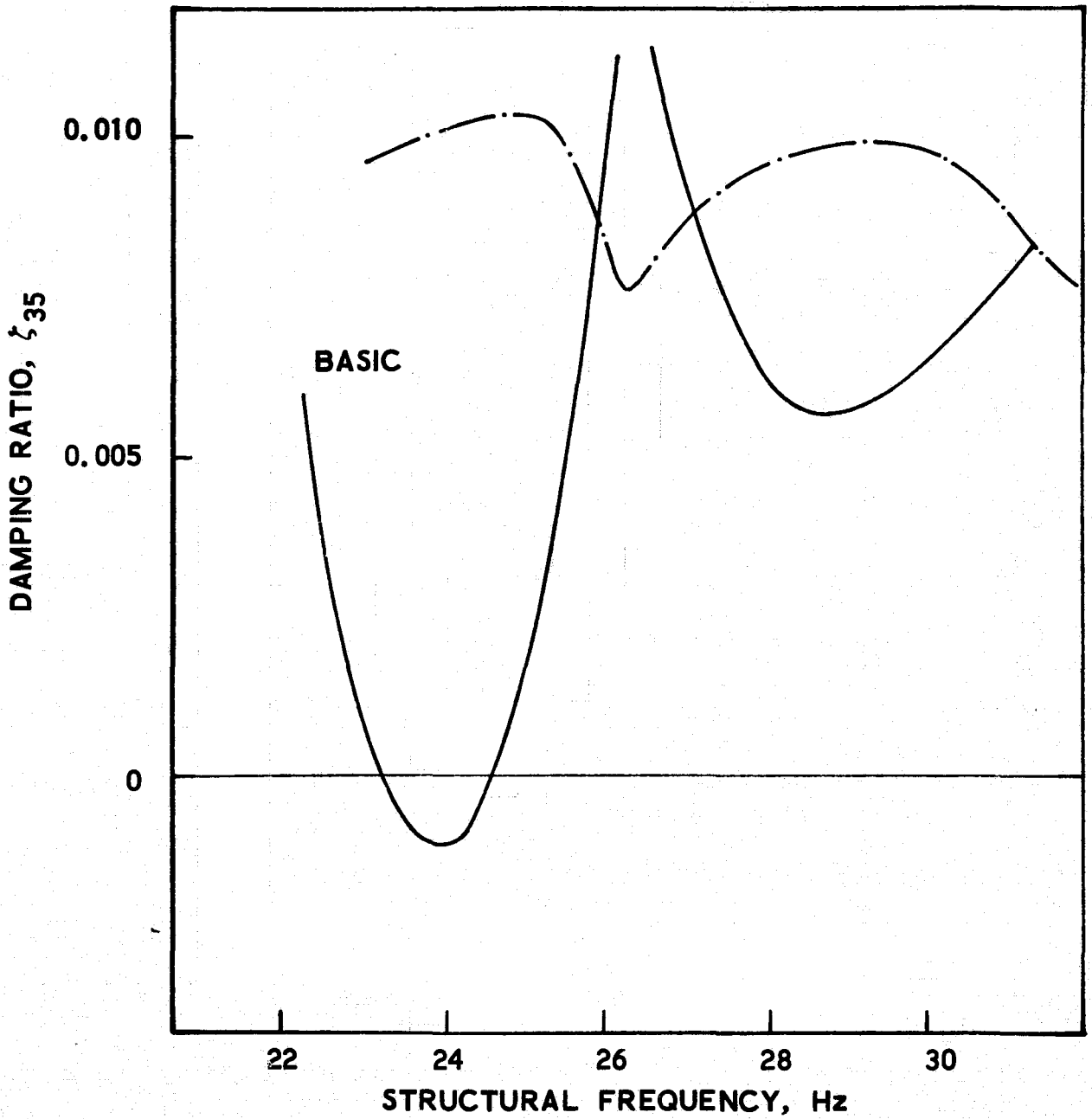Suppressor Design: After SRB Separation

Figure 9b. Stability Results with Aerospace Optimum
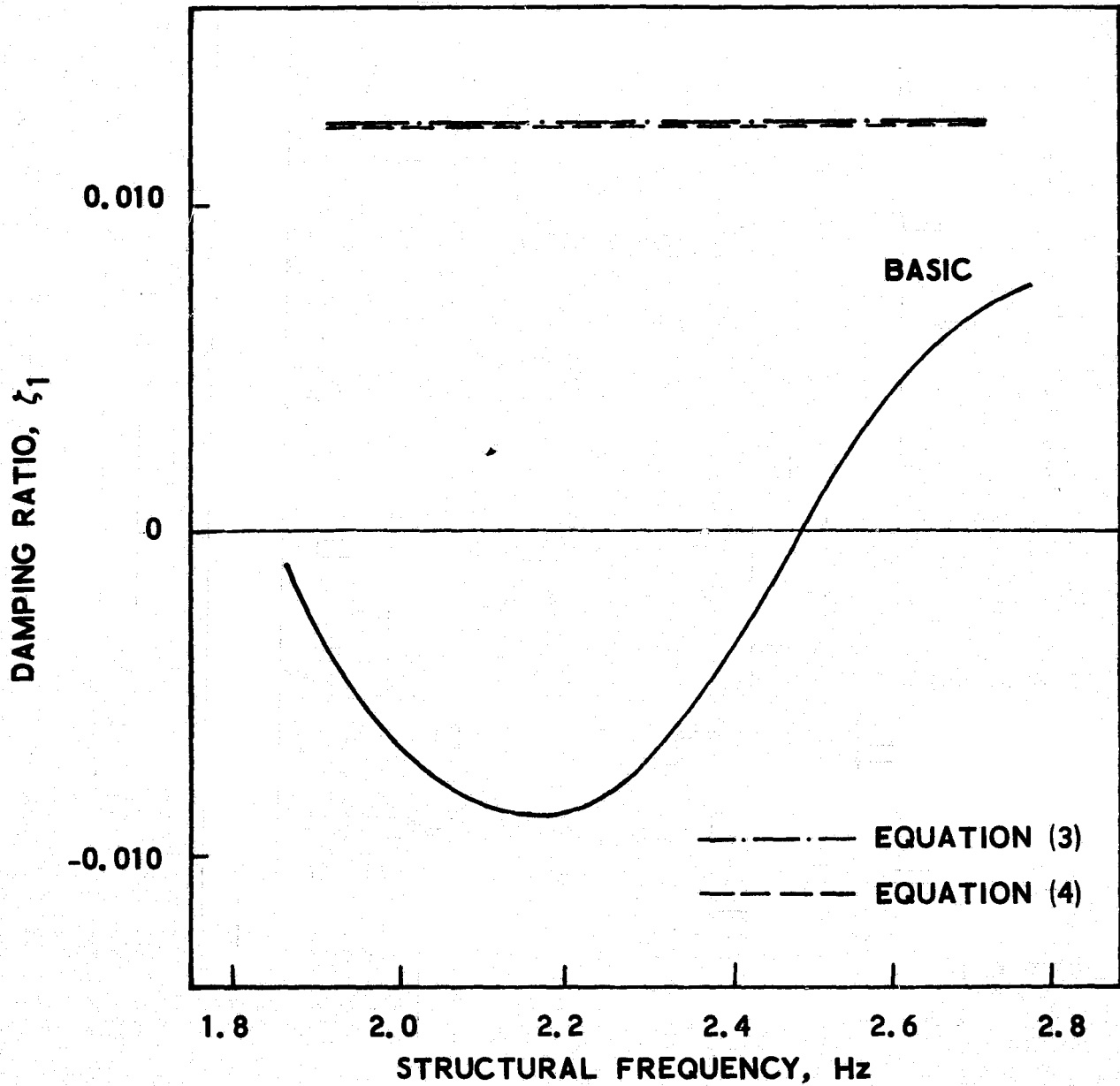Suppressor Design: Orbiter End-Burn

Figure 10a. Stability Results with Aerospace Limiting-Case
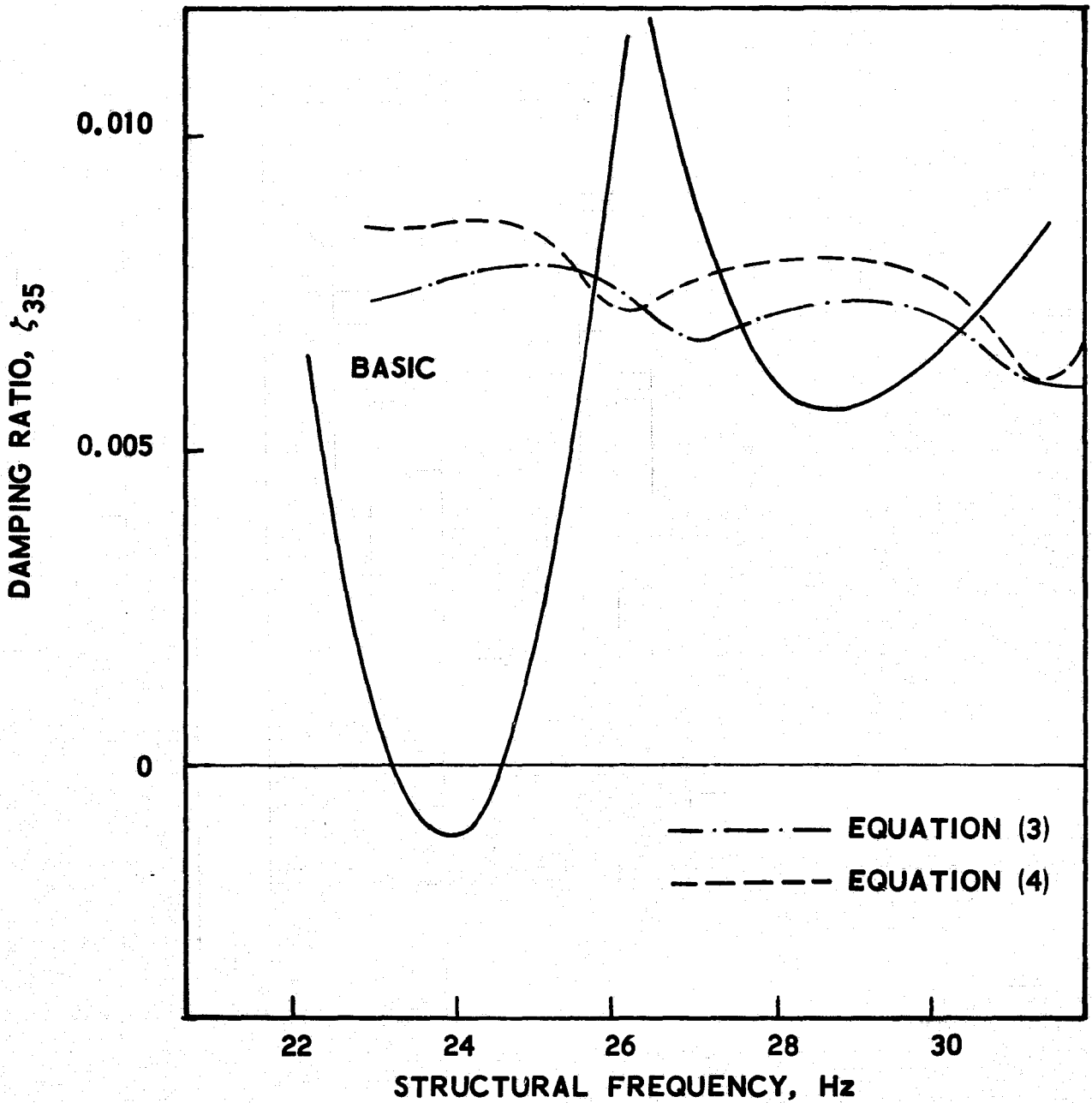Suppressor Designs: After SRB Separation

Figure 10b. Stability Results with Aerospace Limiting-Case
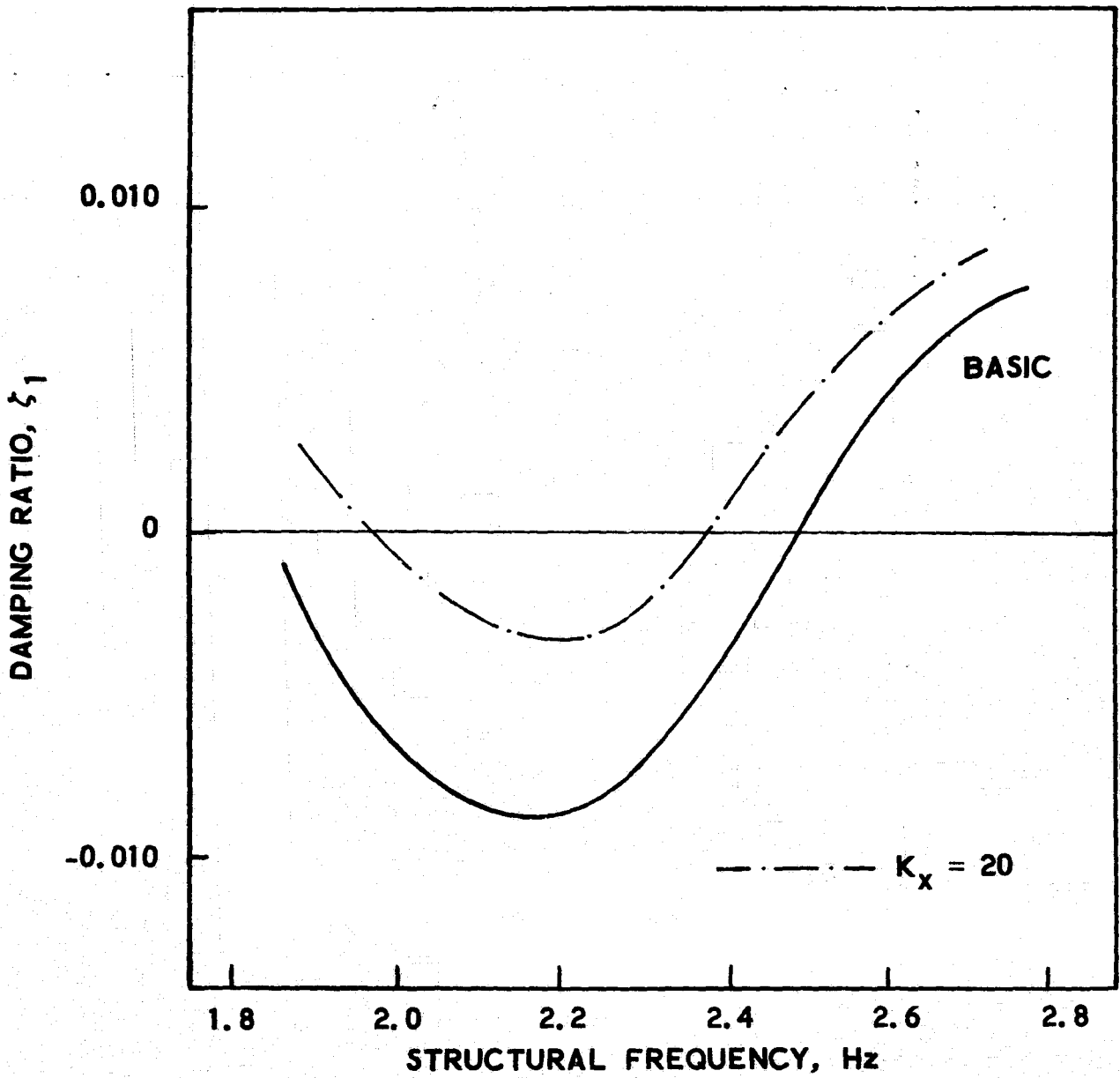Suppressor Designs: Orbiter End-Burn

Figure 11a. Stability Results with Aerospace
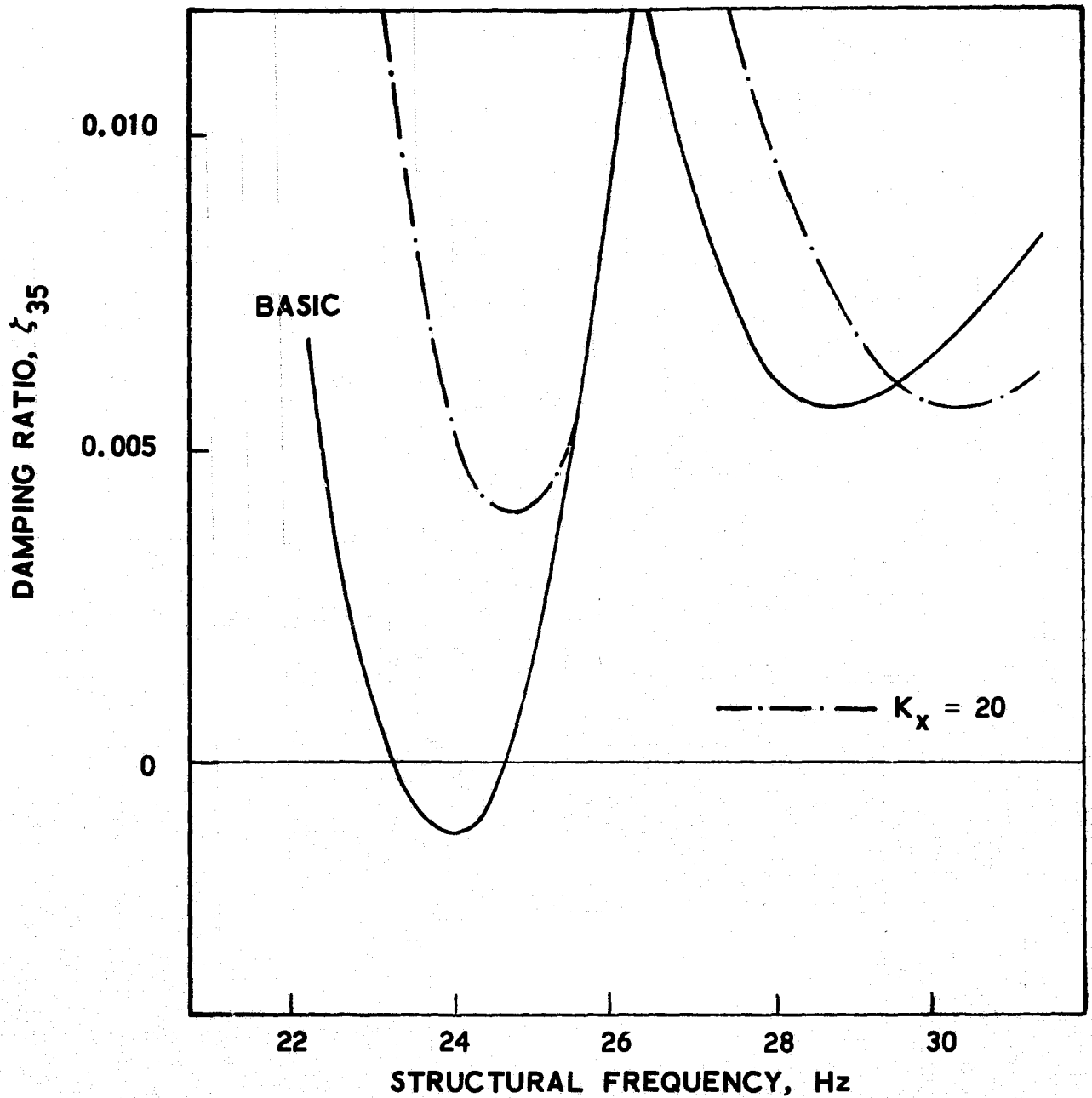Longitudinal-Motion-Feedback
Suppressor: After SRB Separation

Figure 11b. Stability Results with Aerospace
Longitudinal-Motion-Feedback
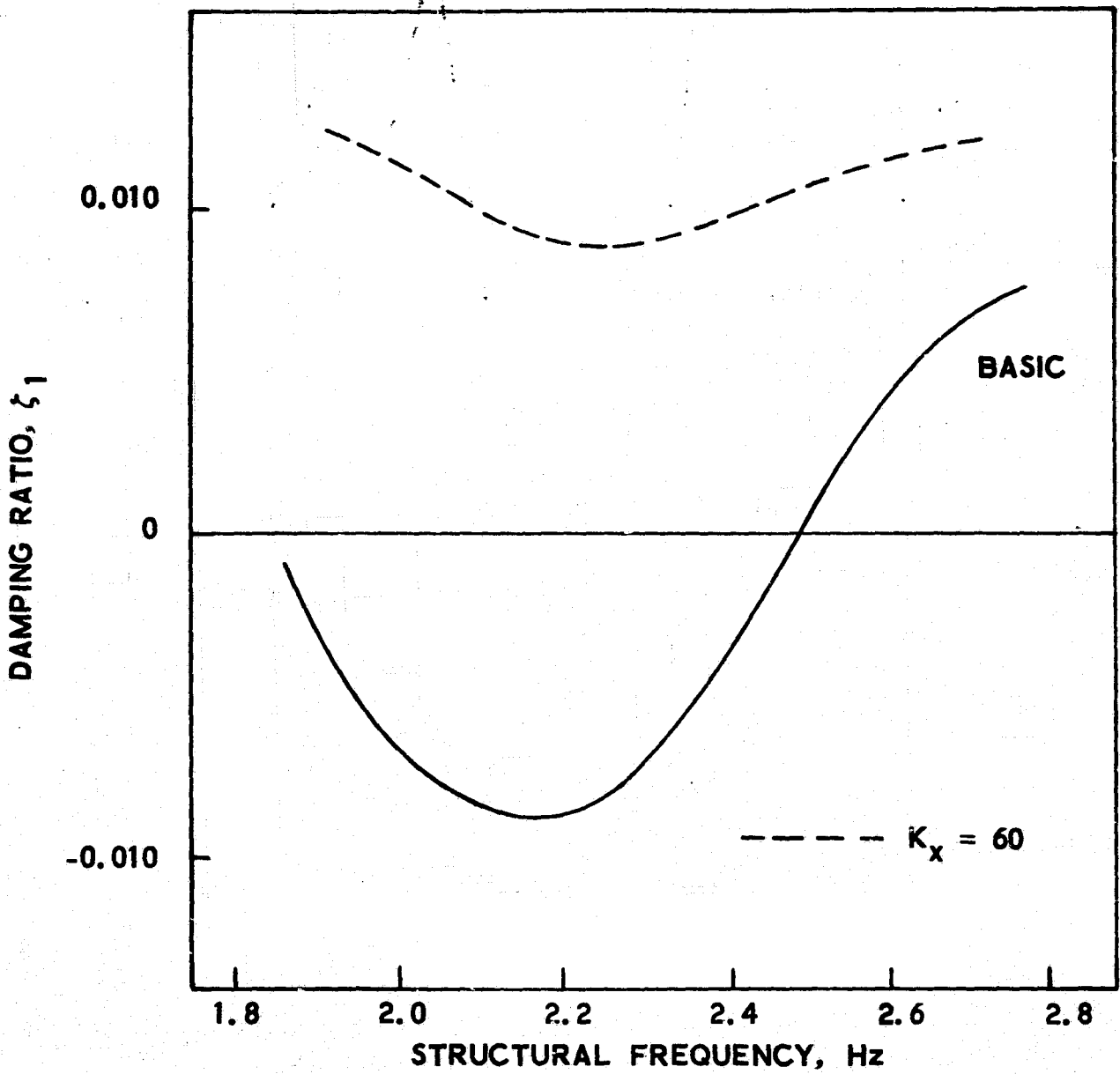Suppressor: Orbiter End-Burn

Figure 11c. Stability Results with Aerospace
Longitudinal-Motion-Feedback
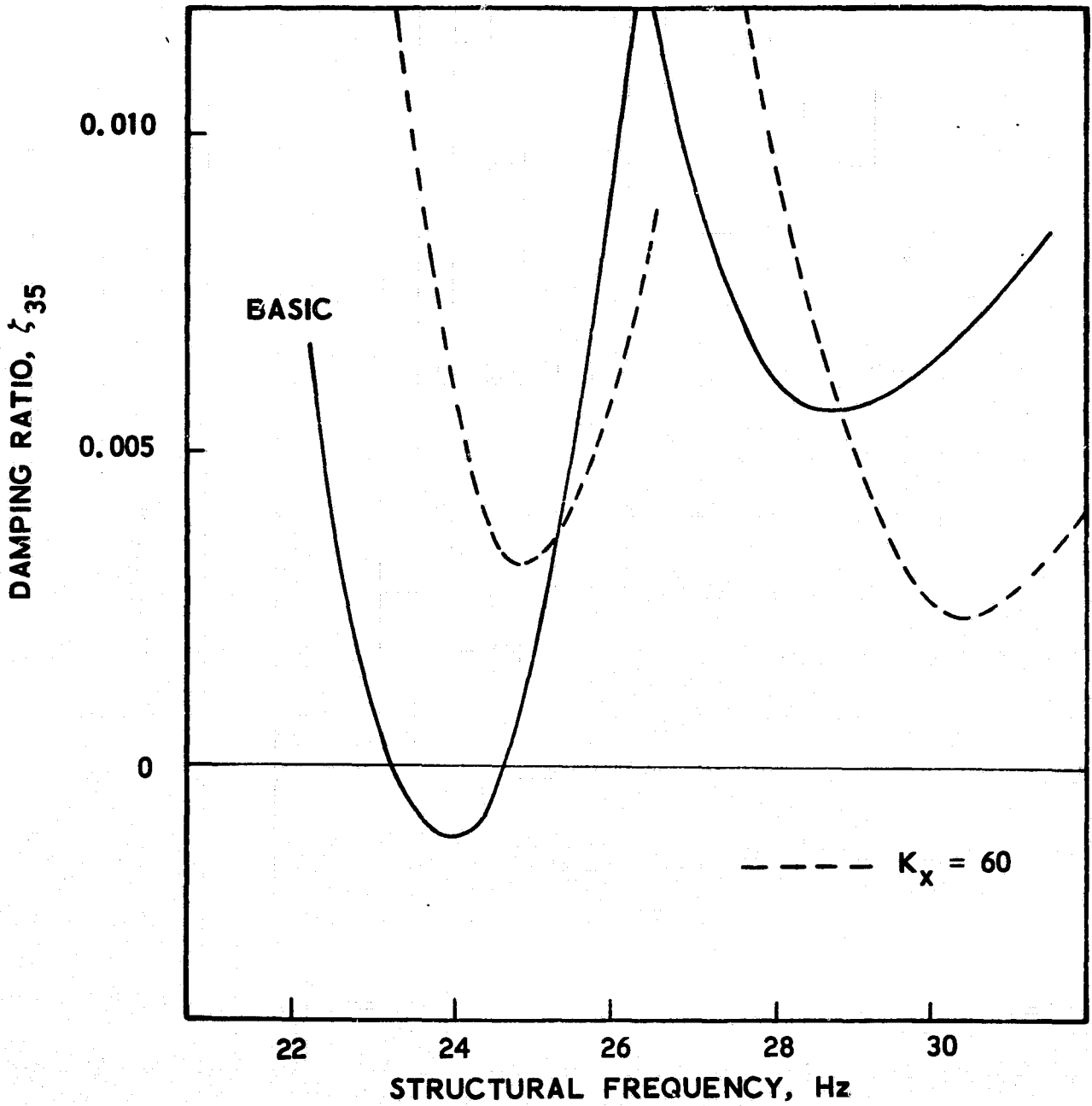Suppressor: After SRB Separation

34

Figure 11d. Stability Results with Aerospace
Longitudinal-Motion-Feedback
Suppressor: Orbiter End-Burn

were undertaken for the case where the suppressor was located at the HPOP inlet. The resulting stability curves are shown in figure 12. There it is seen that both instabilities have been eliminated; however, the performance of the device for the interpump mode instability (fig. 12b) is barely adequate. The performance of the device when the coefficients of the motion feedback were arbitrarily doubled in magnitude was also checked. In this case, the feedline mode instability was eliminated but the interpump mode instability remained. Again the performance of the basic device was checked at the LPOP inlet location. In this instance, the feedline mode instability was eliminated and the interpump mode instability remained.

For the third simple design, the pressure feedback device

$$Q_a = -K_p P_7$$

the HPOP inlet location was first considered.

Stability calculations were made for values of the coefficient K_p between 0.019 m^5/MNs (8 in.^{5}/lb-sec) and 0.6 m^5/MNs (250 in.^{5}/lb-sec). In all cases both instabilities were eliminated with the performance of the device improving with increasing value of the coefficient. To illustrate this behavior, the results for three different values of K_p are shown in figure 13. In contrast to the good performance obtained with this device at the HPOP inlet, the results obtained for the LPOP location were disappointing with the interpump instability remaining when K_p was equal to 0.019 m^5/MNs (8 in.^{5}/lb-sec) and with both instabilities being present when the value of the coefficient was increased to 0.3 m^5/MNs (125 in.^{5}/lb-sec).

3.1.3 Selection of Specific Aerospace Suppressor Designs

The optimum design was clearly the leading candidate for one of the two designs to be selected for more extensive evaluation. For the other suppressor design it was decided to exclude the limiting-case designs since they involved a requirement for flow measurement and to choose the best of the simple feedback systems. From the results presented previously, it is clear that the pressure feedback suppressor located at the HPOP inlet, i.e.,

$$Q_{a3} = -K_p P_7$$

was the best of the concepts that were examined. This concept was therefore selected as the second specific suppressor system. The only remaining question was the selection of the value of the coefficient K_p. It had been seen that the performance of the device improved with increase of the magnitude of K_p (at least up to a value of 0.6 m^5/MNs (250 in.^{5}/lb-sec); however, it was anticipated that indefinite increase of this coefficient might lead to an excessively large physical size for the suppressor. To provide a criterion for the value of K_p, it was decided to require that the chosen design eliminate any destabilizing influence of the propulsion system in the A1 mode and to maintain the minimum value of damping ratio above 0.005 for the E35 mode;
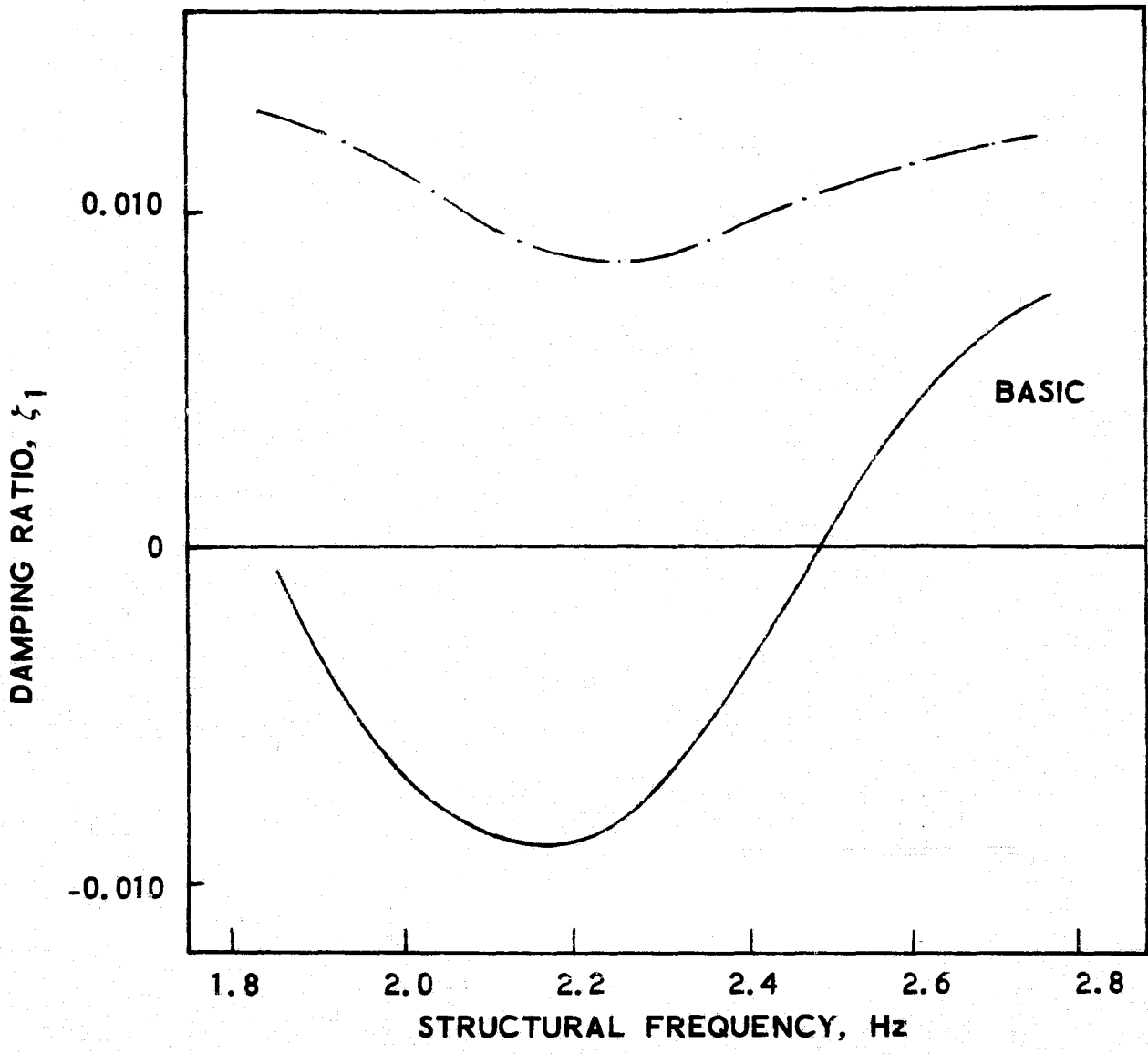
Figure 12a. Stability Results with Aerospace
Longitudinal- and Lateral-Motion-
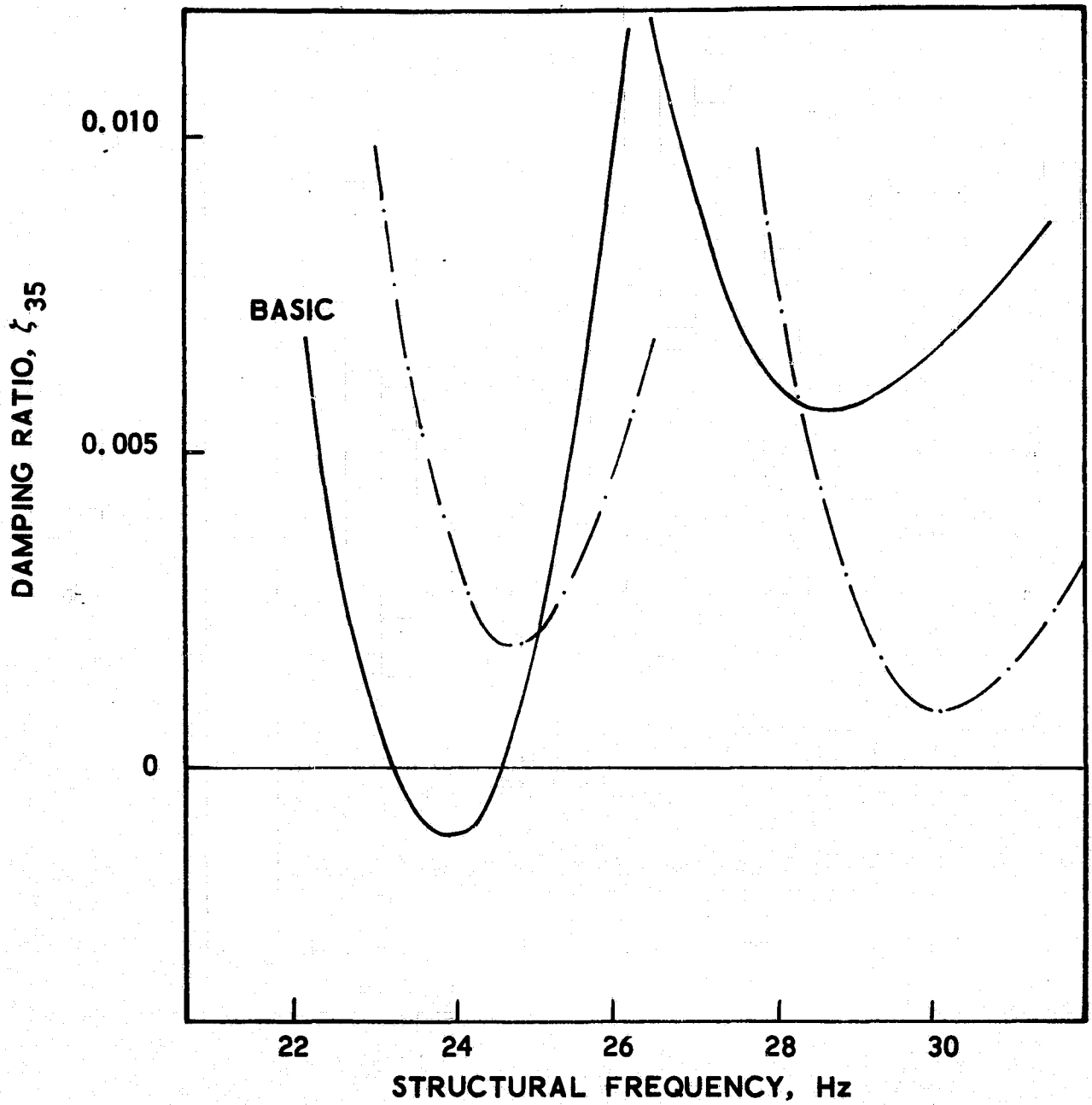Feedback Suppressor: After SRB Separation

Figure 12b. Stability Results with Aerospace
Longitudinal- and Lateral-Motion-
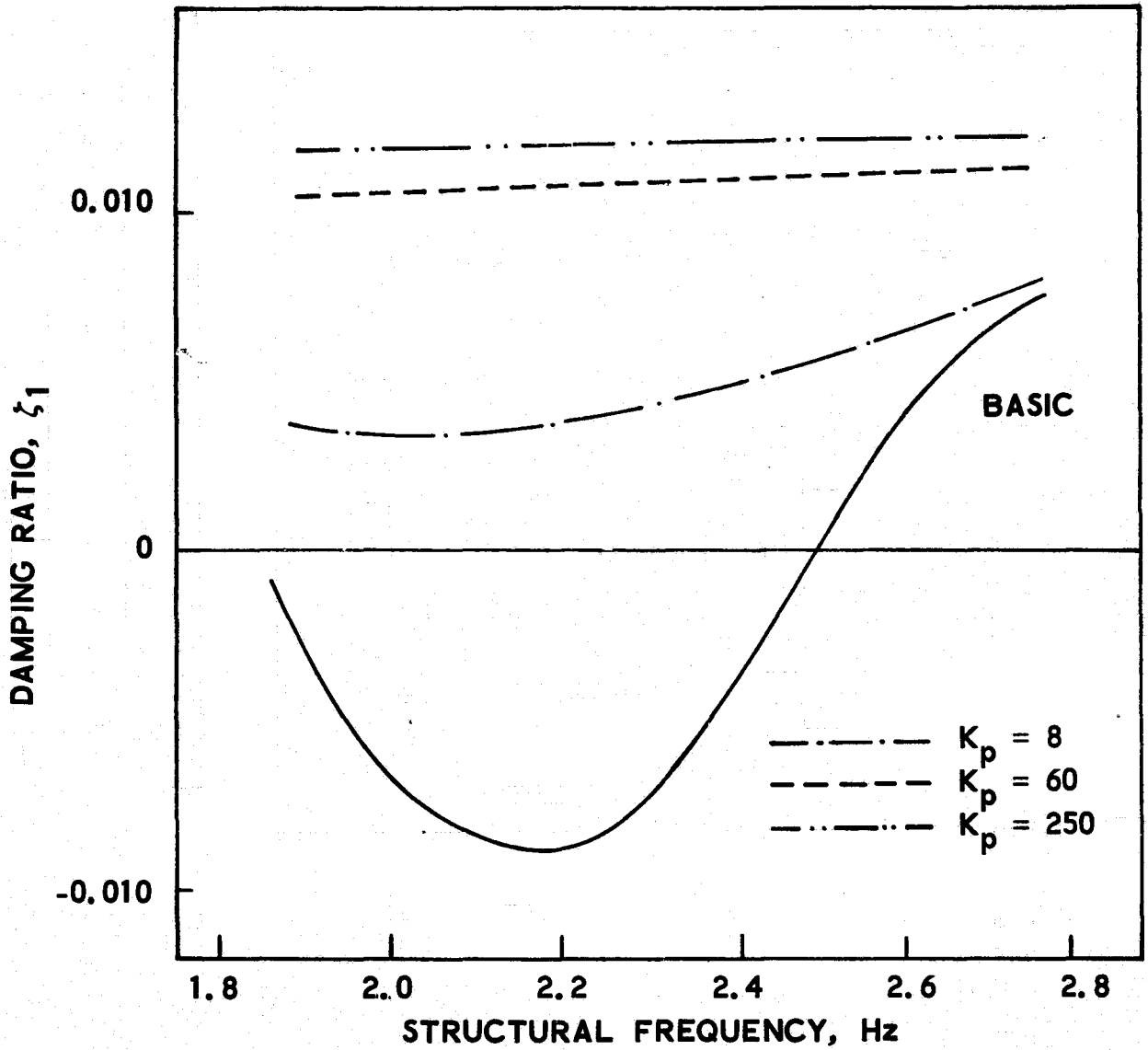Feedback Suppressor: Orbiter End-Burn

Figure 13a. Stability Results with Aerospace
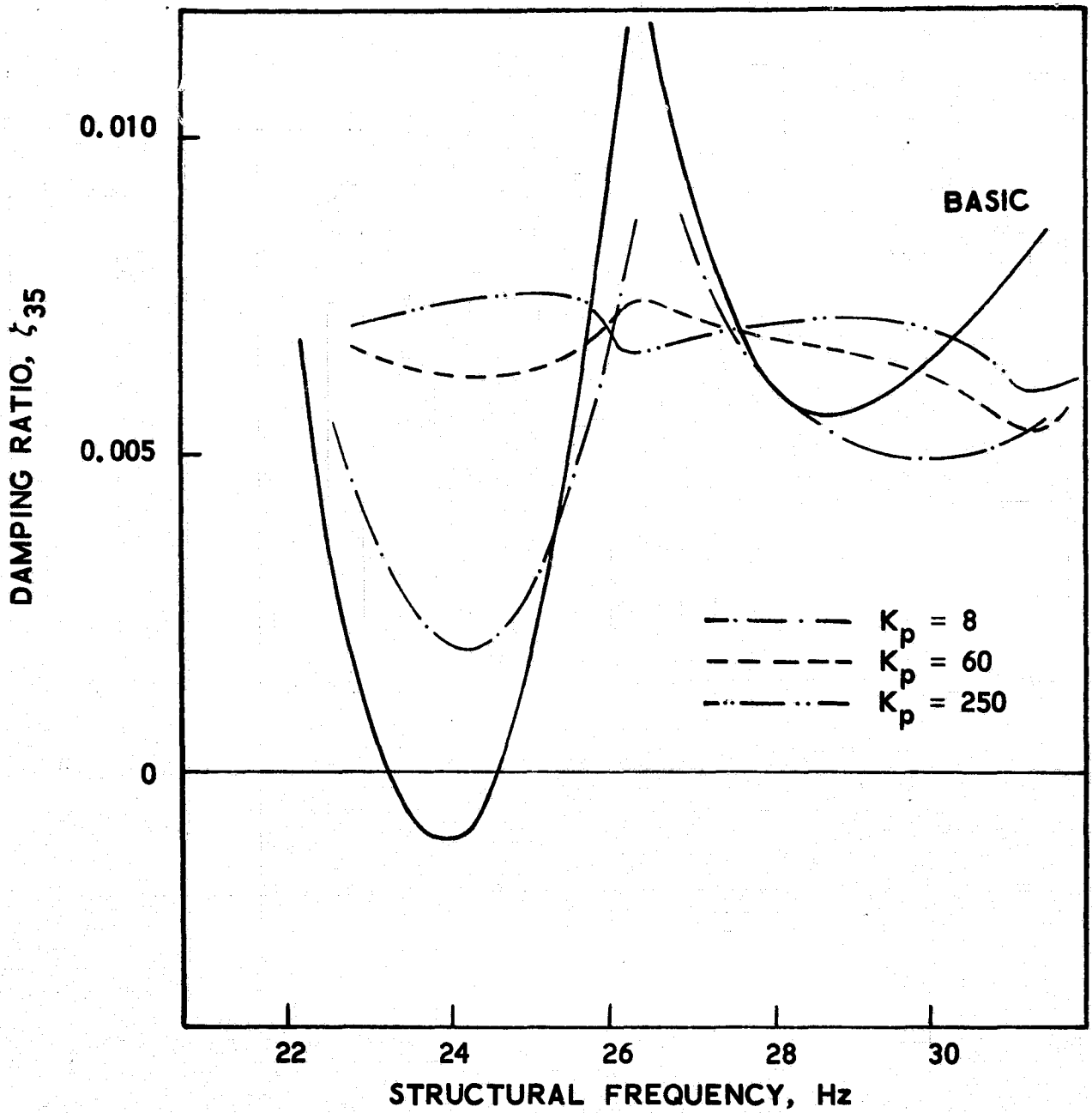Pressure-Feedback Suppressor:
After SRB Separation

39

Figure 13b. Stability Results with Aerospace
Pressure-Feedback Suppressor:
Orbiter End-Burn

these requirements are applied over the specified ±15 percent variation in structural frequency. Although somewhat arbitrary, the requirements are considered to be reasonable. Application of the requirements gave a value of 0. 14 m^5/MNs (60 in.^{5}/lb-sec) for the coefficient K_p. The selected Aerospace designs were thus

$$Q_{a3} = (-Q_7 + A_3 \dot{z}_7) + \overline{C}_{b2} \, s \, P_7$$

$$\overline{C}_{b2} = 2.4 \, 10^{-4} \, m^5/MN \, (0.1 \, in.^5/lb)$$

(9a)

and

$$Q_{a3} = - K_p P_7$$

$$K_p = 0.14 \, m^5/MNs \, (60 \, in.^5/lb-sec)$$

(9b)

These designs will be referred to as the optimum and pressure feedback designs, respectively.

3.2 NASA (Lewis) Suppressor Designs

Two suppressor designs were provided by NASA (Lewis) for detailed evaluation. The first of these designs was related to a system being studied by the Rockwell International/Rocketdyne Division and comprised an HPOP inlet device with a flow rate proportional to the HPOP inlet pressure and the local acceleration of the vehicle in the upstream direction

$$Q_{a3} = - \frac{s^2}{(s^2 + \gamma s + \gamma^2)} \left\{ \frac{Es \, P_7}{(s+\gamma)} - \frac{\alpha A_3 \, s}{(s^2 + s\gamma + \gamma^2)} \, \ddot{z}_7 \right\}$$

(10)

This design concept will be referred to as the NASA/Rocketdyne-type suppressor. The parameter α that is contained in the high pass filter terms that appear in the feedback expression was assigned a value π. These filters provide decoupling of the suppressor at steady-state conditions, as would be required in a practical design. For frequencies above ~1 Hz, the coefficient of the pressure term behaves like an integrator.

Nominal ranges of $0 \leq \alpha \leq 1$ and 0. 3 m^5/MNs (125 in.^{5}/lb-sec) $\leq E \leq$ 0.6 m^5/MNs (250 in.^{5}/lb-sec) had been assigned to the feedback parameters. Specific values for use in the present study were selected upon the basis of a limited set of stability analyses undertaken with this design concept. The selected values were

$$\alpha = 1$$

$$E = 0.3 \, m^5/MNs \, (125 \, in.^5/lb-sec)$$

(11)

The performance of this design for the A1 and E35 modes is shown in figure 14. It may be noted that the stability analyses indicated that the pressure was the most effective feedback parameter with the motion contribution providing a slight improvement in performance at the frequency of the higher mode. This feature of the design is illustrated in figure 15 where the results for zero motion feedback ($\alpha = 0$) and maximum motion feedback ($\alpha = 1$) [both with E equal to 0.3 m^5/MNs (125 in.^{5}/lb-sec)] are presented for the E35 condition.

The second NASA (Lewis) design was a dual-suppressor system that comprised a 0.057 m^3 (2 ft^3) volume compliant accumulator at the LPOP inlet and a NASA/Rocketdyne-type active suppressor at the HPOP inlet. This system was studied since it provided a means of reducing the size of the suppressor located within the engine (i.e., at the HPOP inlet). This size reduction has important practical consideration. The benefit resulting from the use of the additional accumulator at the LPOP inlet had been revealed in some analyses which had shown that the size of the HPOP inlet device was controlled by the need to eliminate the fundamental mode instabilities. Since these instabilities could also be eliminated by a LPOP-inlet device, the dual-suppressor assignment provided a means of size reduction. Again, the specific values of the feedback parameters used in the present study were selected on the basis of a limited number of stability analyses with this design concept. The values selected for the dual system were

$$\alpha = 0$$

$$E = 0.3 \text{ m}^5/\text{MNs (125 in.}^5/\text{lb-sec)} \tag{12}$$

The active device in this case is thus seen to involve only feedback of the inlet pressure. The performance of this dual-suppressor system for the A1 and E35 cases is shown in figure 16.
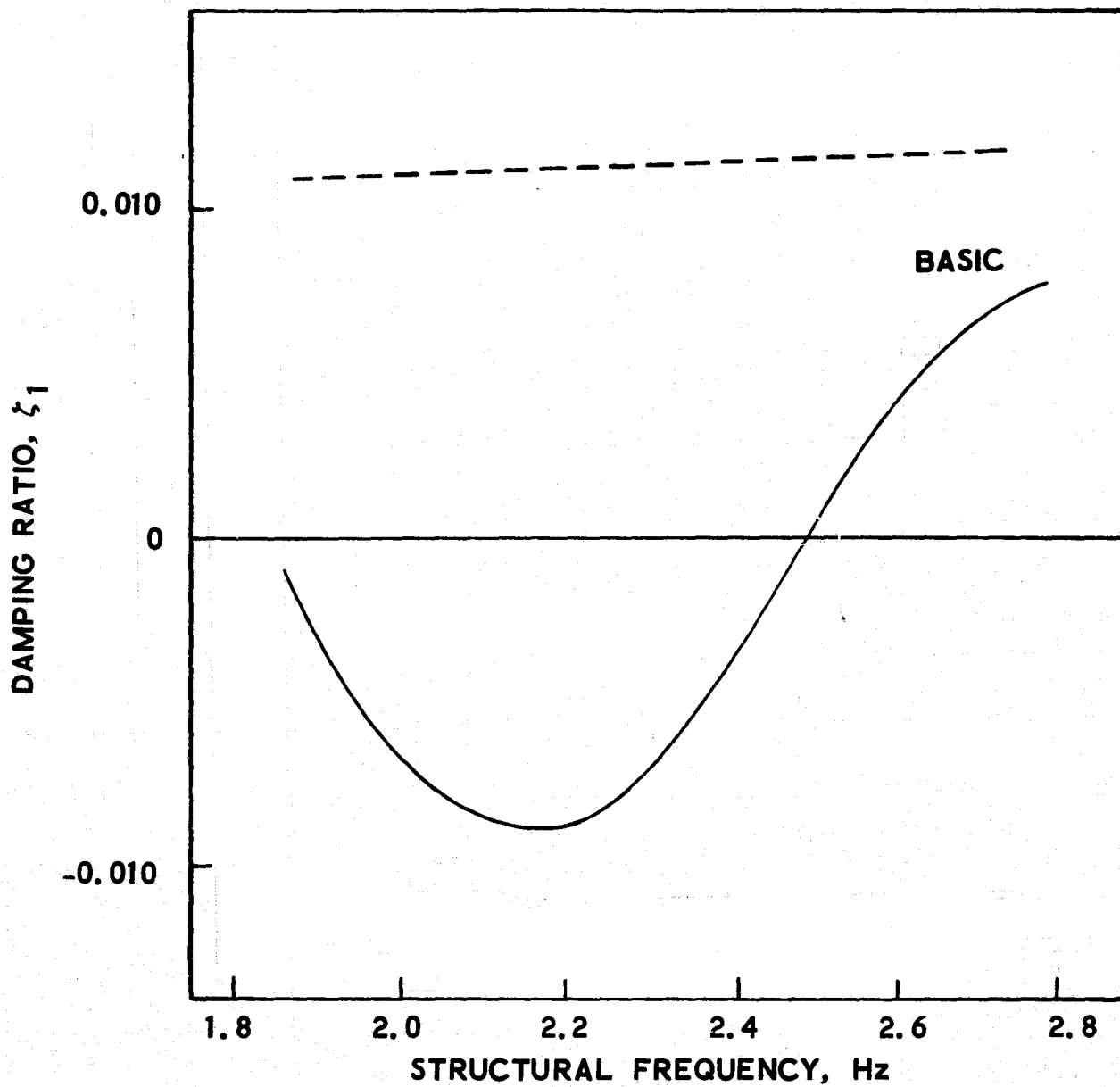
Figure 14a. Stability Results with NASA/
Rocketdyne Suppressor:
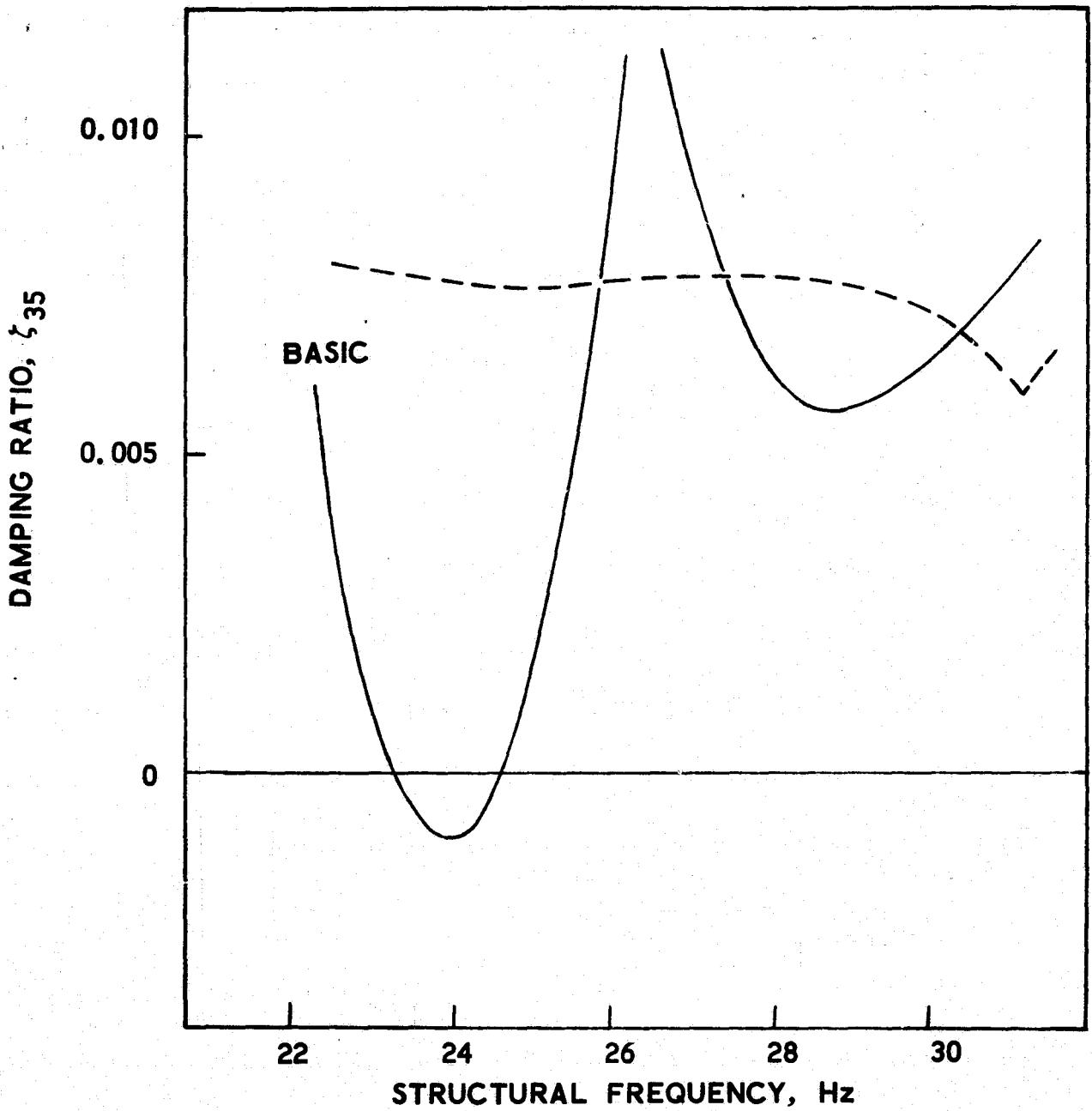After SRB Separation

Figure 14b. Stability Results with NASA/
Rocketdyne Suppressor:
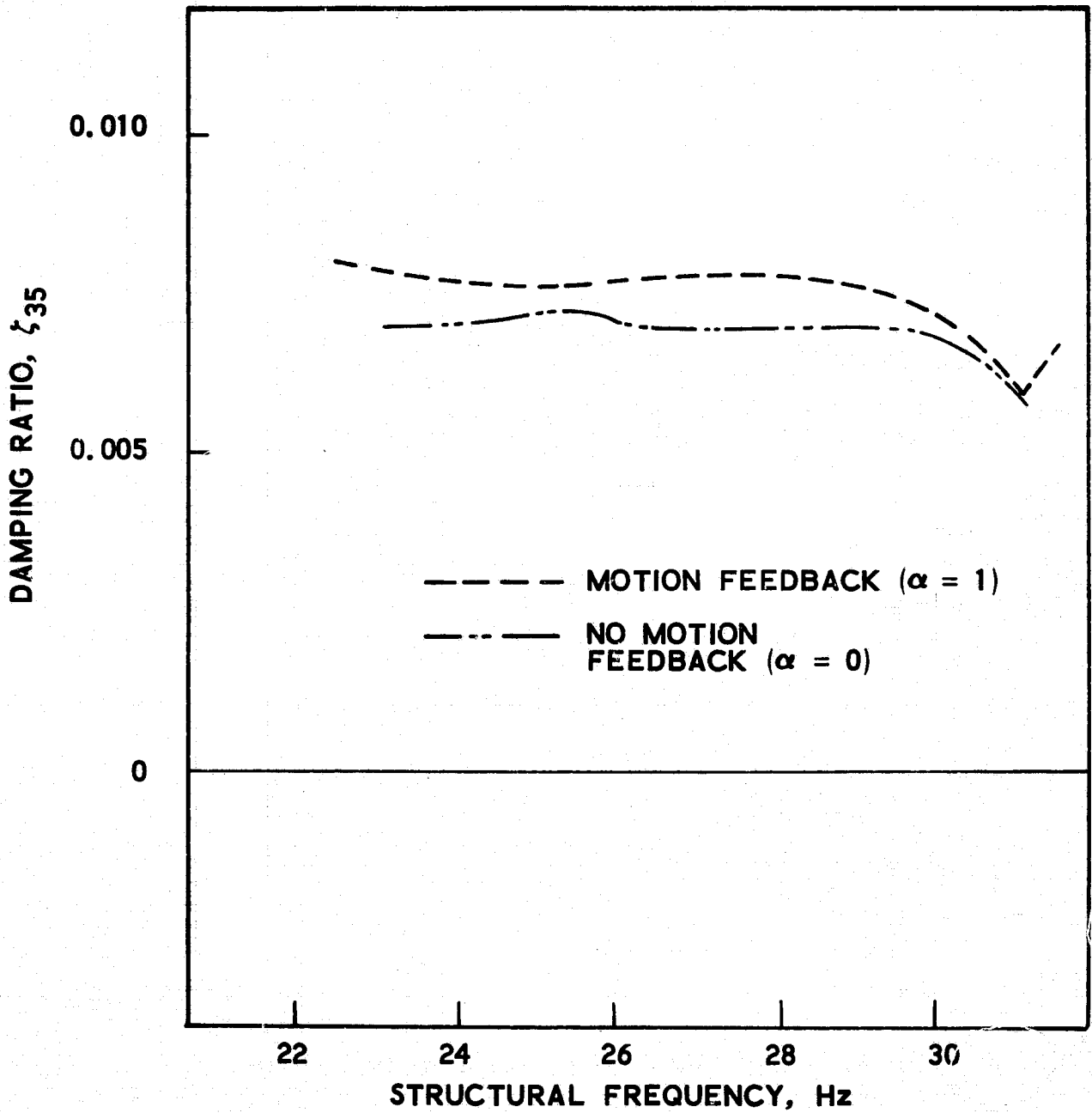Orbiter End-Burn

Figure 15. Effect of Motion Feedback on NASA/
Rocketdyne Suppressor: Orbiter End-Burn
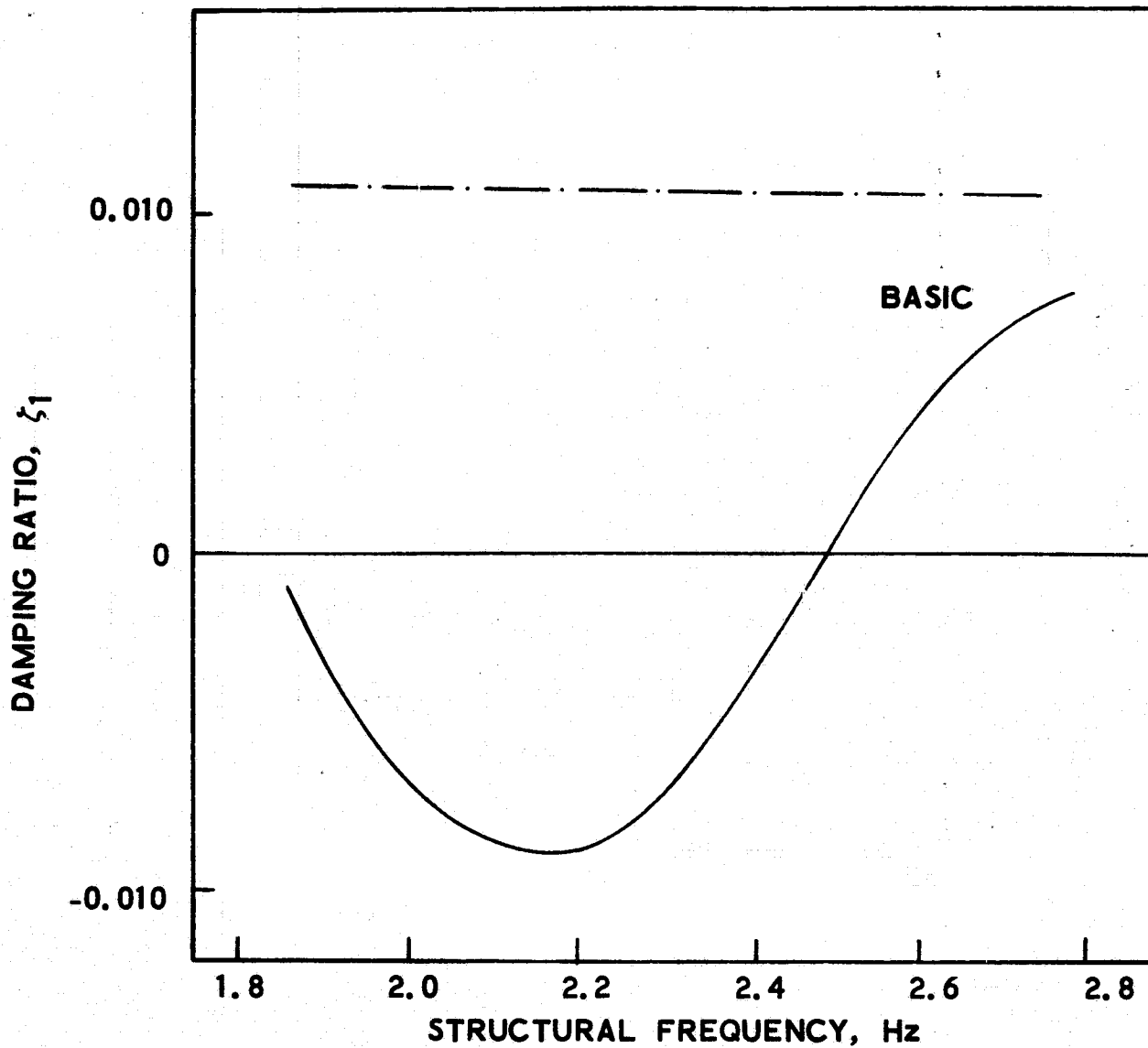
45

Figure 16a.   Stability Results with NASA
              Dual-Suppressor System:
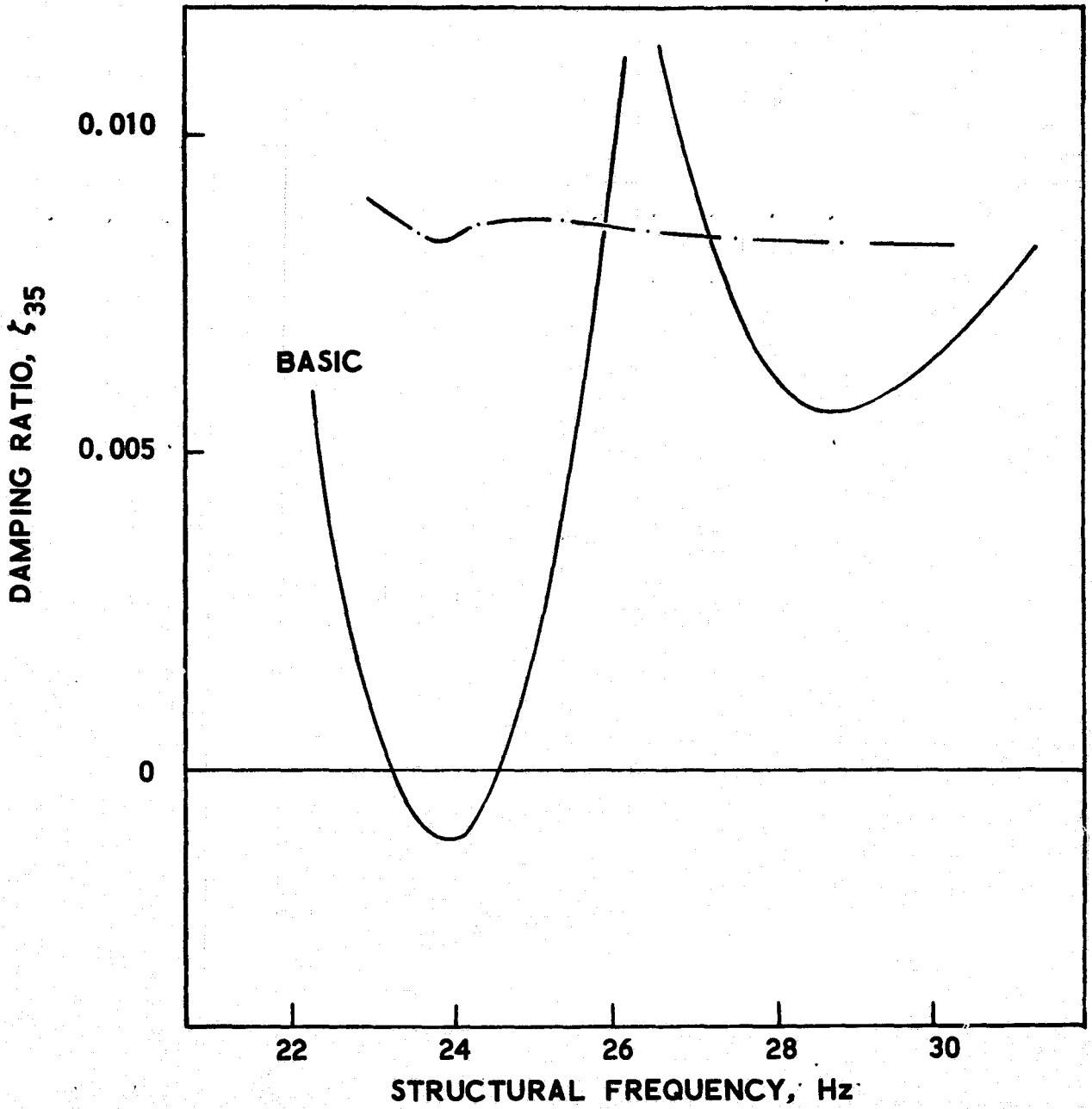   After SRB Separation

Figure 16b. Stability Results with NASA
Dual-Suppressor System:
Orbiter End-Burn

47

4. EVALUATION OF SPECIFIC ACTIVE SUPPRESSOR DESIGNS

The evaluation of the specific suppressor designs discussed in the preceding section was limited to the following areas:

    a.   Control effectiveness

    b.   Performance relative to passive suppressor design

    c.   Sensitivity of performance to feedback error

    d.   Suppressor volume flow requirements

    e.   Suppressor development requirements

Topics such as the suppressor system reliability and the system weight impact were not treated since they involve considerations that were outside the scope of the present study. In the first of the above items, control effectiveness refers to the ability of the suppressor to maintain the system damping ratios at satisfactory levels and does not deal with system frequency response characteristics. In the second item, the reference passive suppressor was taken to be a $0.057 \ m^3$ (2 ft^3) volume compliant accumulator located at the HPOP inlet. The compliant accumulator (no inertance or resistance) is an idealization of the type of passive device commonly used on past vehicles. In the error analysis both magnitude and phase errors in the feedback signal were considered. The size requirements were based upon the response of the suppressors to random oscillations in the system. Consideration of development requirements was limited to the question of providing the necessary feedback measurements. Items such as the development of suitable hydraulic valves and electronic circuitry for the suppressor system were outside the scope of the study.

4.1 Control Effectiveness

A more detailed examination of the effectiveness of the selected suppressor designs was made by undertaking stability analyses for the more extensive sets of modes that had been considered in the study of the basic system (ref. 2). As noted previously these modes had been selected for analysis on the basis of their structural gains. For the end-burn event the additional cases were the E1, E7, E30 and E34 modes. At liftoff, the additional cases were the L18, L26, L49, L51 and L62 modes. At after SRB separation, the additional case was the A46 mode. The general modal data associated with these various cases are given in the tables on pages 15 and 16; the detailed modal data is given in Appendix C. The analyses were run as before with the damping ratios being calculated over the specified ±15 percent variation in the structural mode frequency.

4.1.1 Aerospace Designs

The calculated damping ratios for the basic system and for the two selected Aerospace suppressor designs are shown in figures 17 through 19 for the additional cases at the end-burn, liftoff, and after-SRB-separation events,

Figure 17a. Stability Results with Aerospace Suppressor
Designs: Orbiter End-Burn

Figure 17b. Stability Results with Aerospace Suppressor
Designs: Orbiter End-Burn

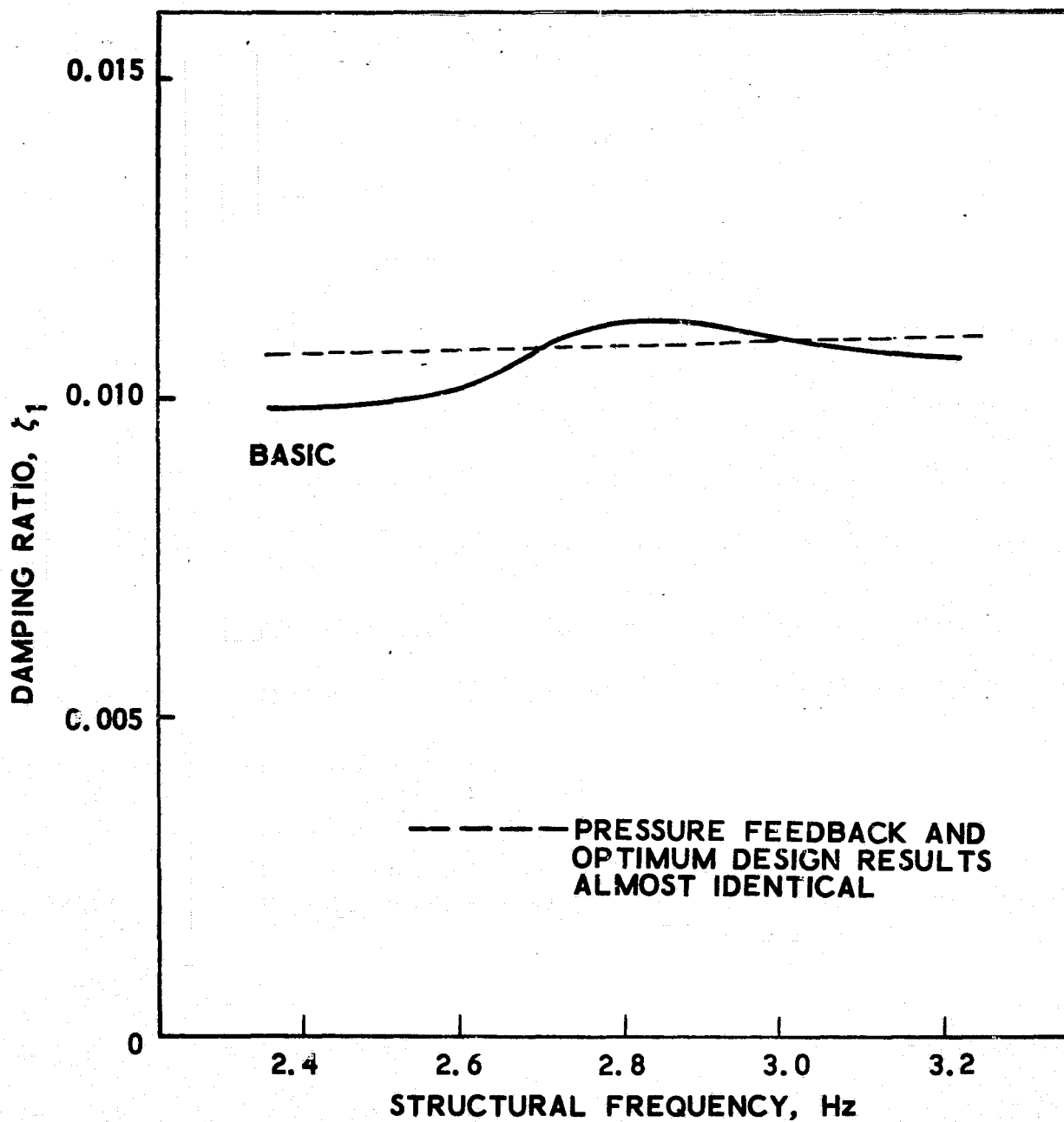Figure 17c. Stability Results with Aerospace Suppressor
Designs: Orbiter End-Burn

Figure 17d. Stability Results with Aerospace Suppressor
Designs: Orbiter End-Burn

Figure 18a. Stability Results with Aerospace Suppressor
Designs: Liftoff

54

Figure 18b. Stability Results with Aerospace Suppressor
Designs: Liftoff

55

Figure 18c. Stability Results with Aerospace Suppressor
Designs: Liftoff

56
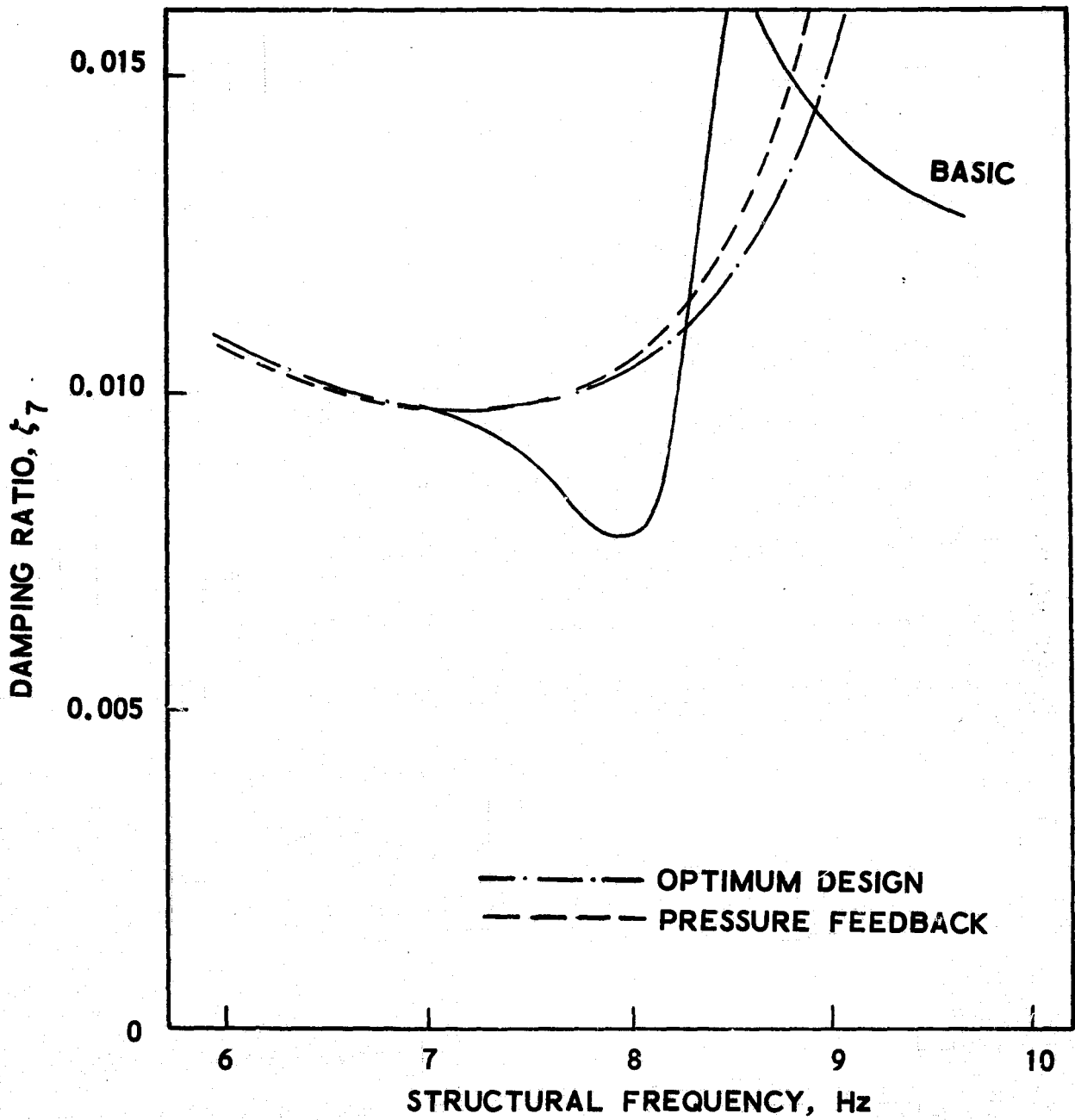
Figure 18d. Stability Results with Aerospace Suppressor
Designs: Liftoff

Figure 18e. Stability Results with Aerospace Suppressor
Designs: Liftoff

Figure 18f. Stability Results with Aerospace Suppressor
Designs: Liftoff

Figure 19. Stability Results with Aerospace Suppressor
Designs: After SRB Separation

respectively (refer to figs. 7 and 8 for the corresponding results for the Al and E35 modes). Examination of the results in figure 17 indicates that the performance of the two suppressor designs is quite similar for the additional end-burn cases. The most severe condition is seen to be the E34 mode ($f \sim 27$ Hz) where the minimum calculated damping ratios in the specified frequency range were around 0.007 and 0.0055 for the optimum and pressure-feedback designs, respectively (fig. 17d). At the liftoff event, it is seen that either design is extremely effective in eliminating the fundamental-mode instability that had been predicted for the basic system (fig. 18a). The performance of the designs for the L18 and L26 modes is similar (figs. 18b, 18c, respectively). The pressure-feedback suppressor is the better performer for the L49 mode ($f \sim 22$ Hz) maintaining the damping ratio above 0.008 while the minimum damping ratio associated with the other design is slightly above the 0.007 level (fig. 18d). The performance of the two devices is similar in the L51 mode ($f \sim 22$ Hz) with minimum damping ratio values of about 0.0065 (fig. 18e). For the L62 mode ($f \sim 27$ Hz) the optimum design is the better performer with a minimum damping ratio of about 0.0065 whereas the damping ratio curve for the pressure feedback suppressor drops to a minimum value of about 0.005 (fig. 18f). For the additional A46 mode ($f \sim 27$ Hz) at the after-SRB-separation condition, it is seen (fig. 19) that the optimum design is the better performer maintaining the calculated damping ratio above 0.008; whereas, in the case of the pressure-feedback design, the damping ratio gets as low as 0.006.

Reviewing the results of the stability calculations, it is seen that both Aerospace designs are effective in eliminating the instabilities predicted for the basic system. The destabilizing influence of the propulsion system has been completely eliminated for the fundamental mode cases and the damping ratios maintained above the 0.005 level for the higher frequency modes ($f \sim 27$ Hz) where coupling with the interpump mode produced a problem for the basic system. The performance of the two designs is comparable insofar as system stabilization is concerned.

4.1.2   NASA (Lewis) Designs

The calculated damping ratios for the basic system and for the two NASA (Lewis) designs are shown in figures 20 through 22 for the additional cases at the end-burn, liftoff and after-SRB-separation events, respectively (refer to figs. 14 and 16 for the corresponding results for the Al and E35 modes). Referring to figure 20, it is seen that the performance of the two designs is comparable for the El mode ($f \sim 2.8$ Hz) that the dual suppressor system is superior in the E7 ($f \sim 8.5$ Hz) and E34 modes ($f \sim 27$ Hz), and that the NASA /Rocketdyne suppressor is superior in the E30 mode ($f \sim 22.5$ Hz). The lowest damping ratio exhibited with the dual-suppressor system was a value of 0.0063 in the E30 mode. The lowest damping ratio exhibited with the NASA/Rocketdyne suppressor was a value around 0.006 in the E34 mode. The results for the liftoff event (fig. 21) indicated that the L51 mode ($f \sim 22$ Hz) and the L62 mode ($f \sim 27$ Hz) were the most severe cases. In the L51 mode the NASA/Rocketdyne and dual-suppressor systems exhibited minimum damping ratios of 0.0066 and 0.0053, respectively. In the L62 mode the single and dual-suppressor systems exhibited minimum damping ratios of 0.0059

Figure 20a. Stability Results with NASA Suppressor
Designs: Orbiter End-Burn

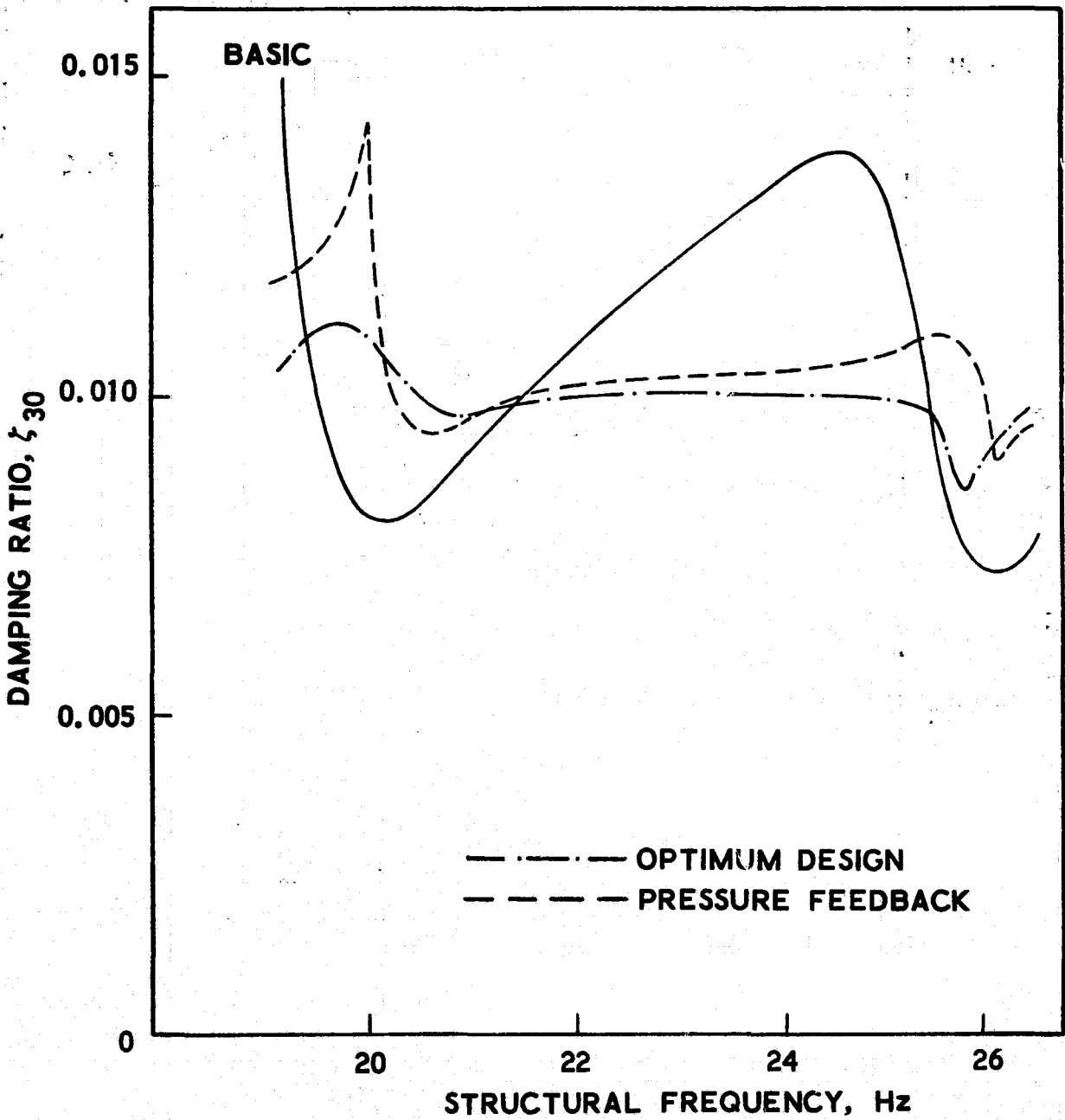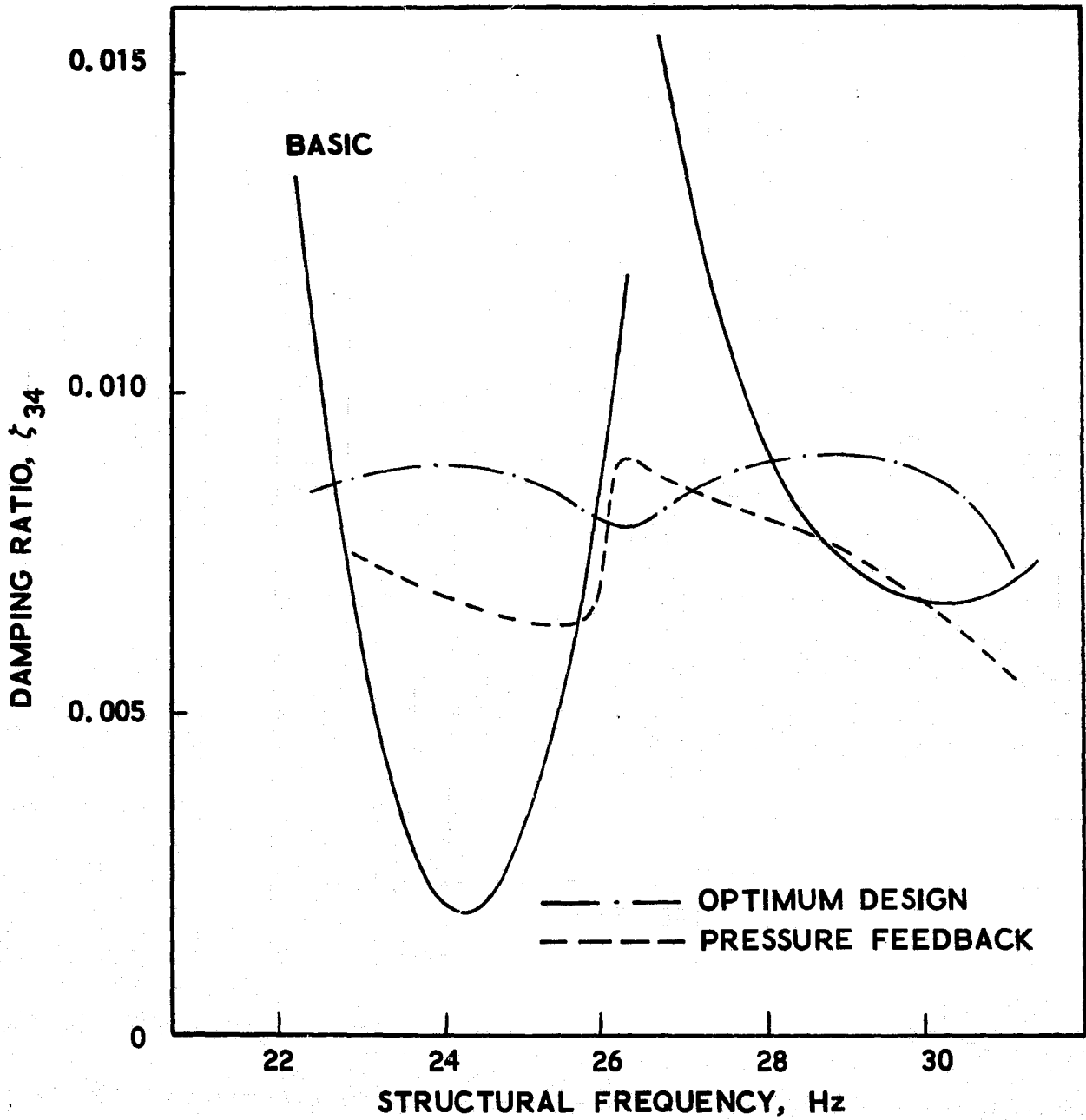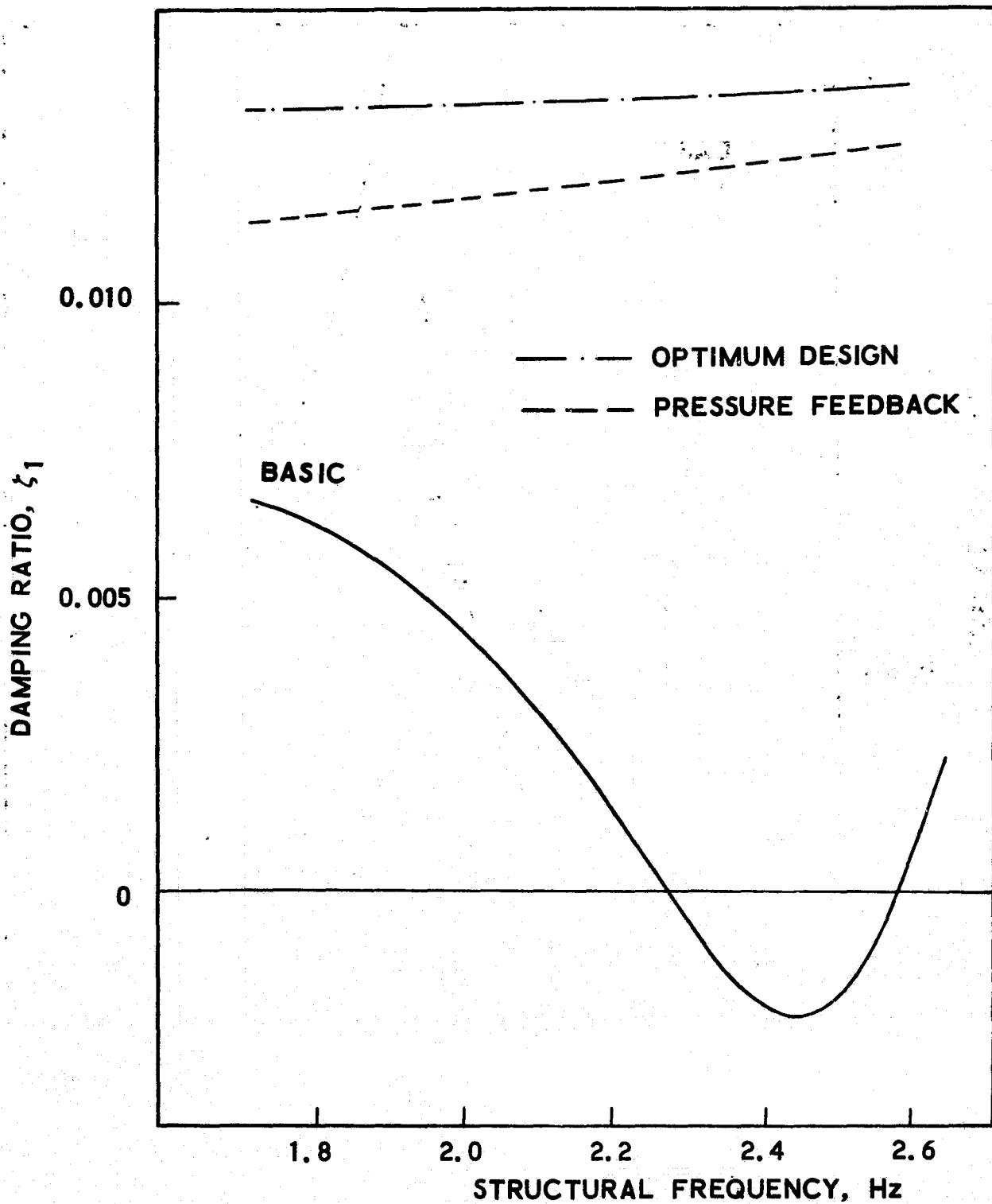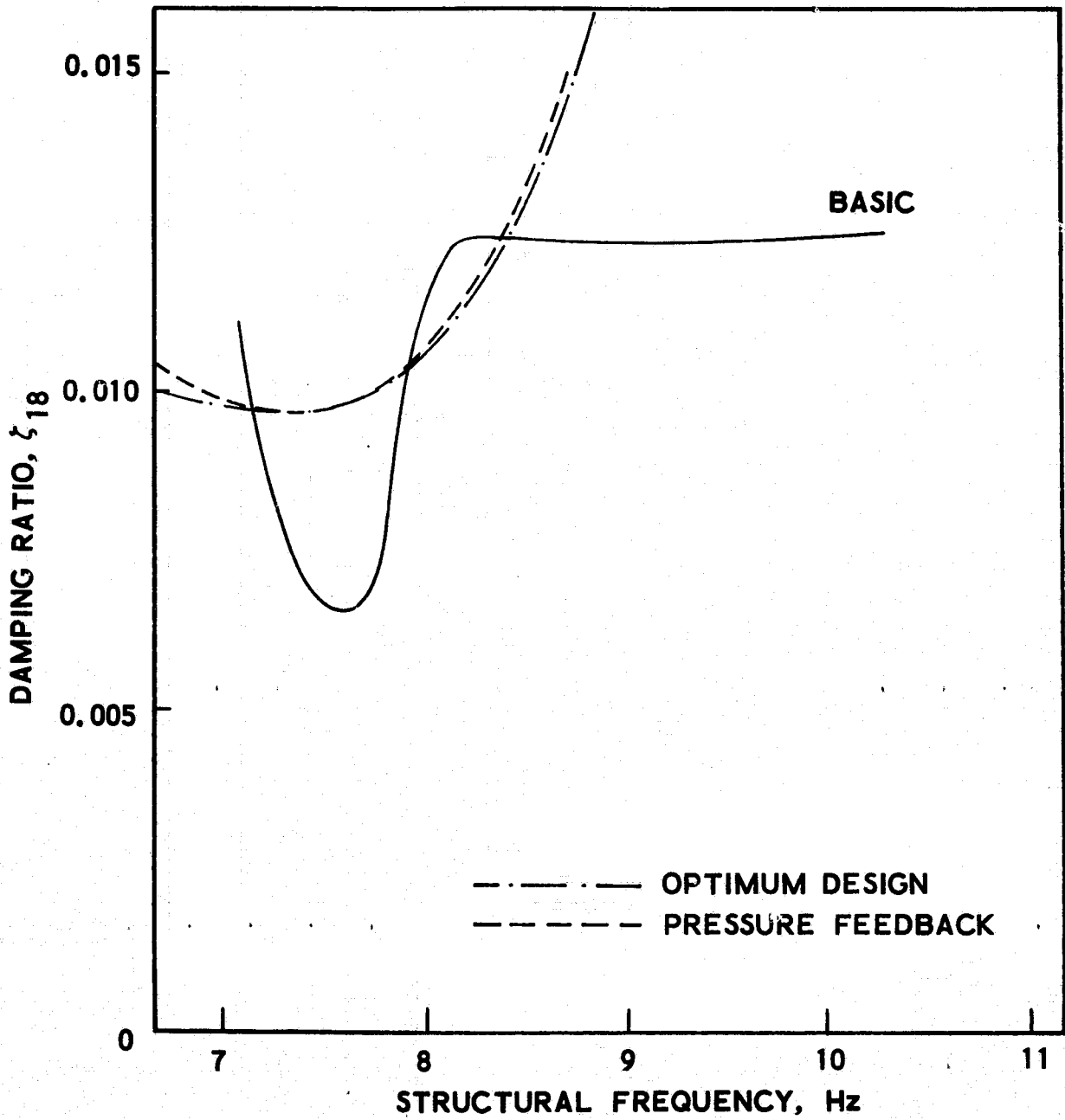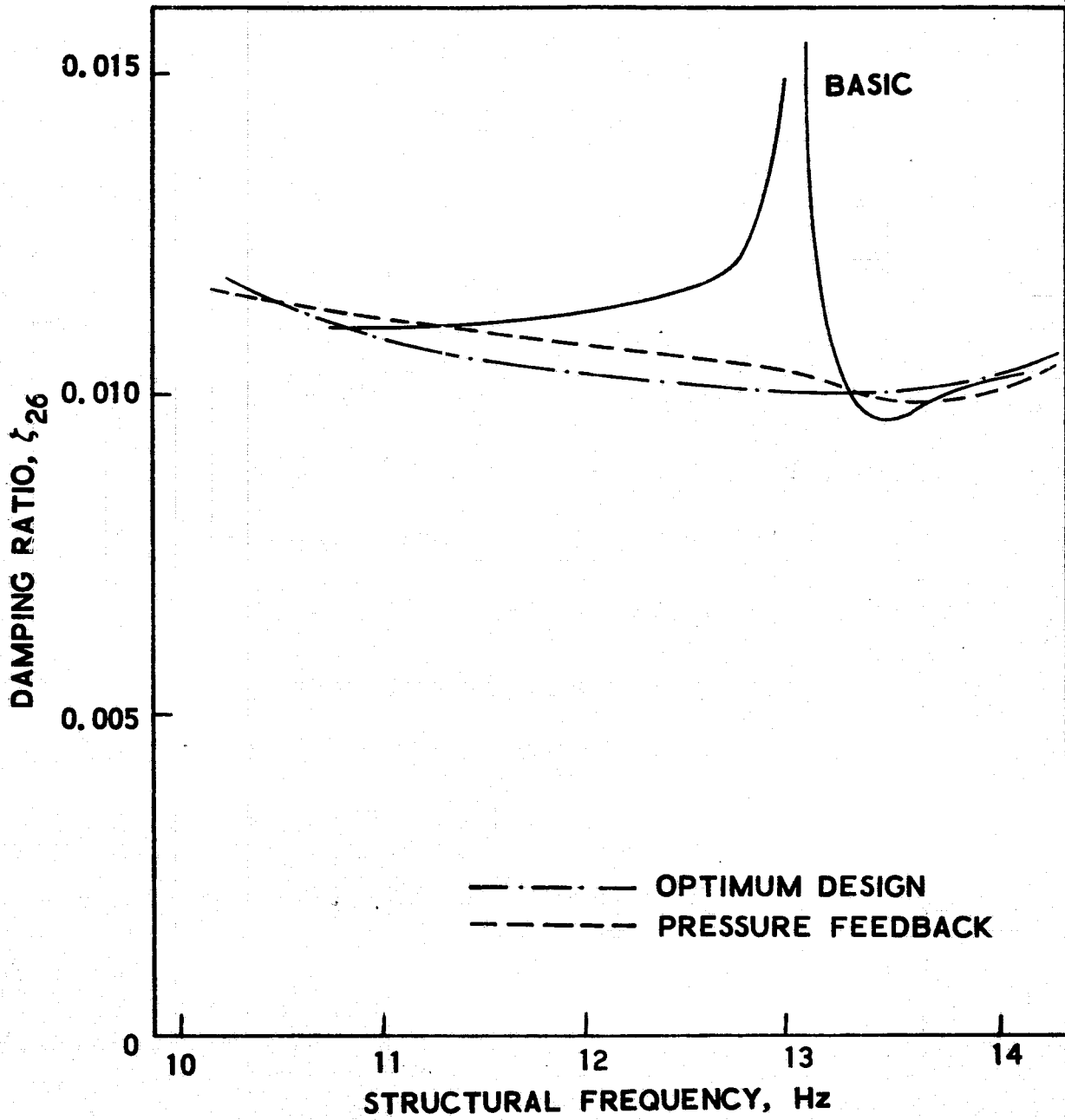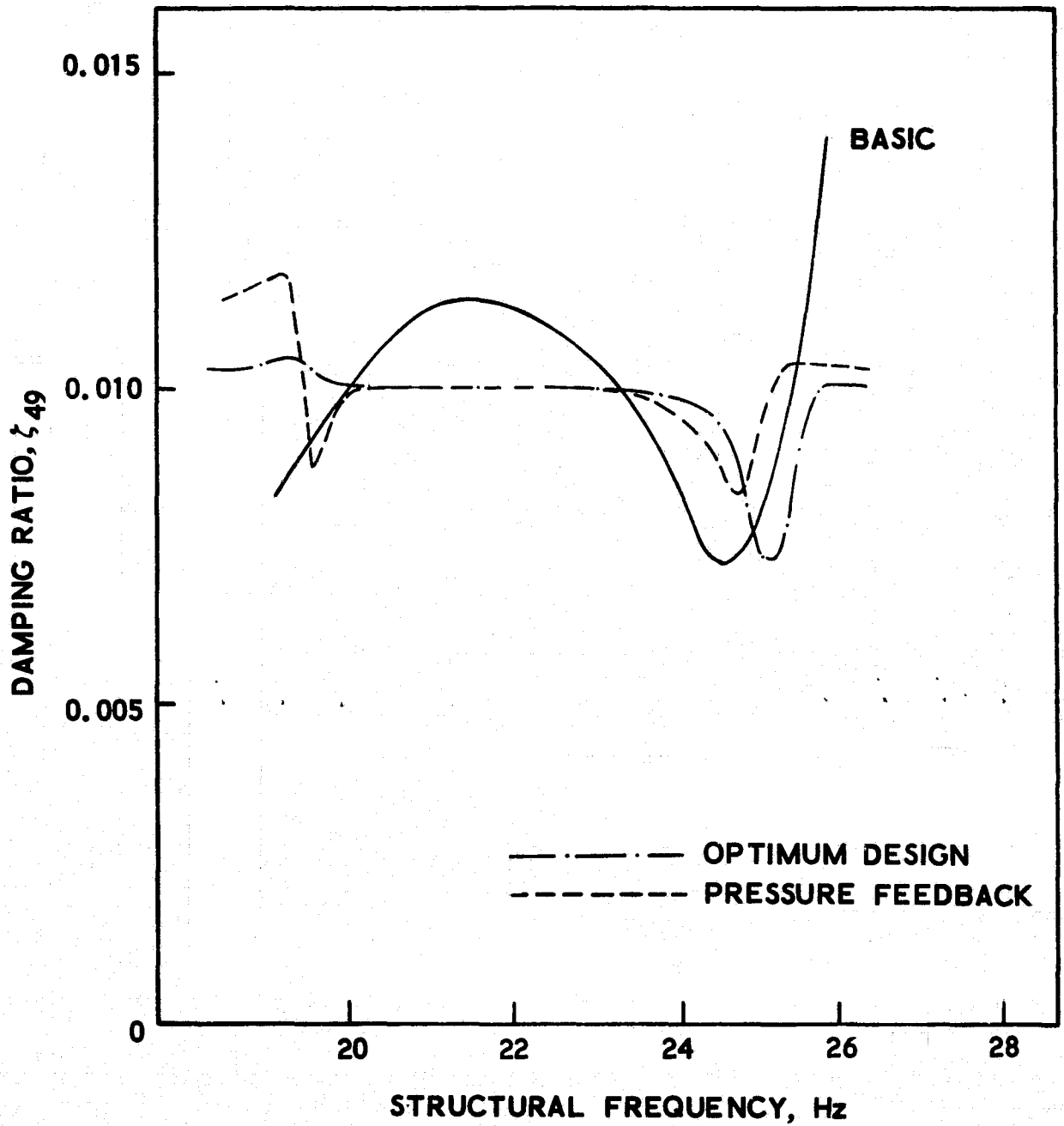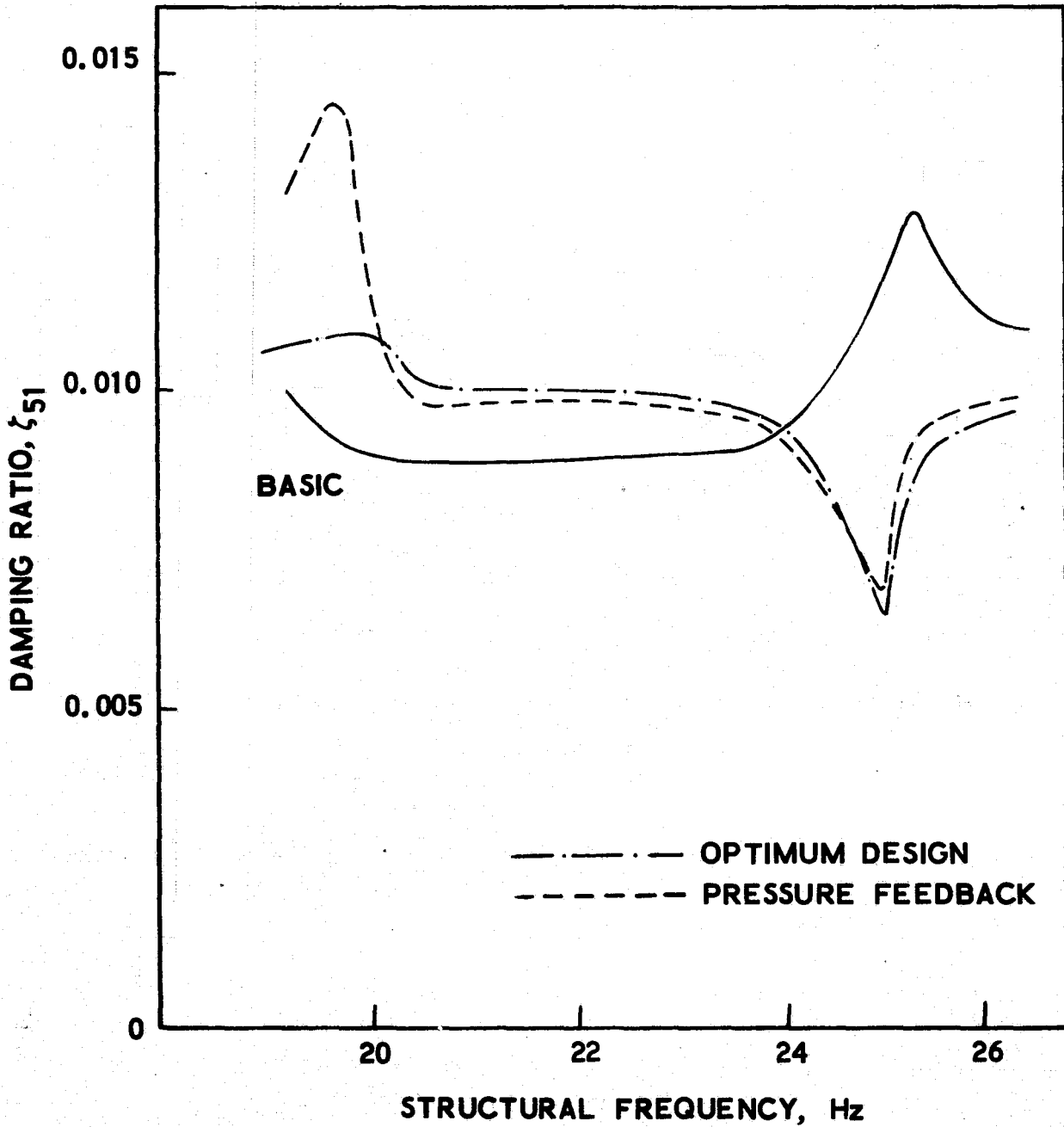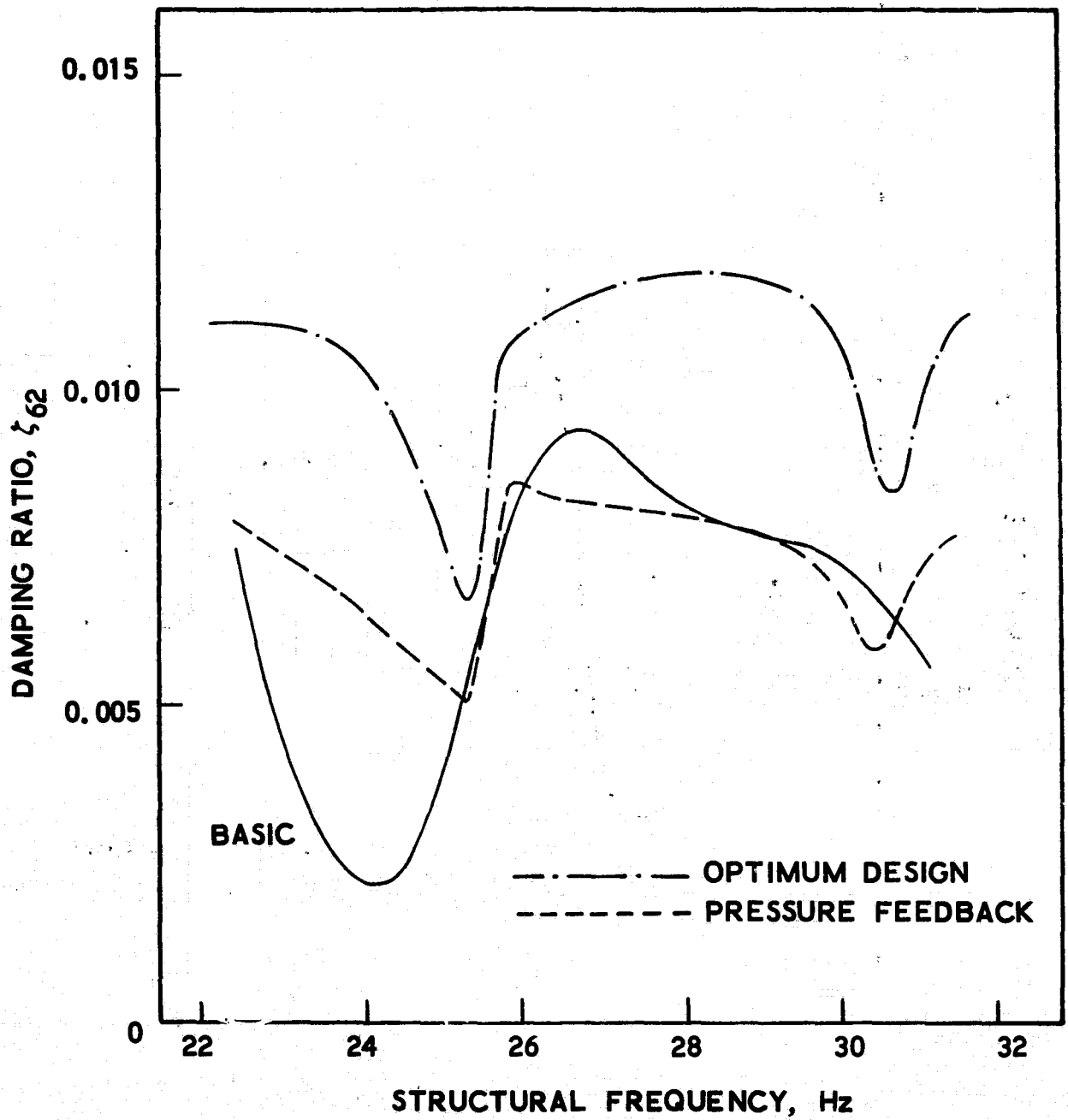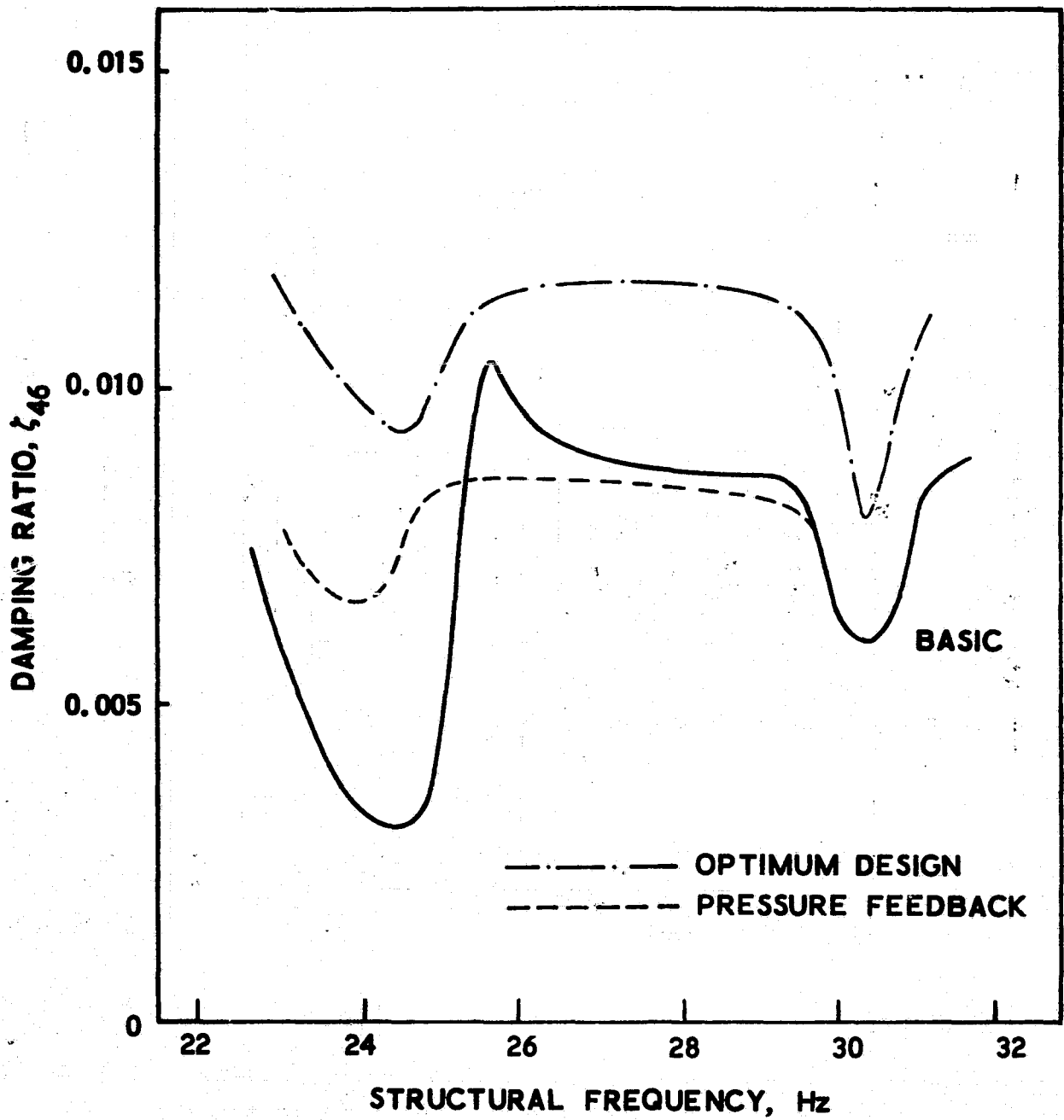Figure 20b. Stability Results with NASA Suppressor
Designs: Orbiter End-Burn

Figure 20c. Stability Results with NASA Suppressor
Designs: Orbiter End-Burn

Figure 20d. Stability Results with NASA Suppressor
Designs: Orbiter End-Burn

Figure 21a.   Stability Results with NASA Suppressor
Designs: Liftoff

Figure 21b. Stability Results with NASA Suppressor
Designs: Liftoff

Figure 21c.   Stability Results with NASA Suppressor
Designs: Liftoff

Figure 21d. Stability Results with NASA Suppressor
Designs: Liftoff
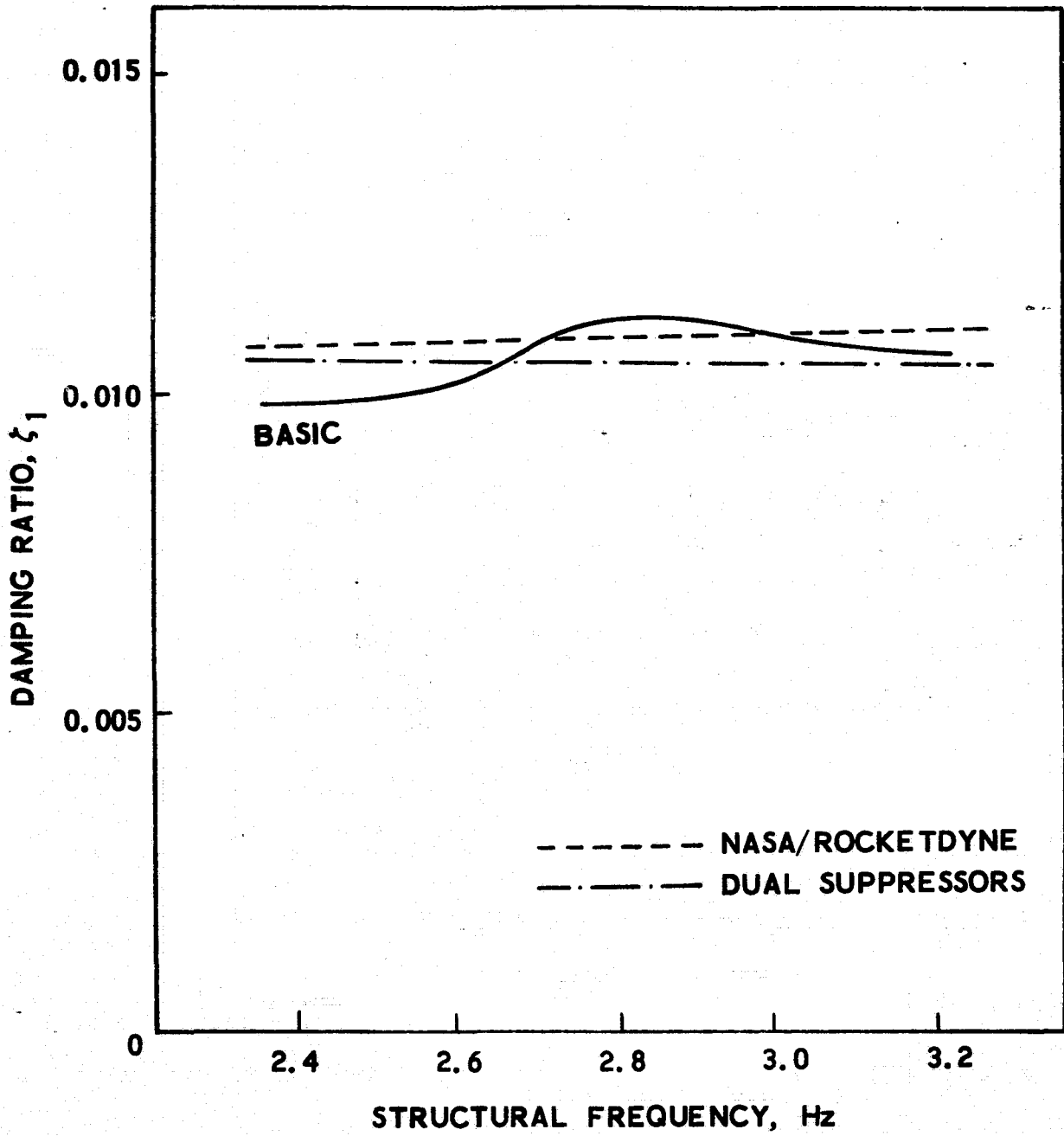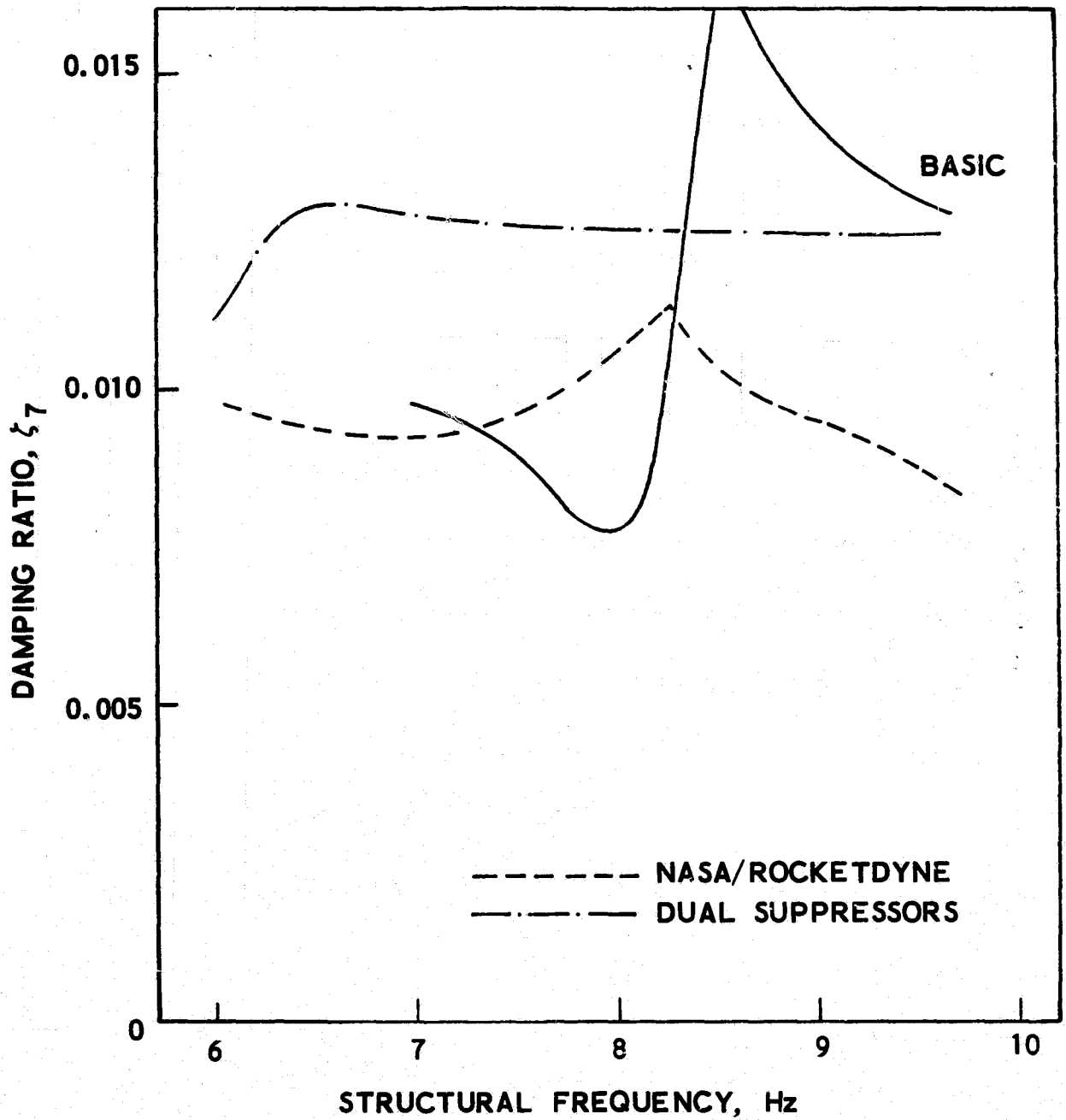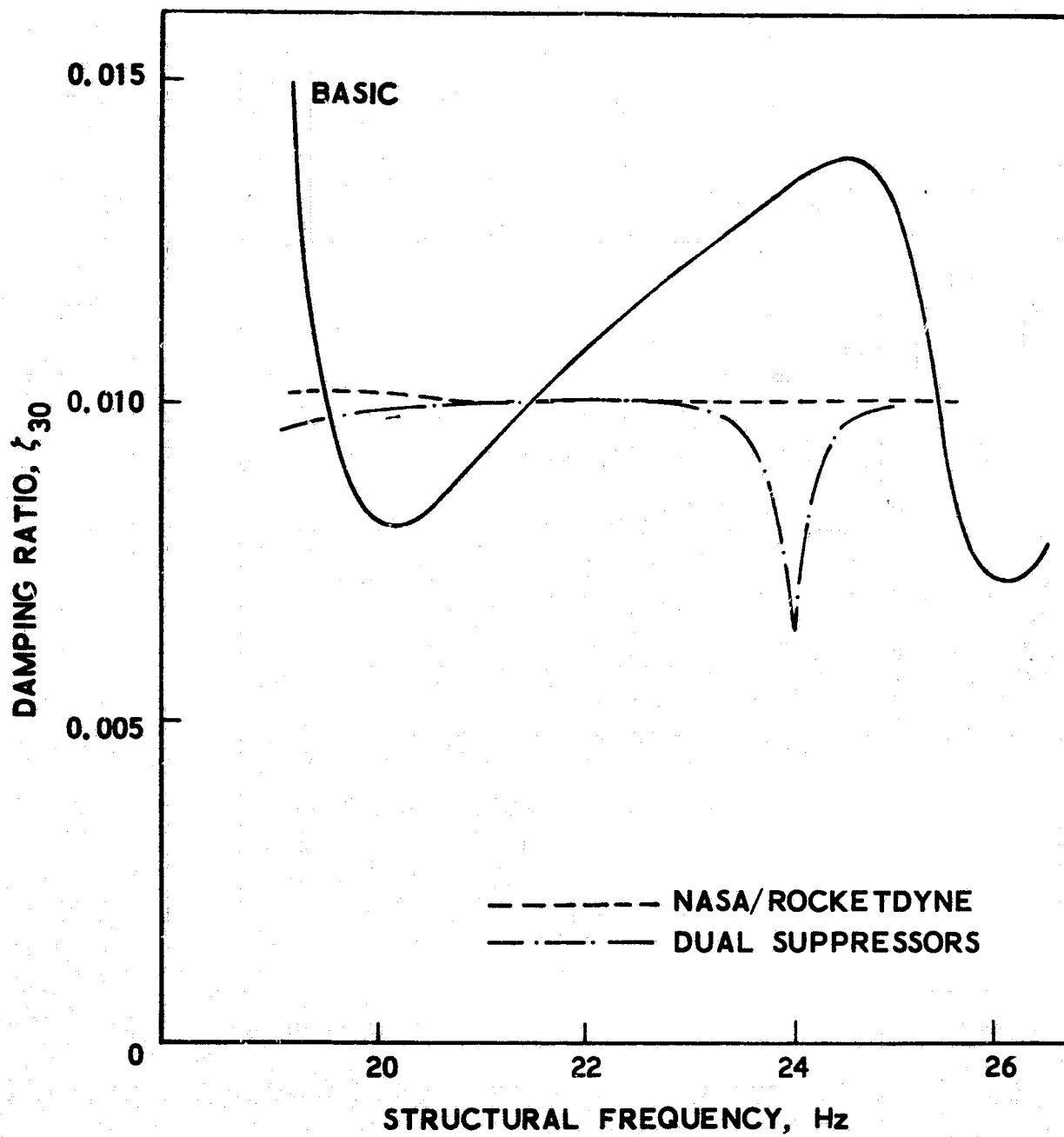
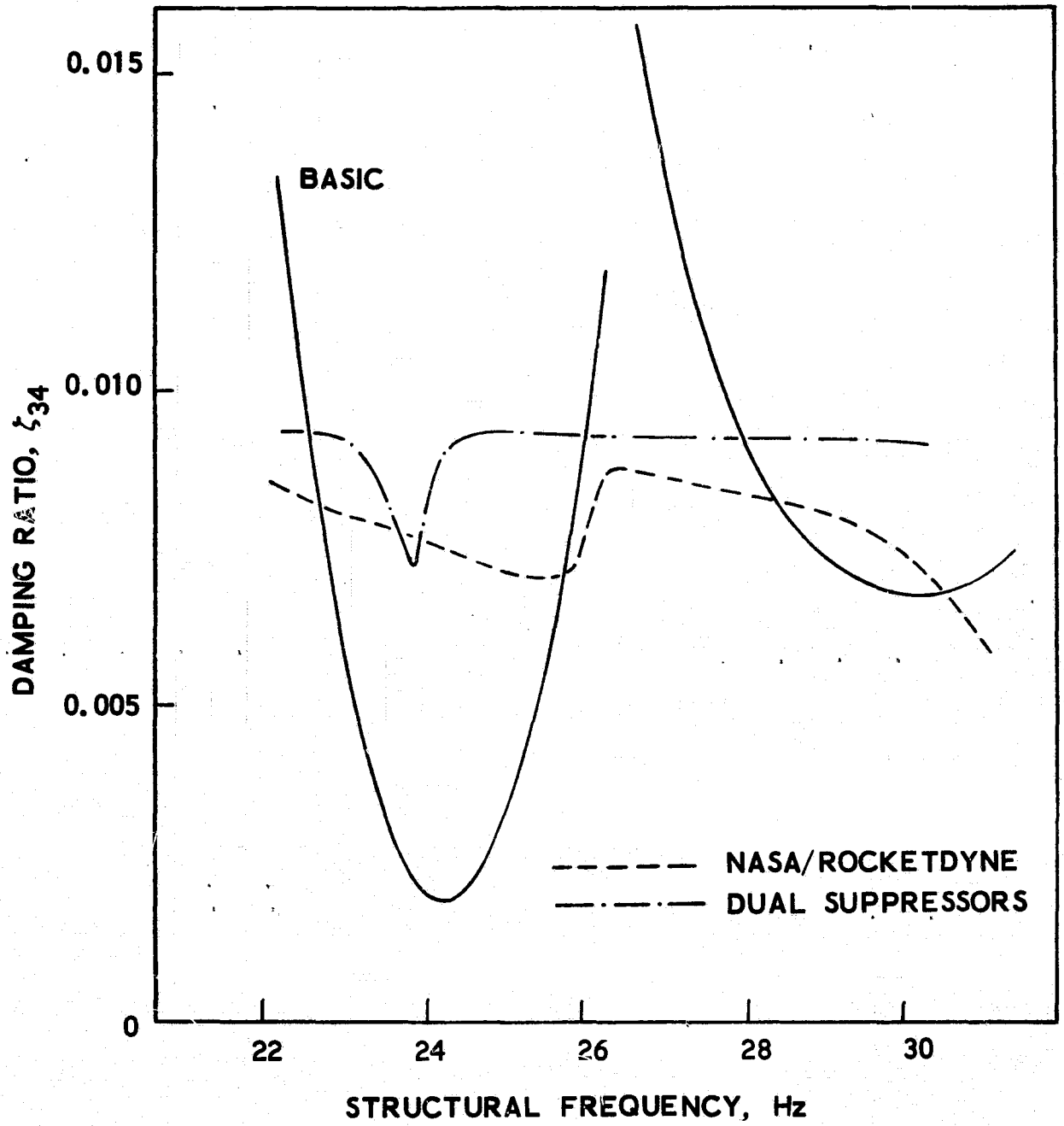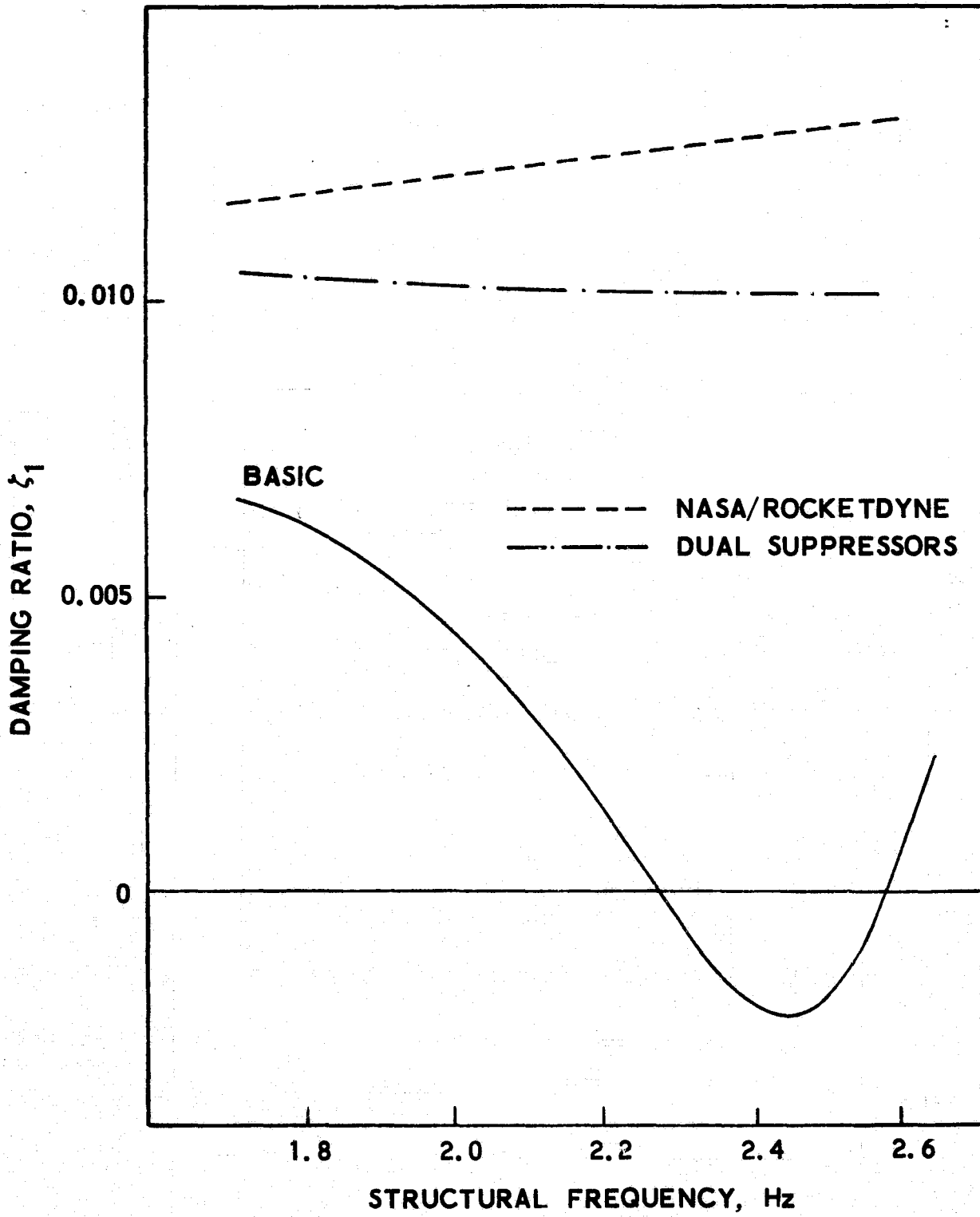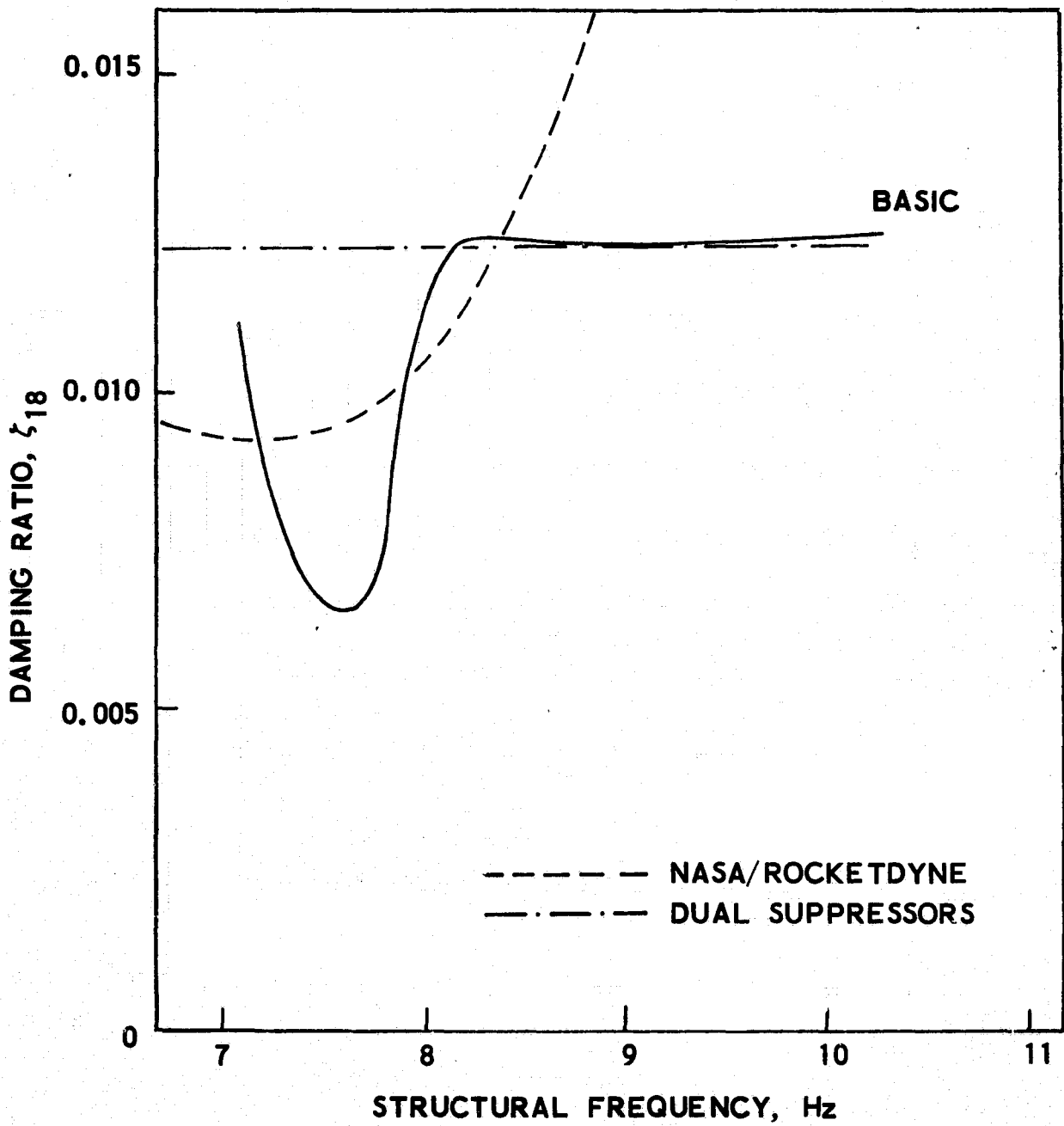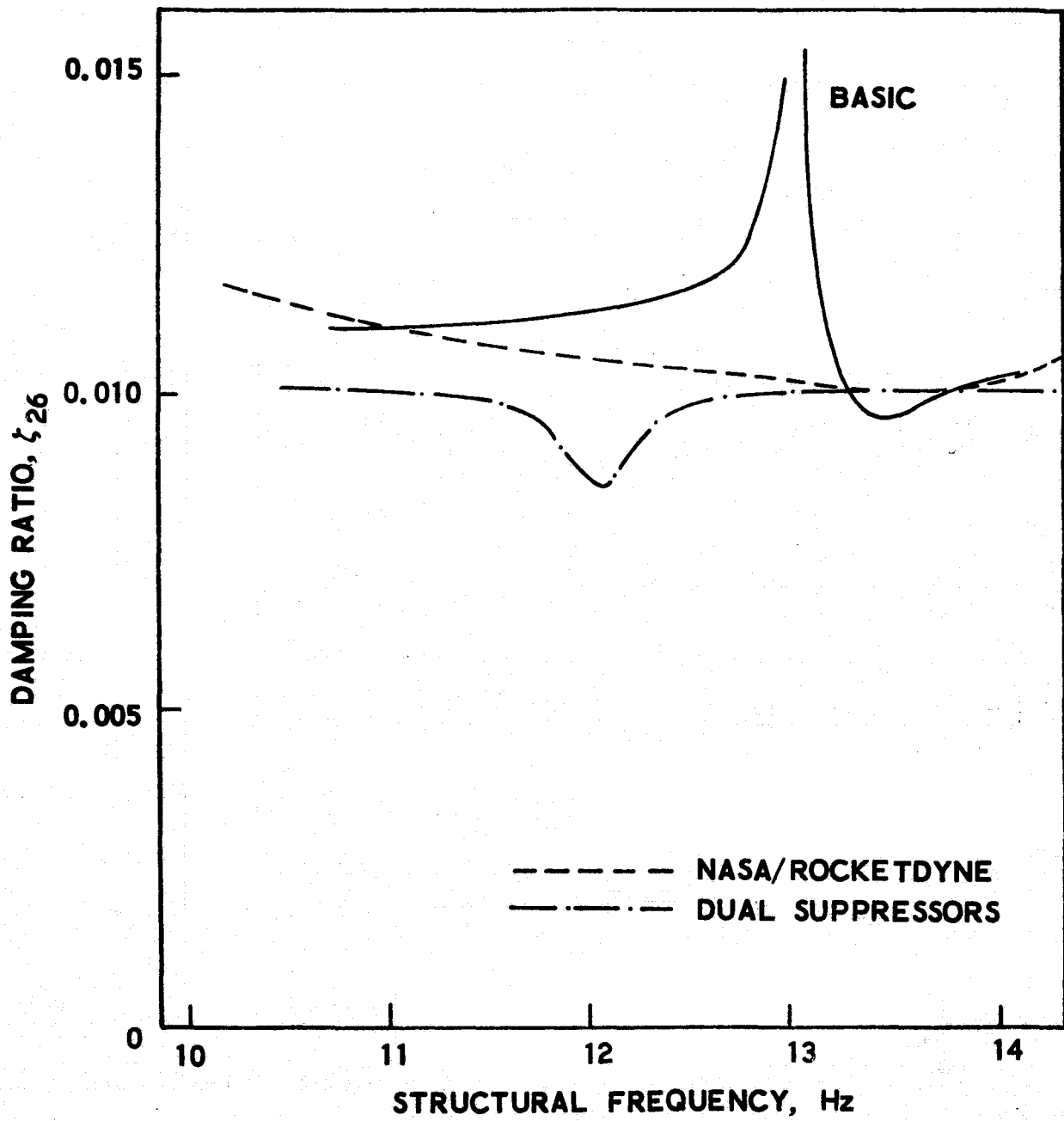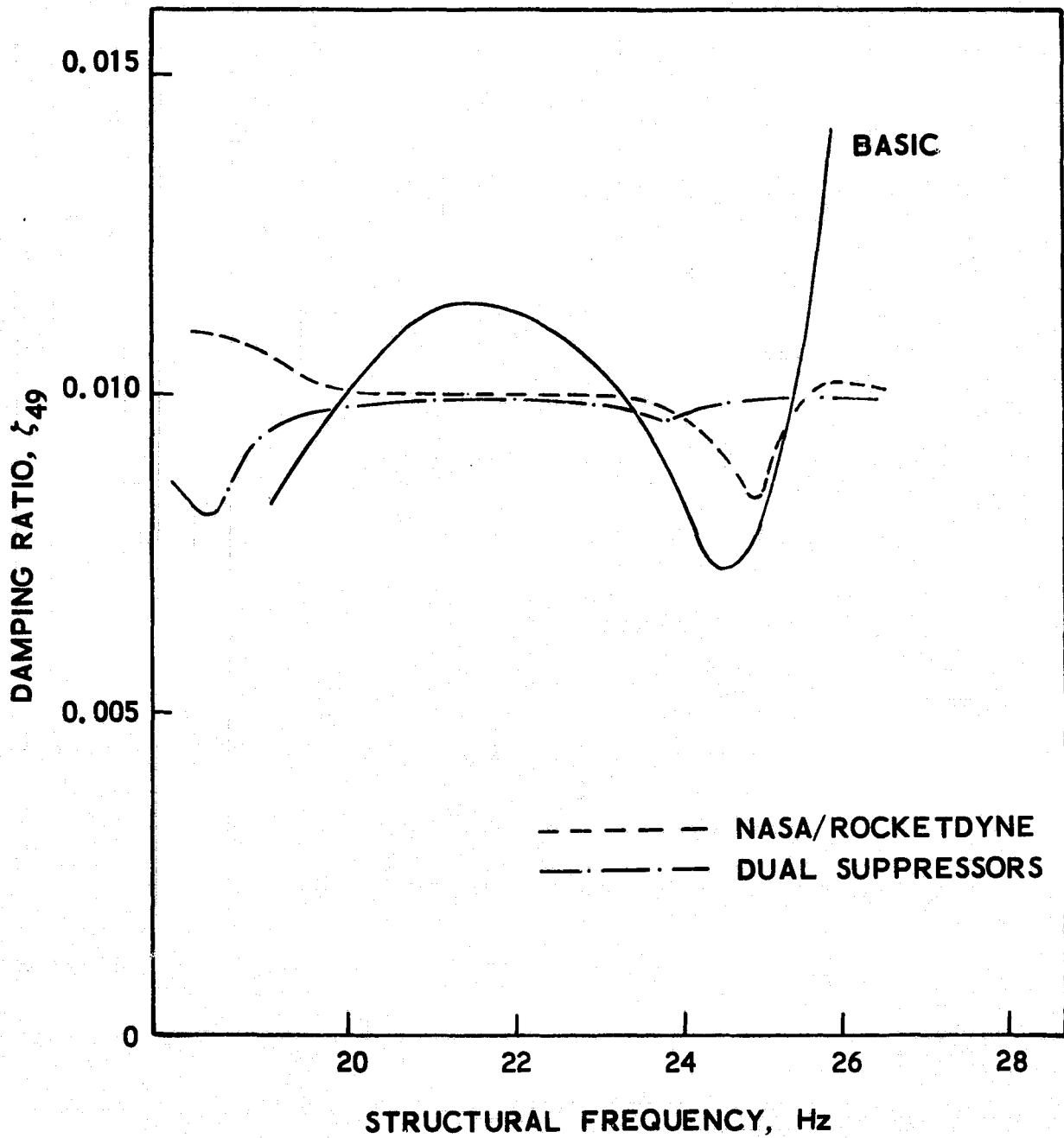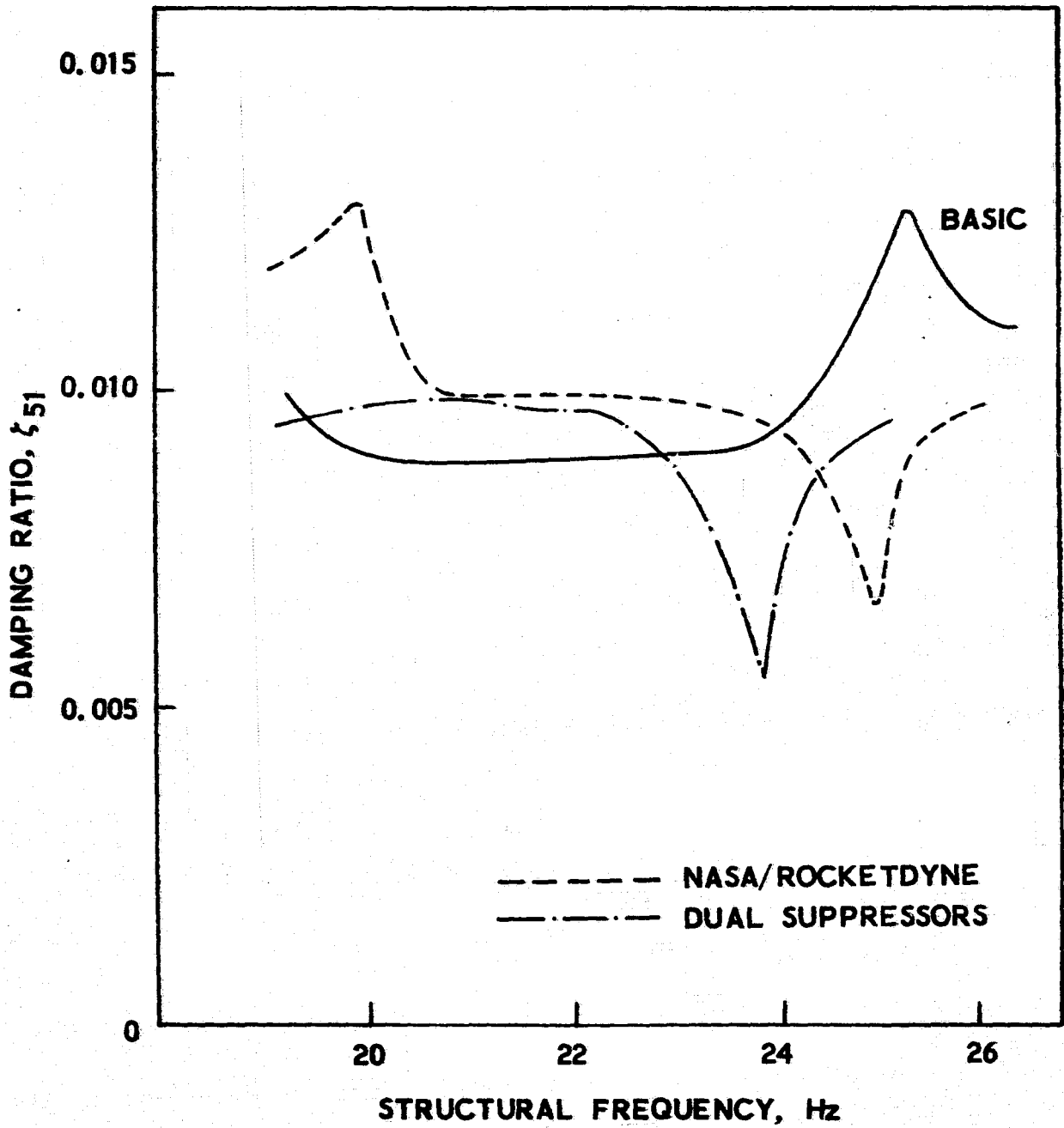Figure 21e. Stability Results with NASA Suppressor
Designs: Liftoff
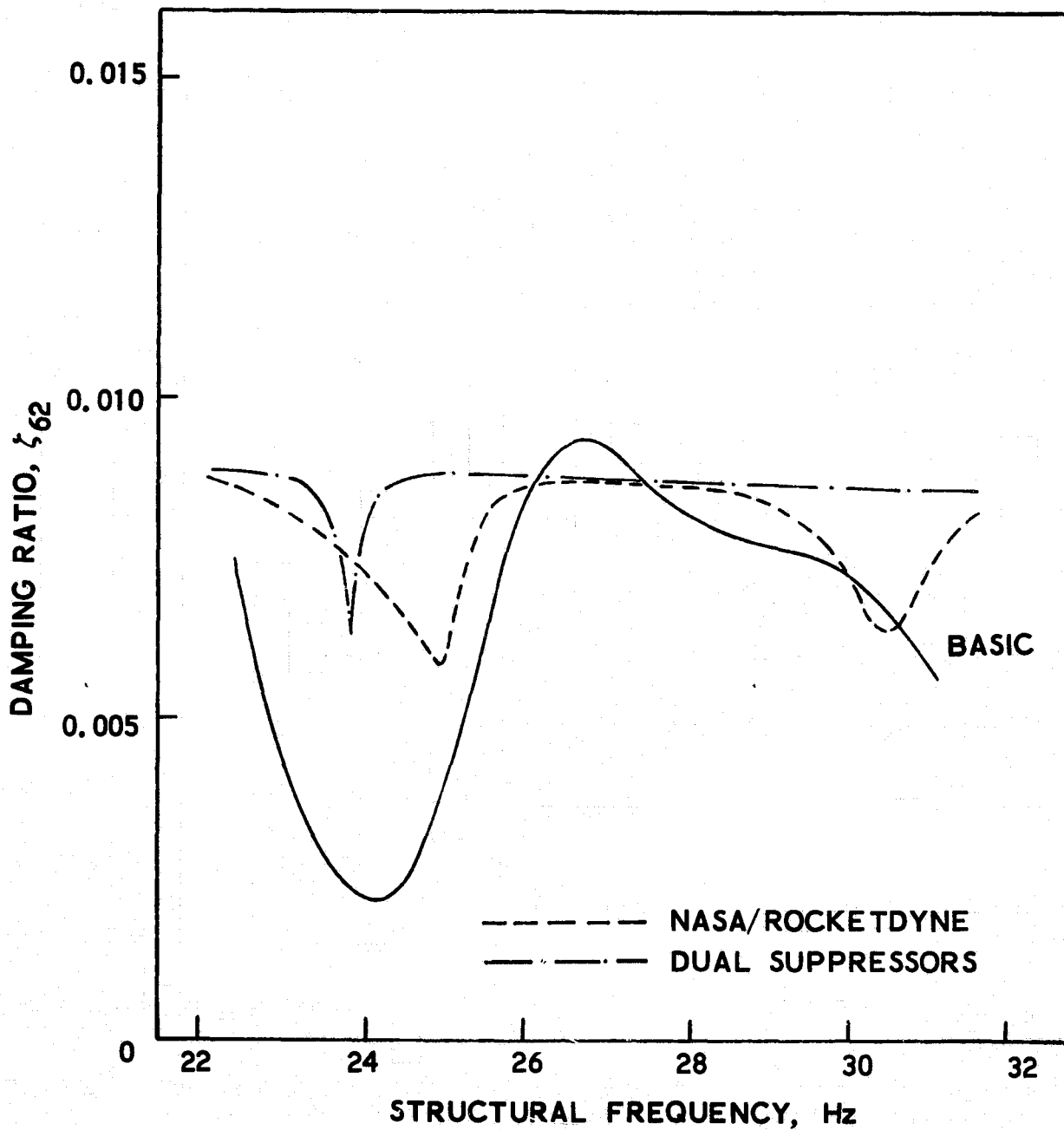
Figure 21f.　Stability Results with NASA Suppressor
Designs:　Liftoff
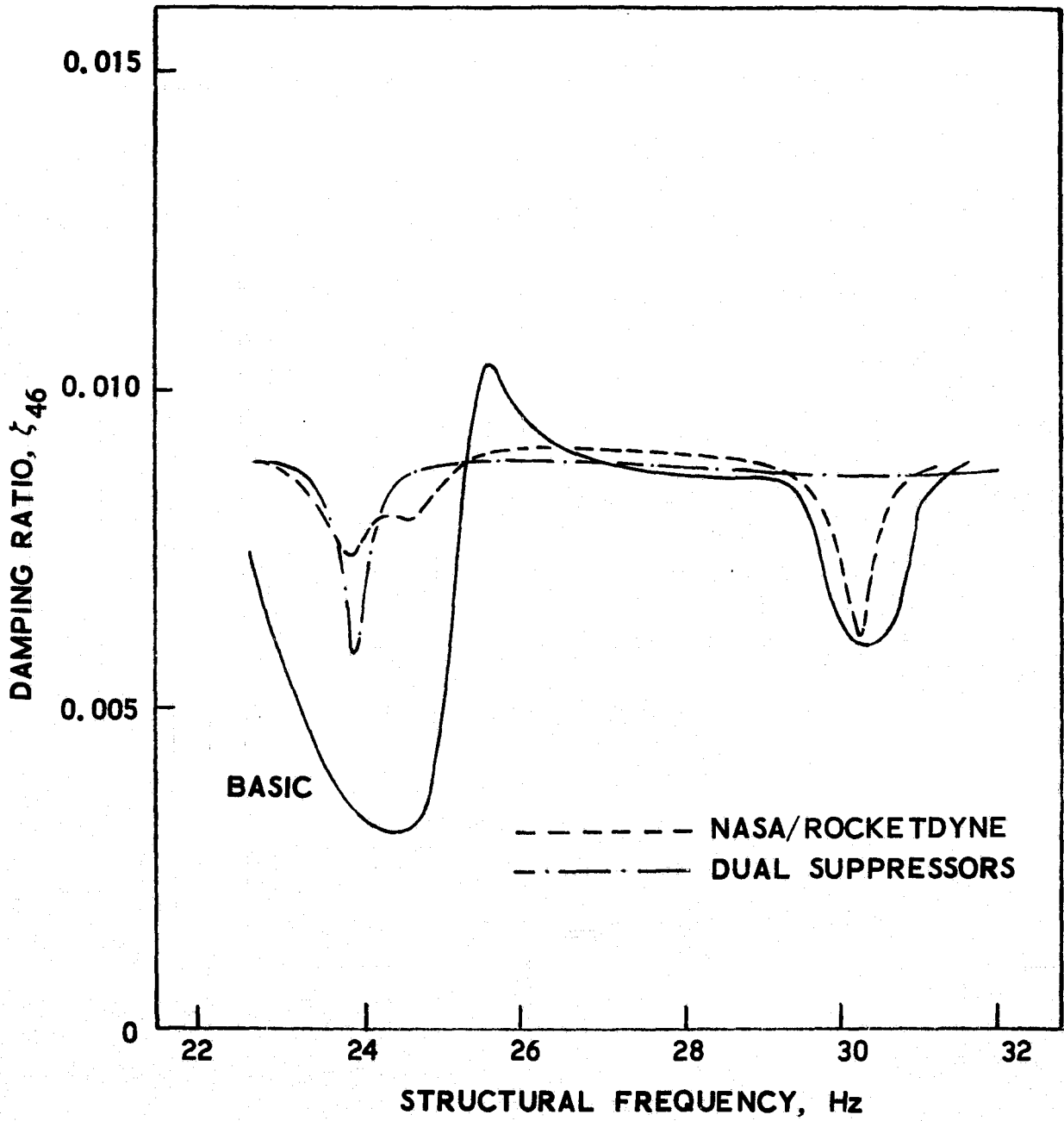
Figure 22. Stability Results with NASA Suppressor
Designs: After SRB Separation

and 0.0064. The damping ratios in the other modal cases at liftoff were maintained above a level of 0.008. For the additional A46 mode ($f \sim 27$ Hz) that was treated at the after-SRB-separation event, the results of the calculations (fig. 22) gave a minimum damping ratio of about 0.0062 for both the NASA/Rocketdyne and dual-suppressor systems.

Review of the results of the stability calculations for the two NASA (Lewis) designs shows that the designs are effective in eliminating the instabilities predicted for the basic system. In the fundamental-mode cases, the destabilizing influences of the propulsion system have been almost totally removed. In the higher modes the system damping ratios have again been maintained above the 0.005 level.

4.2 Comparison with Passive Suppressor Performance

The performance of the four active suppressor designs was next compared with the performance of a reference passive suppressor. The reference passive design was selected on the basis of the results of reference 2 and was taken to be a 0.057 m^3 (2 ft^3) compliant accumulator located at the HPOP inlet. Such a device had been found to provide satisfactory performance and was considered to be a representative passive design. The comparison was largely made on the basis of the minimum damping ratios exhibited with the suppressors over the specified frequency ranges used in the stability calculations. Detailed differences in the performance over these ranges was not considered important (e.g., differences in the variation of the damping ratios with structural mode frequency for a given case).

4.2.1 Aerospace Designs

Comparison of the stability curves calculated for the two Aerospace suppressor designs with the corresponding results for the compliant accumulator revealed very little difference in the performance of the different devices for the E1, E7 and E30 modes at end-burn, the L1, L18, L26, L49 and L51 modes at liftoff, and the A1 mode at the after-SRB-separation event. The differences in the performance in the higher frequency E34, E35, L62 and A46 modes ($f \sim 27$ Hz) are illustrated in figure 23. In these cases, the optimum suppressor design tended to give somewhat superior performance. However, the minimum damping ratios exhibited by the different designs are not greatly different - 0.0067 for the optimum design, u.0051 for the pressure feedback design, and 0.0055 for the compliant accumulator - so that all in all, the performance of these two active suppressor designs can be considered to be comparable to that of the passive device.

4.2.2 NASA (Lewis) Designs

The comparison made with the results for these designs indicated that the performance of the NASA/Rocketdyne suppressor was similar to that of the compliant accumulator for all the cases that were considered (see examples in fig. 24). The minimum damping ratio of 0.0059 calculated for this design compares

Figure 23a. Comparison of Aerospace Active-Suppressor
and Compliant-Accumulator Results:
Orbiter End-Burn

Figure 23b. Comparison of Aerospace Active-Suppressor
and Compliant-Accumulator Results:
Orbiter End-Burn

75

Figure 23c. Comparison of Aerospace Active-Suppressor
and Compliant-Accumulator Results: Liftoff
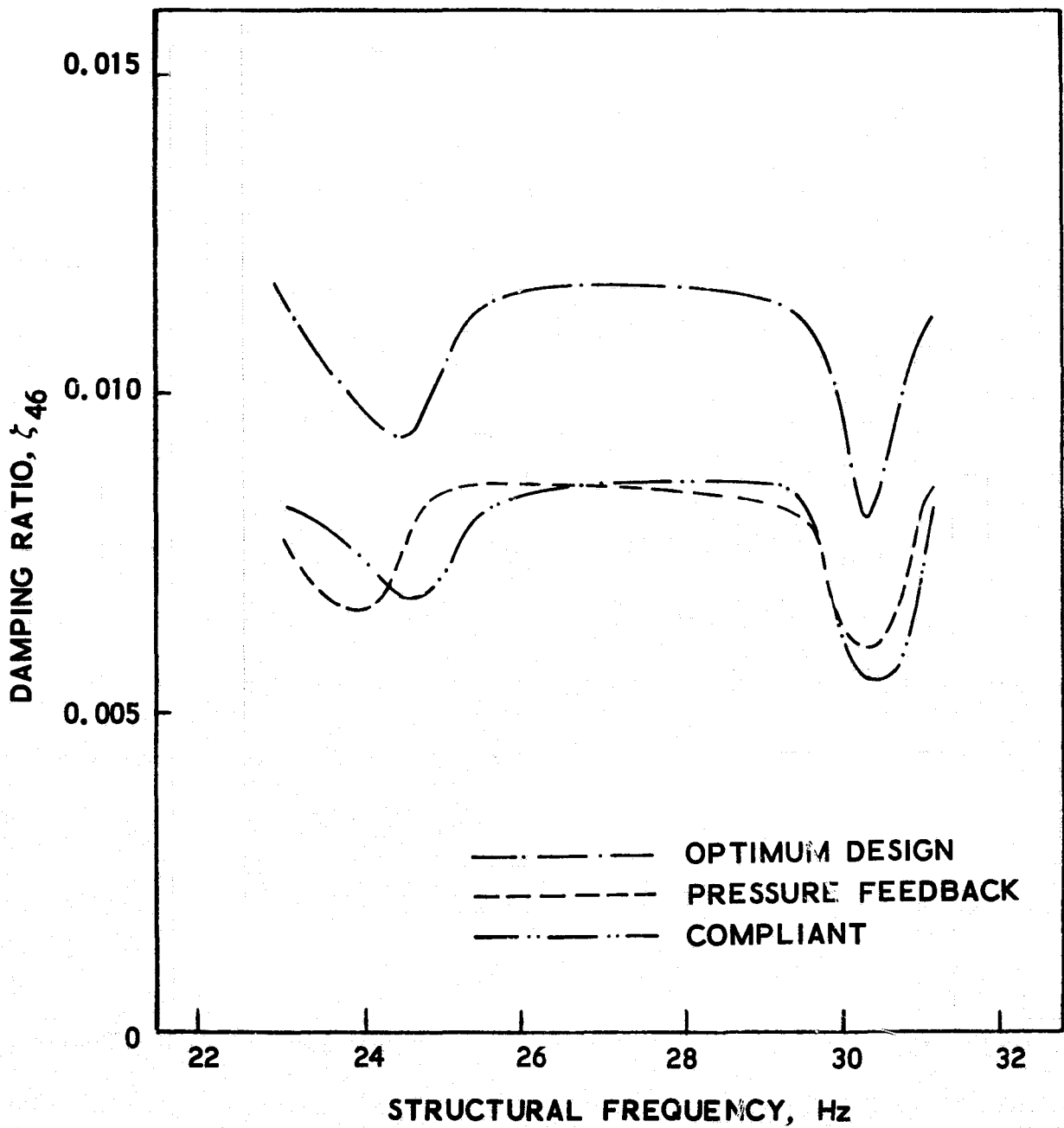
Figure 23d. Comparison of Aerospace Active-Suppressor
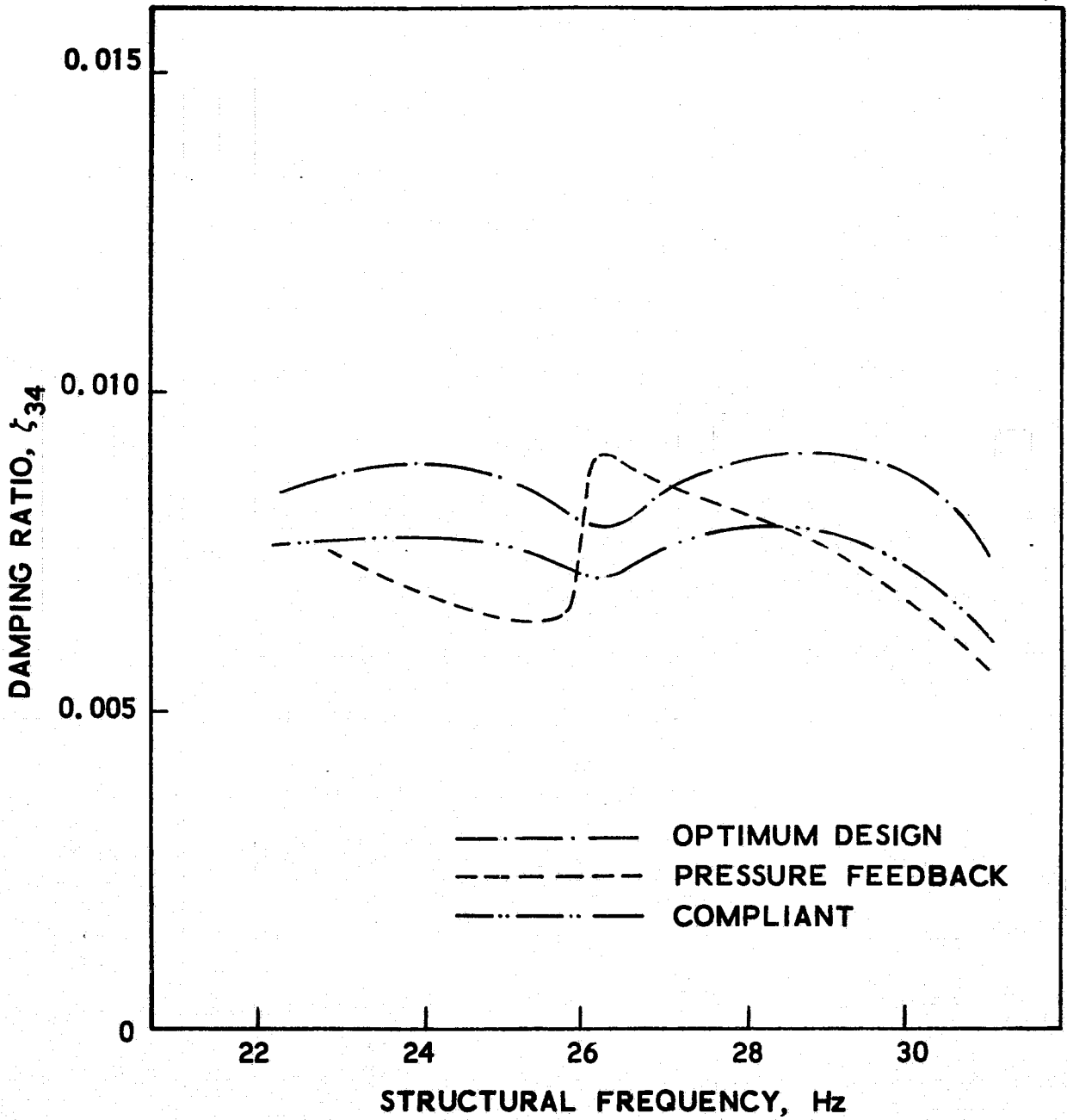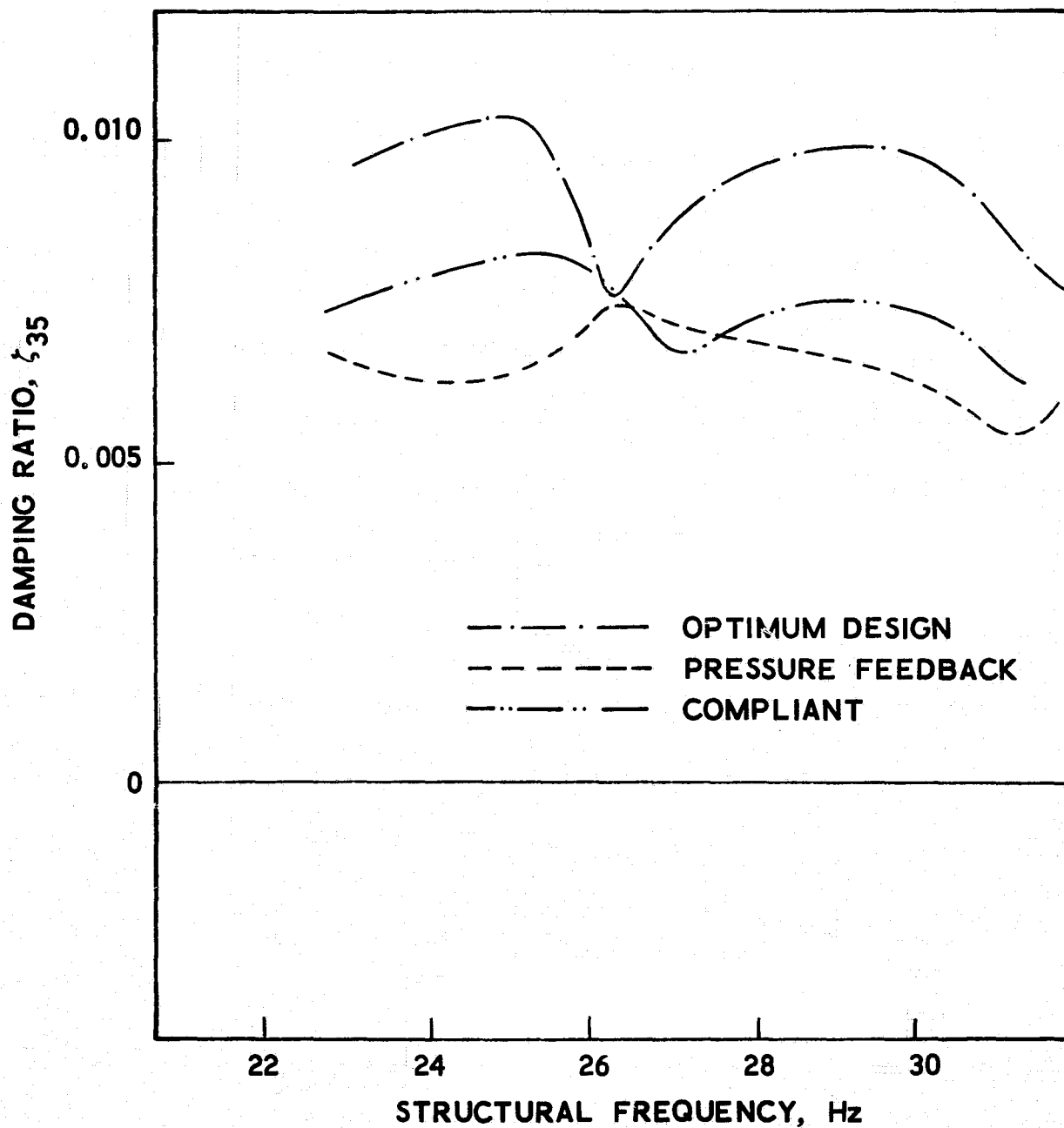and Compliant-Accumulator Results:
After SRB Separation
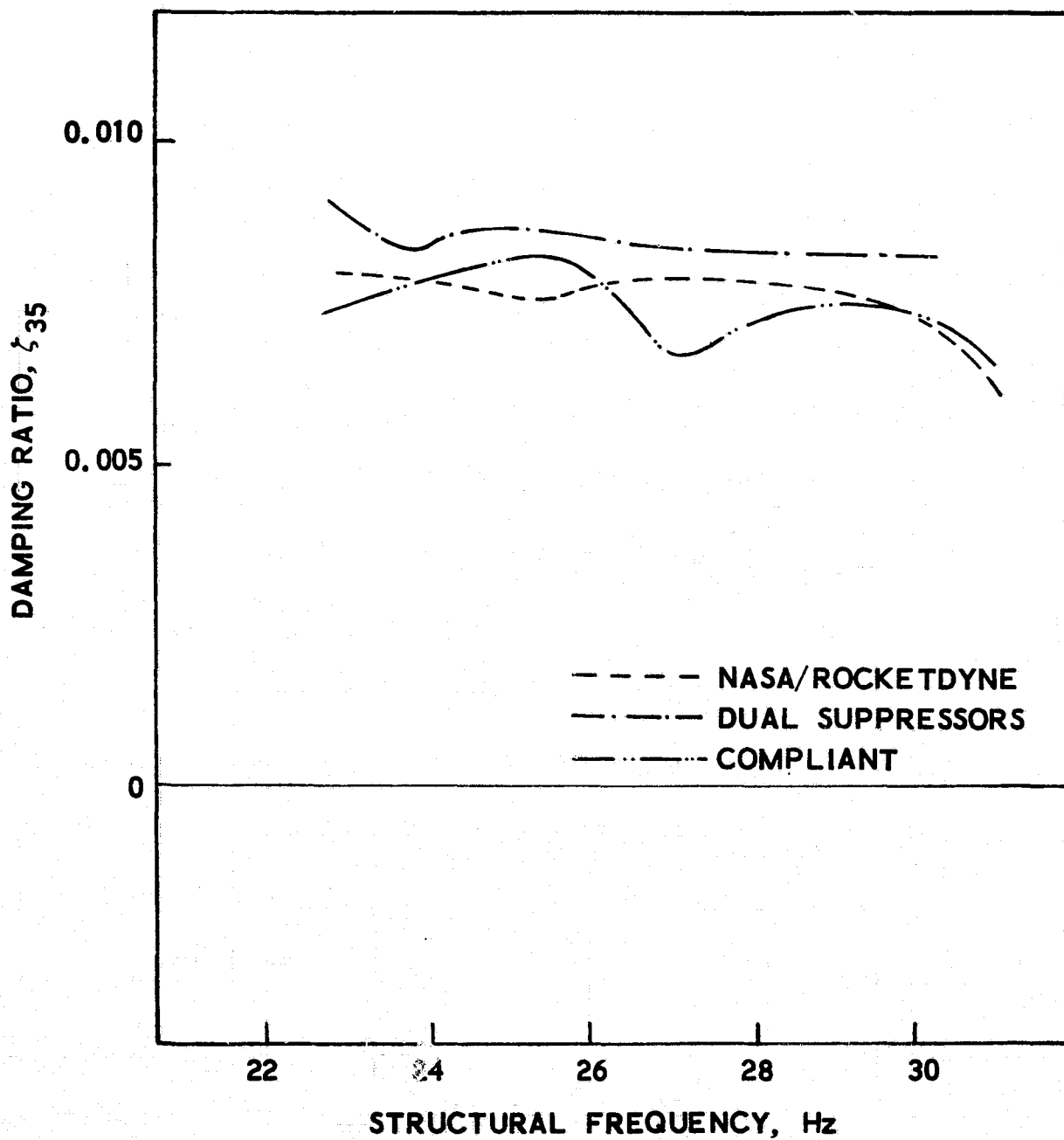
Figure 24a. Comparison of NASA Suppressor and Compliant-
Accumulator Results: Orbiter End-Burn

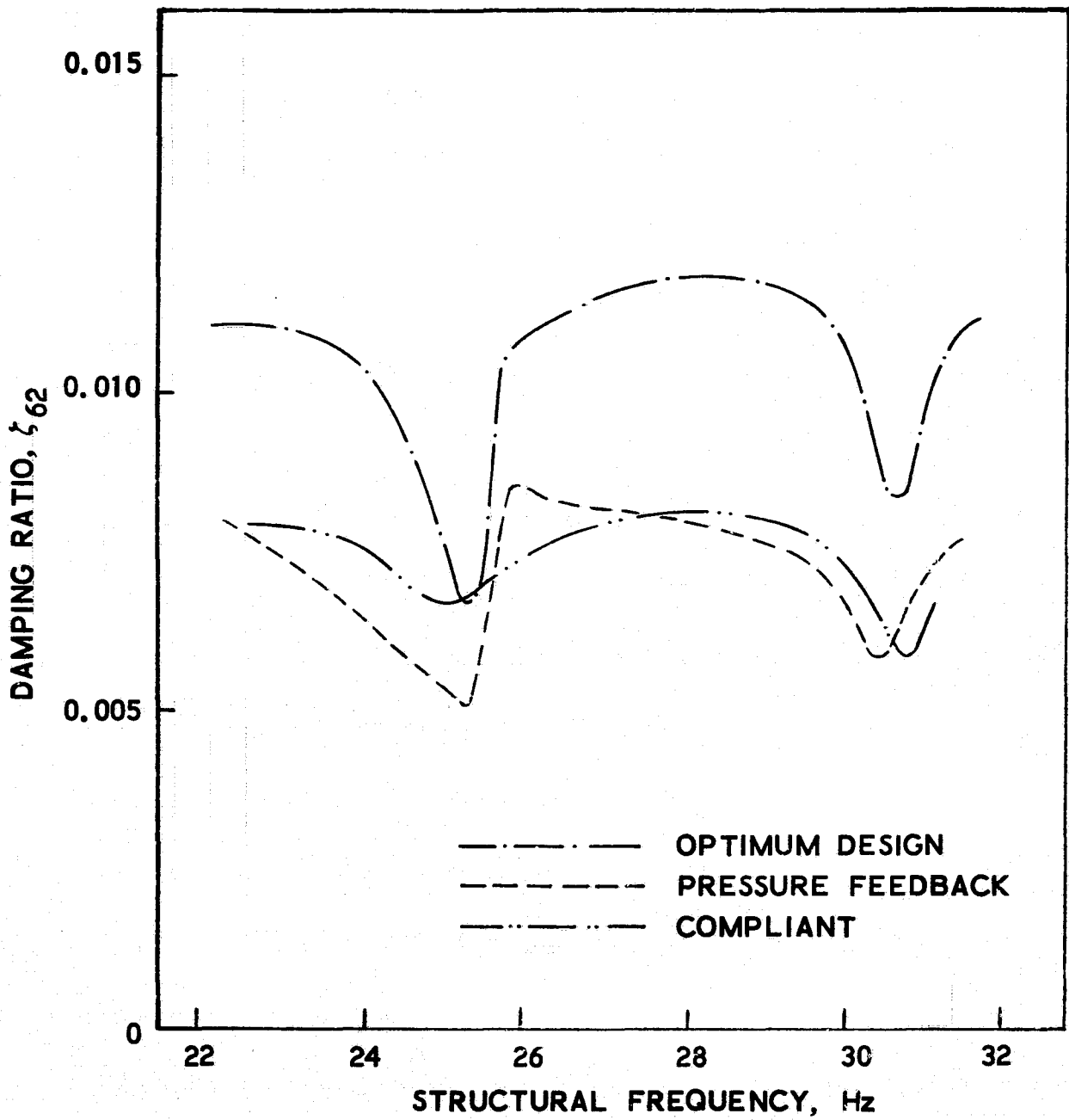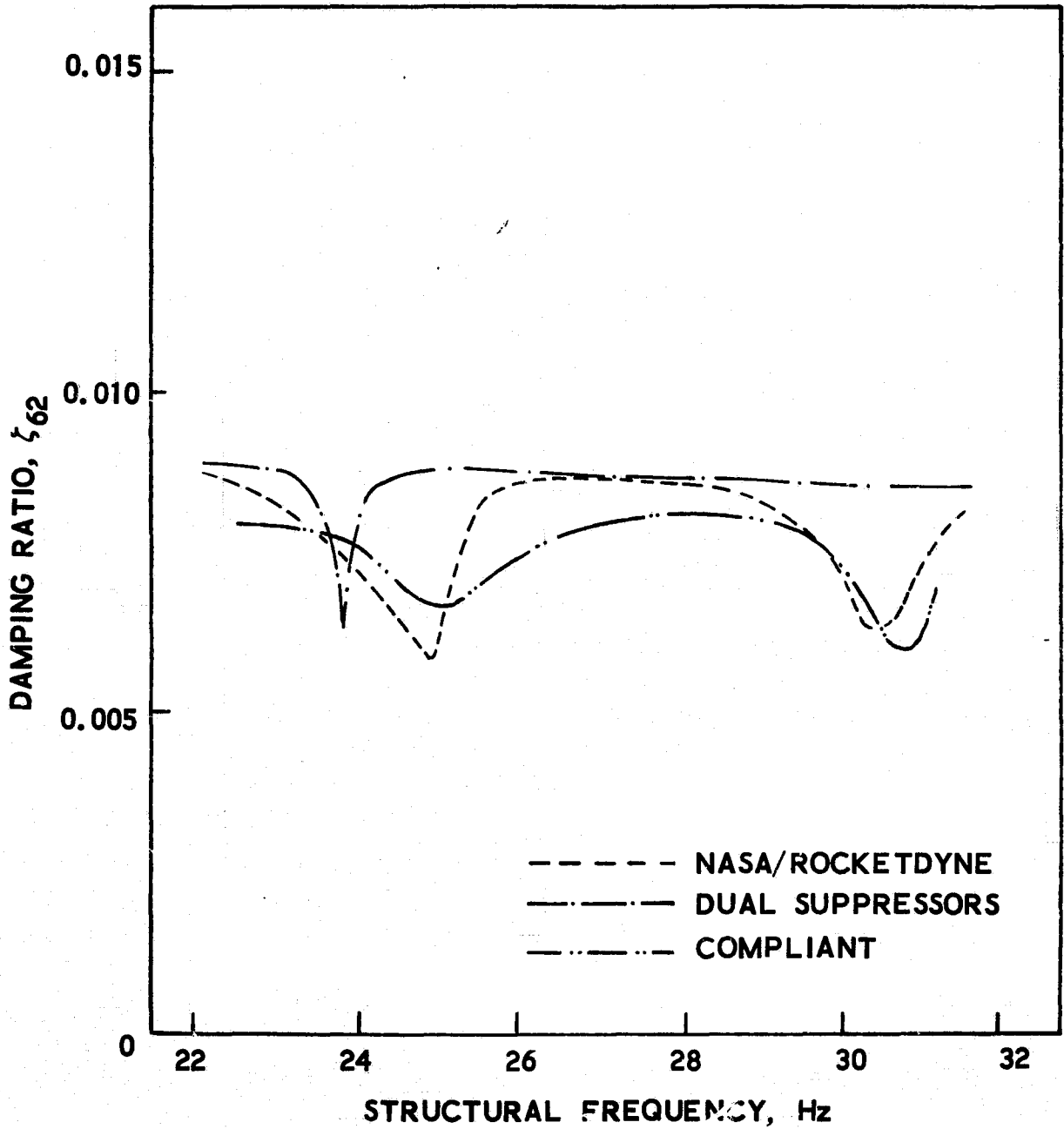Figure 24b. Comparison of NASA Suppressor and Compliant-
Accumulator Results: Liftoff
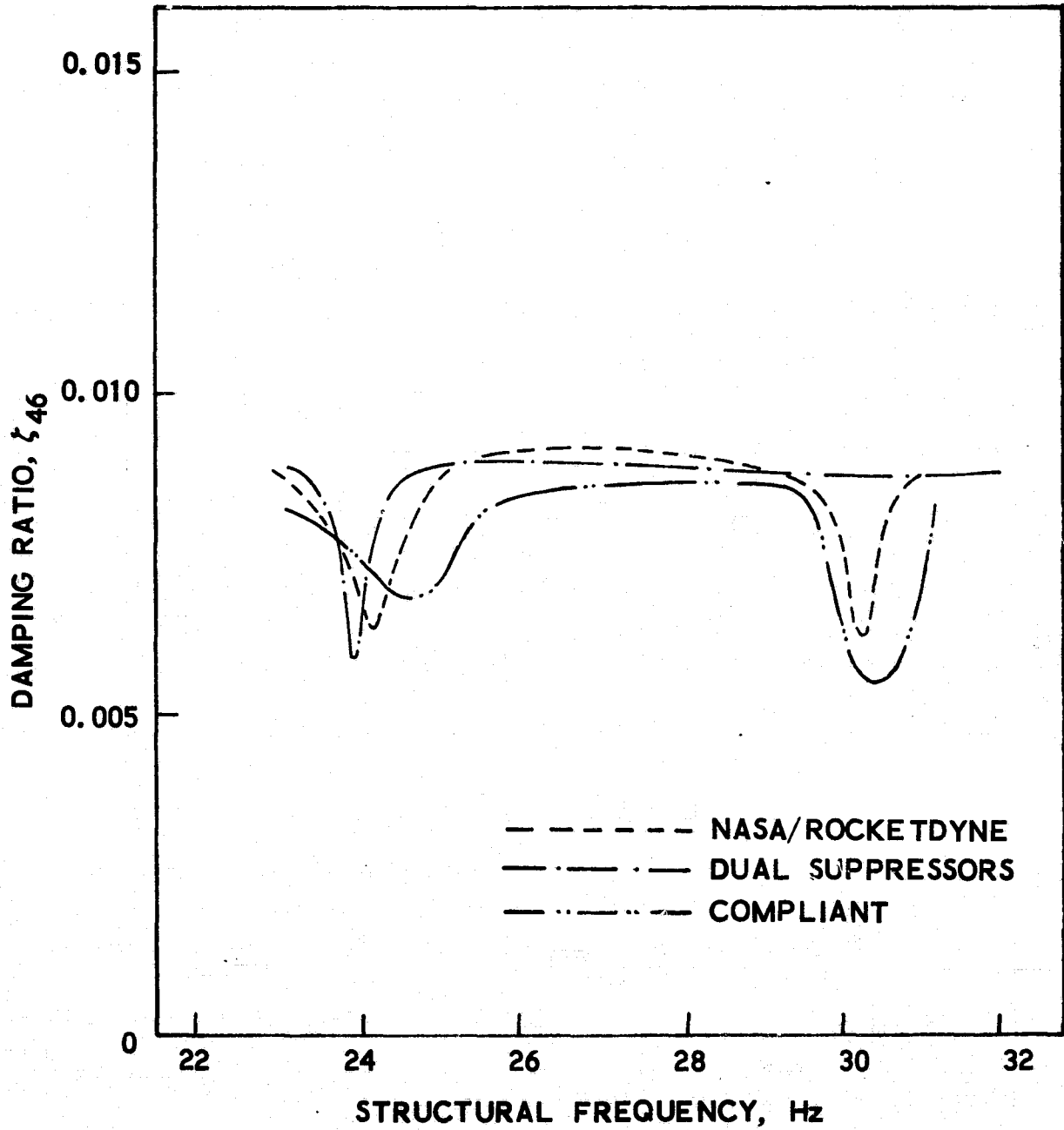
Figure 24c. Comparison of NASA Suppressor and Compliant-
Accumulator Results: After SRB Separation

with a level of 0.0055 calculated for the compliant accumulator. The performance of the dual-suppressor system, relative to the compliant device, would vary from case to case (see examples in fig. 24); however, the minimum damping ratio of 0.0053 calculated for this design was also very close to the corresponding compliant accumulator value of 0.0055. Thus, the performance of the two NASA (Lewis) suppressor designs can also be considered to be comparable to that of the compliant accumulator.

4.3 Sensitivity of Performance to Feedback Error

A limited check of the sensitivity of the performance of the active suppressors to errors in the feedback signals was made using the A1, A46, E34 and E35 stability cases. Nominal errors were taken to be ±15 percent on the magnitude of the signal and ±45-degrees error in the phase of the signal.

4.3.1 Aerospace Designs

In the case of the optimum design, it was found that imposition of the ±15 percent error in the magnitude of the sensed inlet pressure produced little significant change in the performance of this device in the A1 and A46 modes.

In the case of the E34 and E35 modes, there was a reduction in the performance of the device but the minimum damping ratios were still maintained above the 0.005 level. In contrast to the relatively minor degradation in the performance of the suppressor due to errors in the pressure feedback, the imposition of the same percentage errors to the relative flow feedback $(Q_7 - A_3\dot{z}_7)$ provided dramatic changes in the performance of the device. In the case of the A1 mode, the ±15 percent error introduced an unstable condition with damping ratios as low as -0.08. In the E34 and E35 modes the ±15 percent error introduced instabilities with damping ratios down to the -0.004 level. In view of this dramatic change, the variation of the minimum damping ratio with feedback error was investigated for a broader range of error. The results indicated that the performance of the optimum design was extremely sensitive to error in the relative flow feedback. This sensitivity is illustrated in figure 25 where the results for the E35 mode are presented. In the figure it is seen that the performance of this suppressor is degraded markedly by either positive or negative percentage errors in the flow feedback. It may be noted that the sharp break in the curve that appears near the zero error condition results from a change in the critical branch of the calculated damping curves.

In the case of the pressure-feedback design, the performance of the design was found to be insensitive to the imposition of the specified errors in magnitude and phase. This lack of sensitivity is illustrated in figure 26 where the minimum calculated damping ratios are presented as a function of feedback error for the A1 and E35 mode cases.

4.3.2 NASA (Lewis) Designs

The sensitivity of the performance of the NASA/Rocketdyne design to error in the magnitude and phase of both the pressure and the motion feedback signals was checked. The performance of the design proved to be

81
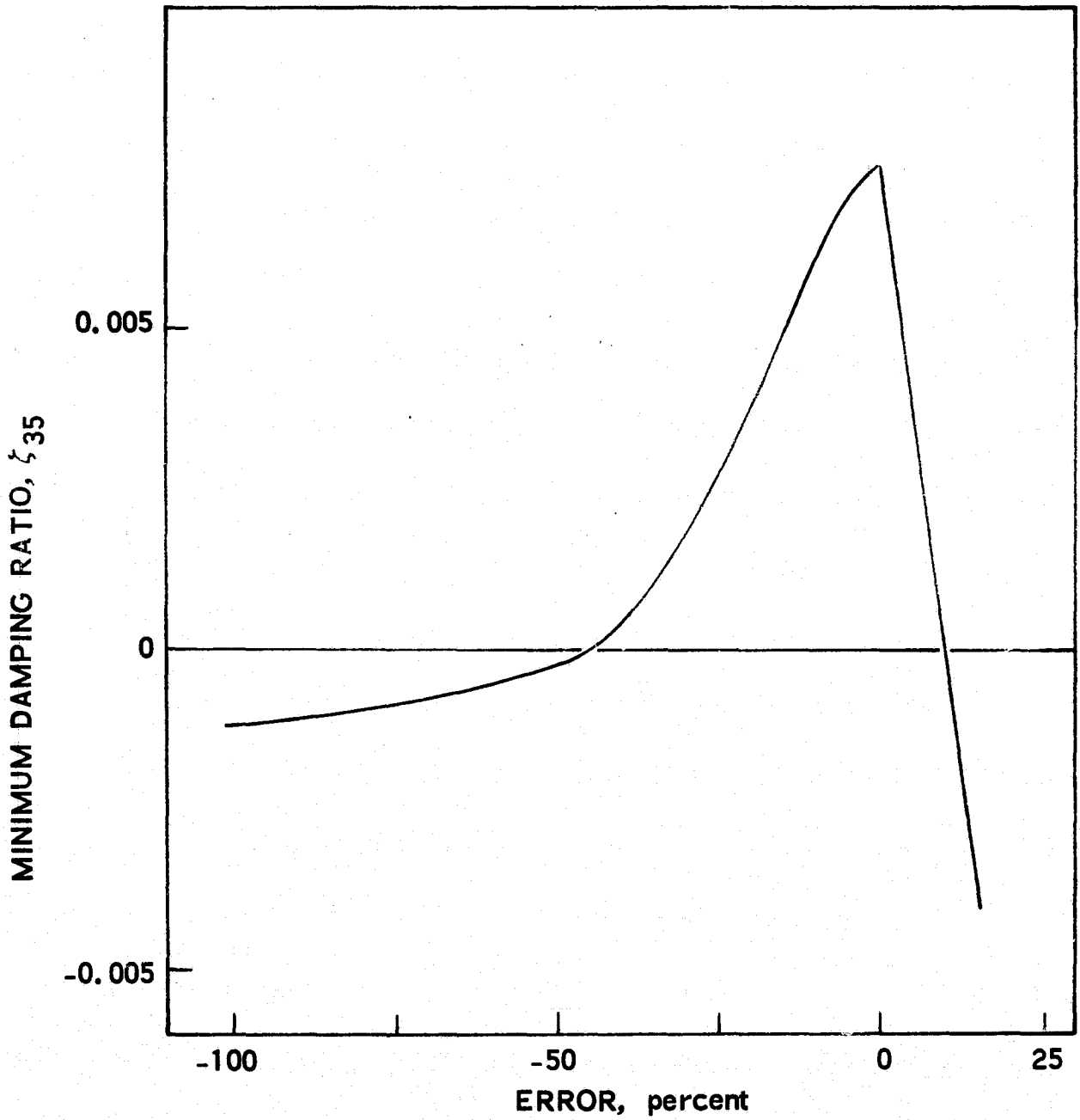
Figure 25.   Effect of Relative-Flow Feedback Error on
Aerospace Optimum Design
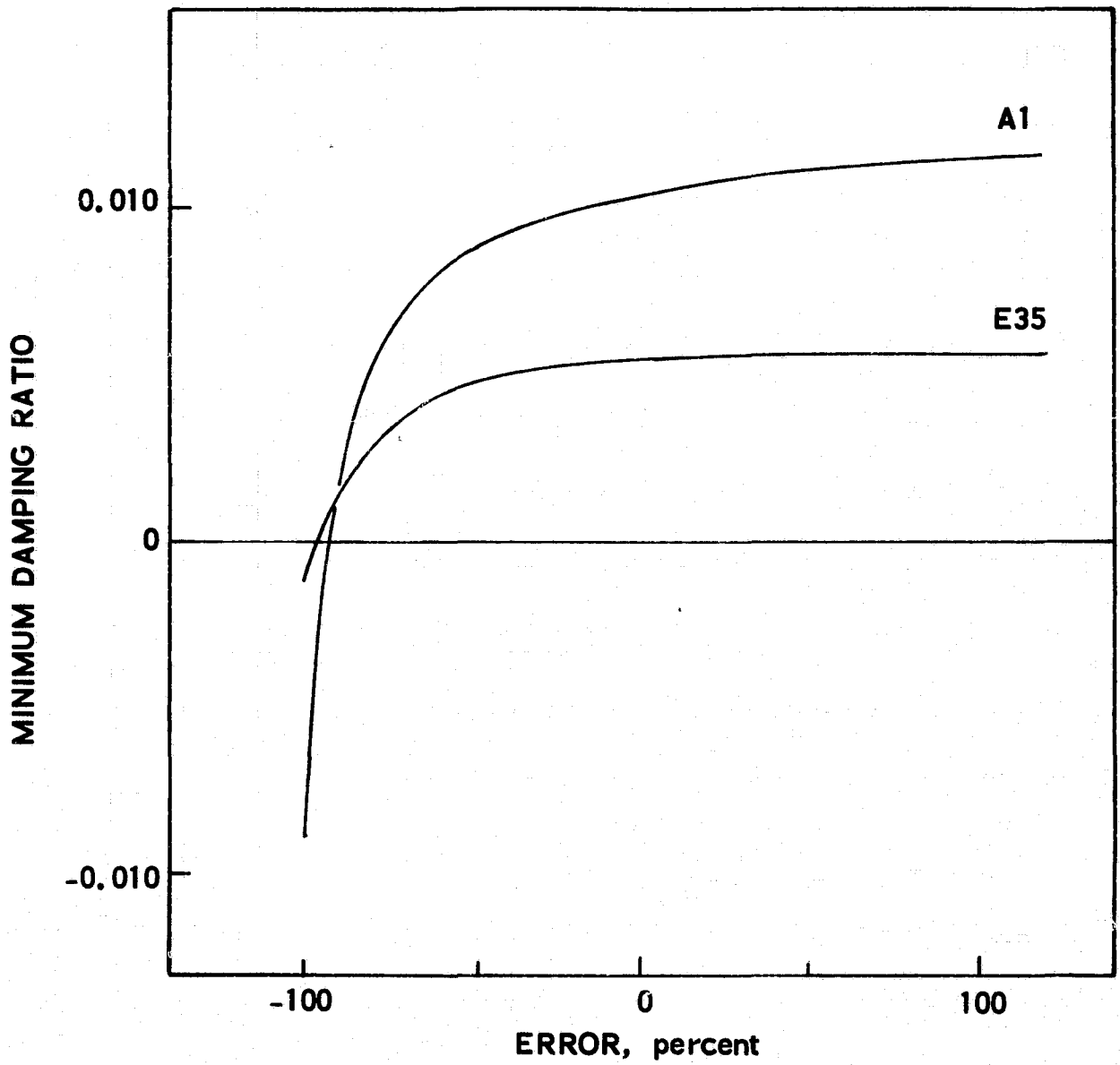
Figure 26a.   Effect of Feedback Error on Aerospace
             Pressure-Feedback Design

83
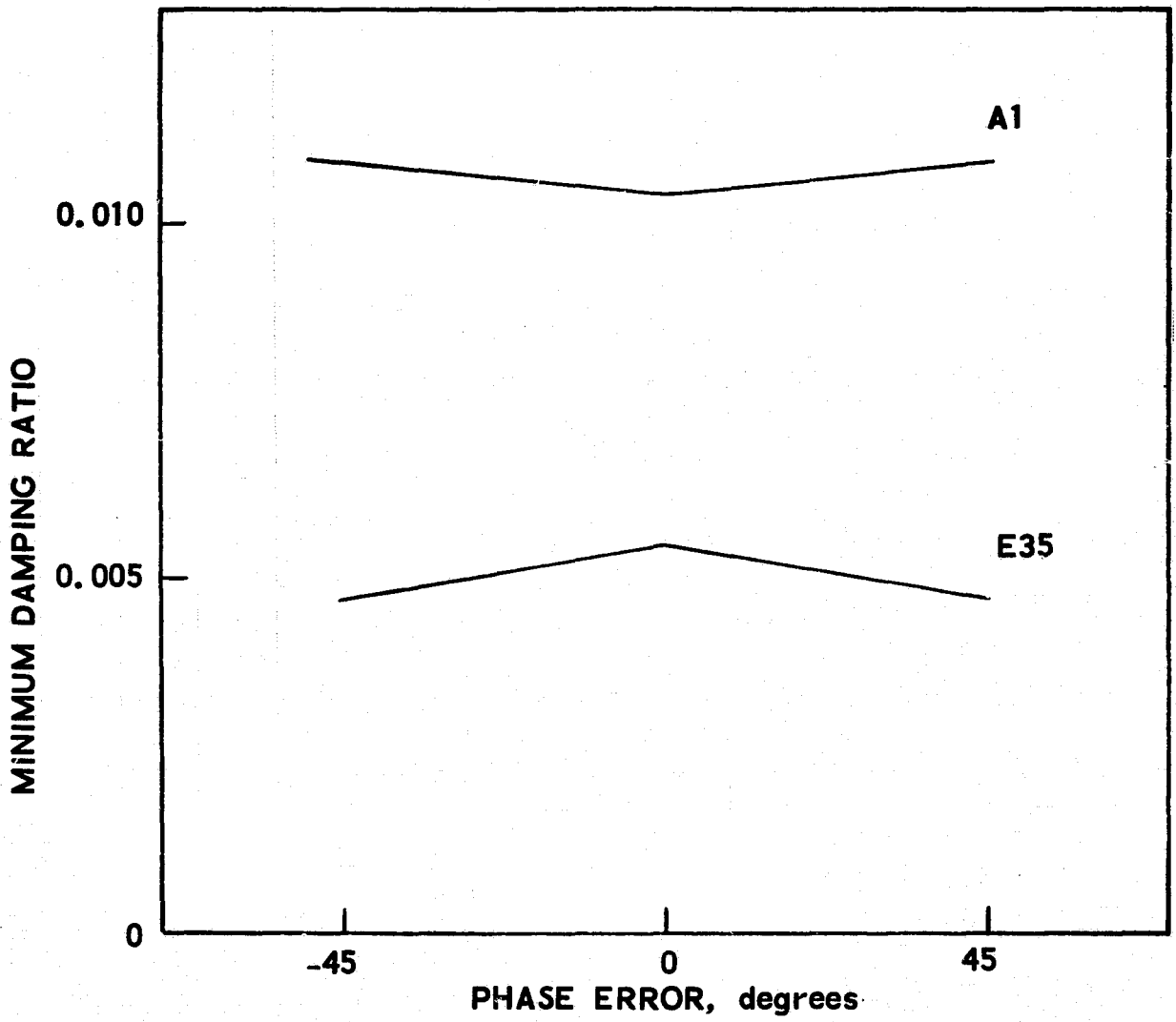
Figure 26b.   Effect of Feedback Error on Aerospace
Pressure-Feedback Design

insensitive to the specified errors in these terms (fig. 27). The same lack of sensitivity was also found for the dual-suppressor design when the effect of errors in the pressure feedback to the HPOP device was checked.

4.4 Suppressor Volume Flow Requirements

In practice the capability of the active suppressors to respond to oscillations in the structural/propulsion system will be limited by constraints imposed by the suppressor design, e.g., hydraulic flow limitations and mechanical stops. Since the suppressor will be exposed to a background "noise" environment, it is essential that the design of the suppressor be such that the capacity of the device is not exceeded by the response to this noise. This response thus provides a lower bound on the volume flow capability required of the device.[*] To provide illustrative estimates of such bounds for the present study it was assumed that a representative measure of the system noise response was provided by the peak engine acceleration level of 0.25 g (along the longitudinal axis) that was specified in the Shuttle engine interface requirements. This level was viewed as an extreme value that would be appropriate for use at the lower frequencies of the system.

4.4.1 Aerospace Designs

The results of the stability analyses indicated that the response in the fundamental mode of the system provided the most severe size requirement for the active suppressors. For both the optimum and pressure feedback designs, it was found that the suppressor flow rate per unit longitudinal engine acceleration in this mode was

$$Q_a / \ddot{x}_e \approx 0.0032 \text{ m}^2 \text{ sec } (5 \text{ in.}^2 \text{ sec})$$

Substitution of the assumed response level of 0.25 g results in an estimated suppressor flow rate of 0.0079 m^3/sec (482 in.^{3}/sec). This value represents a minimum flow rate which the suppressors must accommodate if they are to be effective. The flow rate, which is associated with the fundamental-mode response, can be converted to suppressor volume requirements (i.e., suppressor-stroke and area) when the fundamental-mode frequencies are specified. Such a conversion will be illustrated in the following section when the NASA (Lewis) designs are discussed. In addition to the suppressor size estimates, the flow rate can also be employed to estimate the hydraulic flow requirements that would be necessary to operate the device. Such estimates require detailed knowledge of the suppressor design and are out of the scope of the present study.

---

[*]A similar requirement applies to passive suppressors; however, for the devices being considered for the Space Shuttle it was found that this requirement was overshadowed by the need to maintain fluid within the suppressor during transient operating conditions.
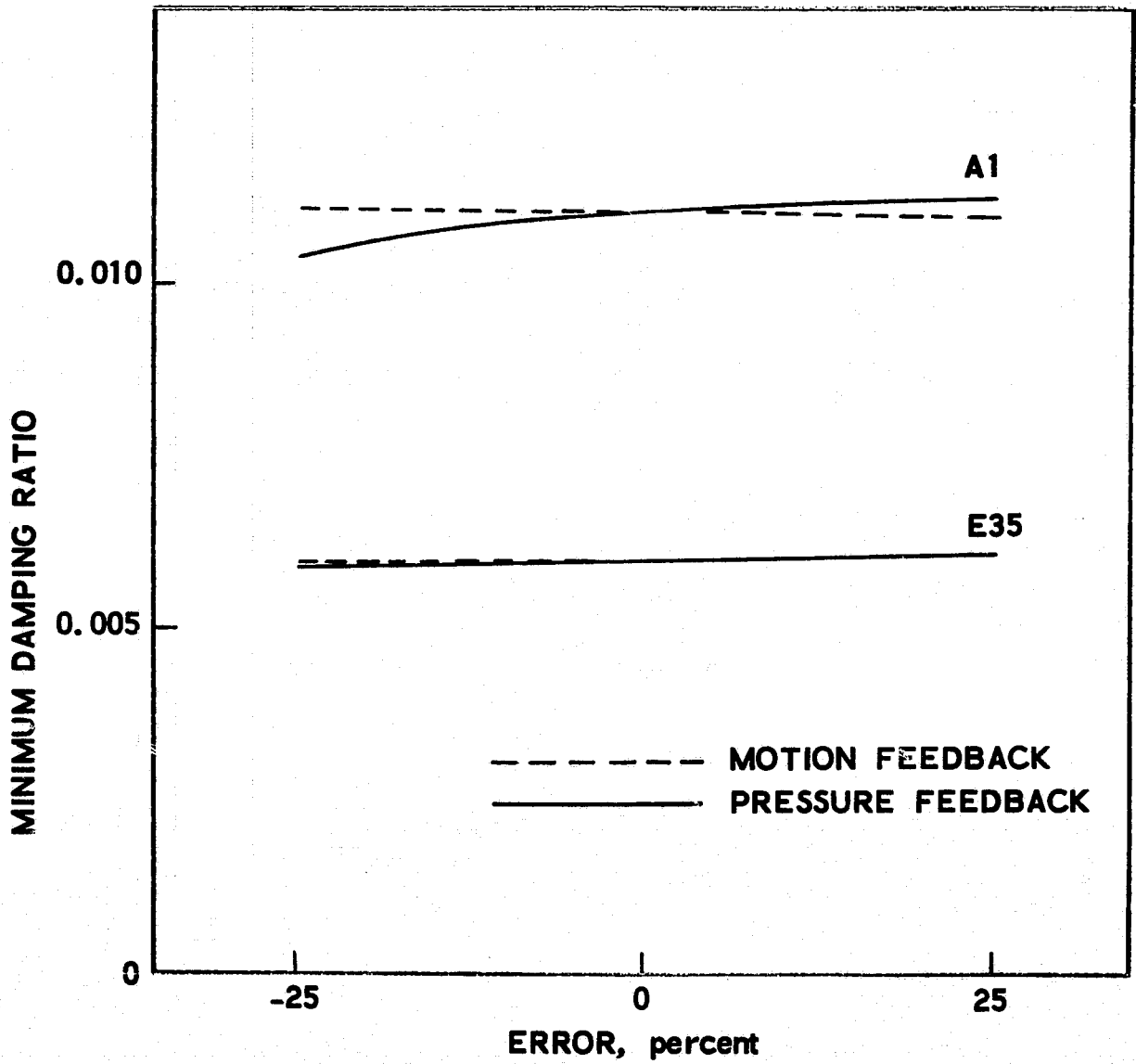
Figure 27a. Effect of Feedback Error on
NASA/Rocketdyne Design
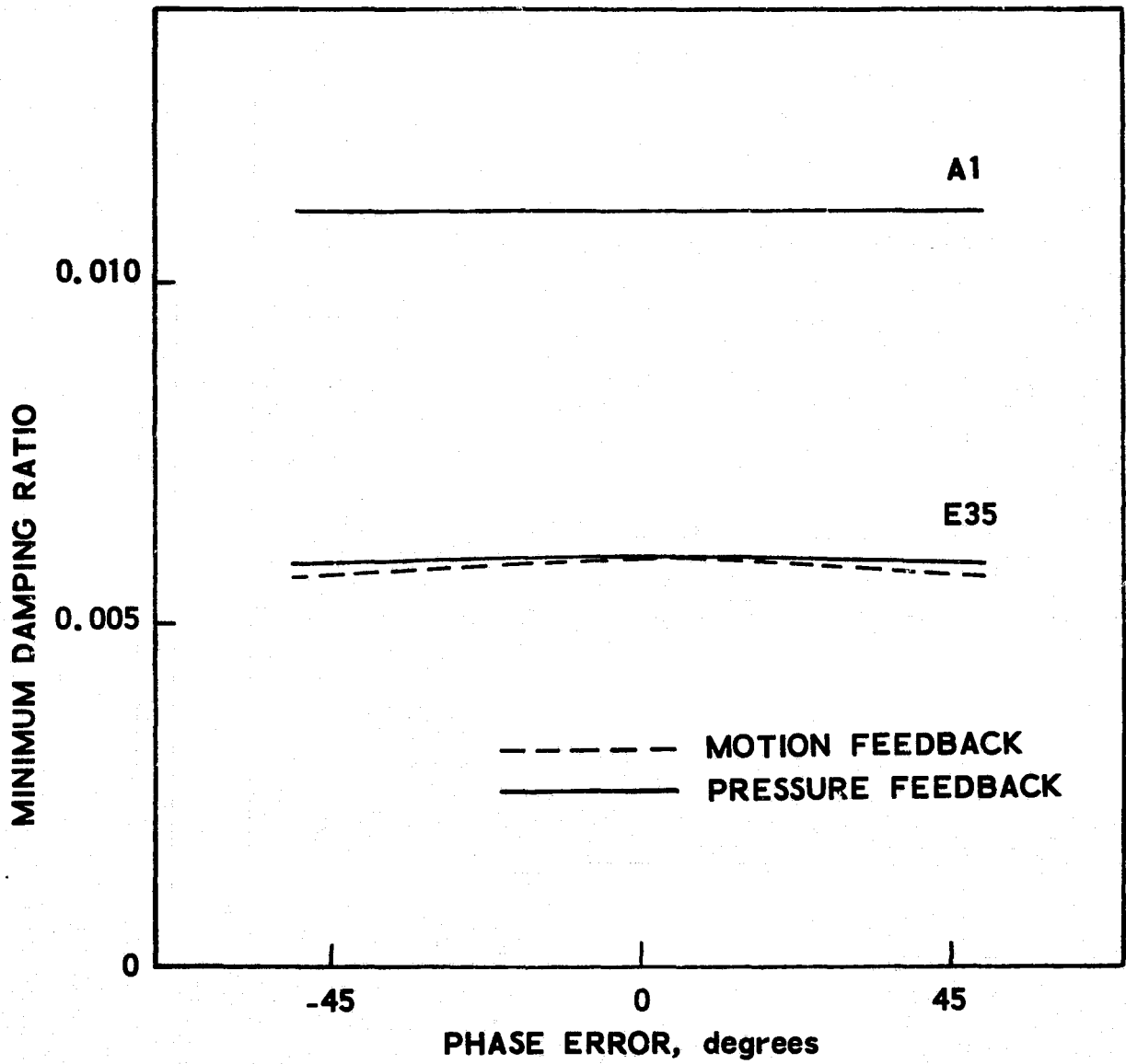
Figure 27b. Effect of Feedback Error on
NASA/Rocketdyne Design

4.4.2 NASA (Lewis) Designs

The results of the stability analyses for the NASA (Lewis) designs also indicated that response in the fundamental modes provided the governing conditions insofar as the suppressor size requirements were concerned. For the NASA/Rocketdyne design, the estimated flow rate per unit longitudinal acceleration of the engine in the fundamental mode was essentially the same as for the Aerospace designs.

$$Q_a/\ddot{x}_e \approx 0.0032 \text{ m}^2 \text{ sec } (5 \text{ in.}^2 \text{ sec})$$

For the dual-suppressor design, the flow rate was reduced by more than a factor of three to

$$Q_a/\ddot{x}_e \approx 0.00097 \text{ m}^2 \text{ sec } (1.5 \text{ in.}^2 \text{ sec})$$

This reduction indicates the benefit that results from the simple addition of the compliant accumulator at the LPOP inlet. The benefit could be increased further by introducing a shaping function that would inhibit response of the suppressor in this mode. In such a case, the size of the suppressor would be determined by the requirements in the modes above the fundamental. According to the results of the present analysis, action of the suppressor in the higher modes is only required to eliminate the instability that appears in the E35 mode. Thus, an upper limit on the size reduction is provided by the flow rate associated with response in this mode. This flow rate was found to be

$$Q_a/\ddot{x}_e \approx 0.000065 \text{ m}^2 \text{ sec } (0.1 \text{ in.}^2 \text{ sec})$$

Thus, an additional decrease of an order of magnitude in the flow rate requirement is possible if the response of the HPOP inlet device in the lower frequency modes is suppressed.

Turning to the NASA/Rocketdyne design, the suppressor flow rate associated with the assumed 0.25 g response level is 0.0079 m³/sec (482 in.³, sec), the same rate as estimated for the Aerospace designs. To convert this flow rate to a volume requirement, a representative fundamental mode frequency of 2.5 Hz was assumed. The resulting volume requirement was 0.0005 m³ (30.8 in.³). This volume requirement can be translated into suppressor stroke and area requirements. These latter are illustrated in figure 28 where the shaded zone defines the permissible region of stroke and area values. A design that was outside this zone would be ineffective since the response capability of the suppressor would have been taken up by the random oscillations present in the system.

Finally, it should be noted that the flow rate and volume requirements for the suppressors were developed with use of both assumed noise
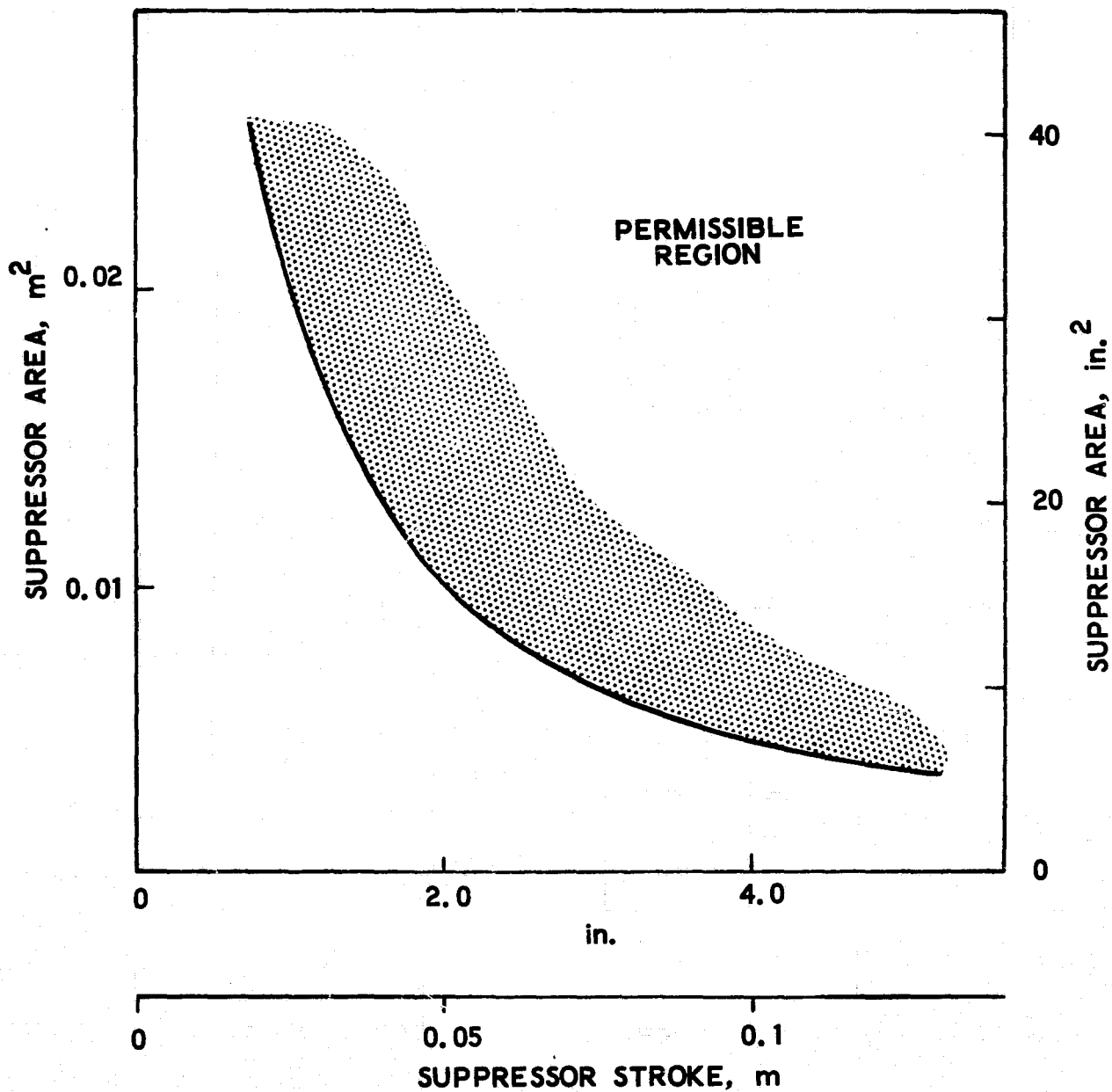
Figure 28. Representative Suppressor Size Requirements for NASA/Rocketdyne Design

89

response levels and the modal characteristics of the coupled structural/ propulsion system. Thus, it is seen that the sizing of an active suppressor is indeed dependent upon knowledge of the dynamic characteristics of the system. In addition this knowledge would also be required to develop the hydraulic supply requirements for the suppressor.

4.5 Suppressor Development Requirements

The considerations in this section are limited to the question of providing the measurements of the feedback quantities required for the different devices. These quantities are the local accelerations in the engine system, the HPOP inlet pressure, and the relative flow into the HPOP. In the case of the acceleration and pressure variables, there is clearly no fundamental problem since similar measurements are presently made on a routine basis on space vehicles. However, it should be noted that special attention must be given to the signal/noise aspects so that adequate sensitivity to small unsteady pressures is achieved. With respect to the measurement of relative flow, required for the optimum design, the prospect for in-flight measurement is doubtful. This doubt is primarily the result of the present unavailability of a satisfactory dynamic flowmeter even for ground testing.[*] In view of the probable unavailability of in-flight flow measurement, it is natural to seek the replacement of the relative flow feedback by some equivalent set of parameters that would be more amenable to measurement. Examination of the equations for the coupled structural/ propulsion system indicates that the absolute flow Q_7 can be written

$$Q_7 = \frac{1}{Z_i} (P_5 - P_7) + \frac{A_3 R_3 \dot{z}_7}{Z_i}$$

where Z_i and R_3 are the impedance and resistance of the interpump line, respectively and P_5 is the pressure at the LPOP discharge. Using this result, the feedback for the optimum design can be written in the alternative form

$$Q_{a3} = \frac{1}{Z_i} (P_7 - P_5) + \frac{A_3 L_i}{Z_i} \ddot{z}_7 + \overline{C}_{b2} \, s \, P_7$$

---

[*]Development of a dynamic flowmeter for possible use on the Shuttle is presently being undertaken by Panametrics, Inc. under contract to the NASA Langley Research Center (ref. 9).

where L_i is the inertance of the interpump line. From this expression, it is seen that the optimum design can be represented by an equivalent system of pressure and motion feedback which should be more easily attainable. However, there is a snag. The feedback requires the pressure differences (P_7-P_5) across the interpump line and examination of these pressures in the feedline mode type of instability (fig. 5) indicates that the differential is of the order of 5 percent of the magnitude of the individual pressure components. Such a small differential would be difficult to measure accurately with separate transducers and introduces the possibility of significant feedback error in a device that has shown itself to be sensitive to error (see section 4.3). There is the possibility of the use of a differential pressure transducer; however, difficulties could remain with problems associated with relatively long sensing line(s) (2 ~ 4 m) such as the effects of trapped gas and line vibration. Thus, the approach of replacing the relative flow measurement by equivalent pressure (and motion) measurements does not appear to be a viable approach. The combination of the uncertainty of satisfactory relative flow measurements and the previously demonstrated sensitivity of the optimum design to errors in the relative flow feedback indicates that the optimum design should be considered unsatisfactory.

5. SUMMARY, AND CONCLUDING REMARKS

The elements and findings of the study can be summarized as follows:

a. Stability analyses undertaken with various suppressor design concepts led to the selection of the following two Aerospace designs for more detailed evaluation

$$Q_{a3} = (-Q_7 + A_3 \dot{z}_7) + \overline{C}_{b2} \, s \, P_7$$

$$\overline{C}_{b2} = 2.4 \, 10^{-4} \, m^5/MN \, (0.1 \, in.^5/lb)$$

$$Q_{a3} = -K_p P_7$$

$$K_p = 0.14 \, m^5/MNs \, (60 \, in.^5/lb\text{-}sec) \cdot$$

where $(Q_7 - A_3 \dot{z}_7)$ represents the relative flow into the HPOP and P_7 denotes the pressure at the HPOP inlet. The first of these designs represents an "optimum" design based upon the idea of eliminating the oscillatory thrust perturbations. The second design represents a simple feedback design.

b. The results of the Aerospace design selection studies indicated that the suppressors required location at the HPOP inlet to be effective.

c. The purely motion feedback devices treated in the Aerospace design selection studies proved to be unsatisfactory.

d. Two design concepts were provided by NASA (Lewis) for detailed evaluation. The first of these designs was a single suppressor at the HPOP inlet that obeyed the law

$$Q_{a3} = \frac{-s^2}{(s^2 + \gamma s + \gamma^2)} \left\{ \frac{E \, s \, P_7}{(s+\gamma)} - \frac{A_3 s}{(s^2 + s\gamma + \gamma^2)} \ddot{z}_7 \right\}$$

$$E = 0.3 \, m^5/MNs \, (125 \, in.^5/lb\text{-}sec)$$

This design was based upon studies undertaken by Rockwell International/Rocketdyne Division. It was found that the pressure feedback was the most important factor in the effectiveness of this design and that the ac coupling terms did not influence the performance. The second NASA design concept

93

comprised a dual-suppressor system that consisted of a 0.057 m^3 (2 ft^3) compliant accumulator at the LPOP inlet and the following active device at the HPOP inlet

$$Q_{a3} = \frac{-s^2}{(s^2 + \gamma s + \gamma^2)} \left\{ \frac{E \, s \, P_7}{(s + \gamma)} \right\}$$

$$E = 0.3 \text{ m}^5/\text{MNs} \quad (125 \text{ in.}^5/\text{lb-sec})$$

The rationale for this dual system was the idea of reducing the size requirements for the HPOP inlet device by the use of an additional LPOP inlet device.

e. All four specific suppressor designs were effective in eliminating the instabilities predicted for the basic system. For the stability cases that were treated in the study, the suppressors maintained the system damping ratio above the 0.005 level (the assumed structural damping ratio was 0.01).

f. The performance of the four specific active suppressor designs was comparable to that of a representative passive device - a 0.057 m^3 (2 ft^3) compliant accumulator at the HPOP inlet.

g. The performance of the Aerospace "optimum" design proved to be highly sensitive to errors in the relative flow feedback $(Q_7 - A_3 \dot{z}_7)$. In view of this sensitivity and the uncertainty associated with a satisfactory relative flow (or equivalent) measurement, the "optimum" design was deemed to be unsatisfactory. The other Aerospace design and the two NASA designs were insensitive to imposed feedback signal errors of ± 15 percent in amplitude and ± 45 degrees in phase.

h. Size estimates were developed for the active suppressor designs. These requirements were governed by the fundamental-mode response of the system.

i. Relief in the stroke and hydraulic requirements by at least a factor of three can be obtained by the addition of an accumulator at the LPOP (see section 4). Further relief of up to an order of magnitude is possible by also introducing a shaping function in the feedback to eliminate the suppressor response in the fundamental mode. The sizing is then governed by the higher mode response.

In conclusion, it has been seen that the initial examination of active suppressors undertaken in this qualitative study has provided HPOP inlet suppressor designs that will give performance that is comparable to that of passive devices. The design studies indicate that a device involving feedback of the HPOP-inlet pressure (i.e., $Q_a = -K_p P_7$) provides an effective and

simple design that is relatively insensitive to errors in both the magnitude and phase of the feedback signal. Regarding the sensitivity of the active suppressor design to the system dynamic characteristics, it has been seen that the suppressor sizing and hydraulic supply requirements are dependent upon such characteristics. Finally, as regards future pogo suppression studies for the Shuttle, it is recommended that active suppressor designs continue to be considered. The basic concepts employed in such studies can be guided by the results of the present investigation. In addition, the use of sophisticated control methods, such as time and frequency optimum control, should be investigated in order to determine if the effectiveness of active devices could be enhanced above the levels found in the present study.

APPENDIX A

SYSTEM EQUATIONS

A. 1 Fluid Dynamic Equations for Propulsion System

The fluid dynamic equations for the individual elements of the propulsion system model are given below.

First Feedline Segment

$$P_1 = \alpha_{11}P_t + \alpha_{12}Q_t + \alpha_{13}\dot{x}_{\ell 1}$$

$$Q_1 = \alpha_{21}P_t + \alpha_{22}Q_t + \alpha_{23}\dot{x}_{\ell 1}$$

First Feedline Corner

$$P_1 = P_2$$

$$Q_2 - A_2\dot{z}_1 = Q_1 + A_1\dot{x}_1$$

Second Feedline Segment

$$P_3 = \tilde{\alpha}_{11}P_2 + \tilde{\alpha}_{12}Q_2 - \tilde{\alpha}_{13}\dot{z}_{\ell 2}$$

$$Q_3 = \tilde{\alpha}_{21}P_2 + \tilde{\alpha}_{22}Q_2 - \tilde{\alpha}_{23}\dot{z}_{\ell 2}$$

Second Feedline Corner

$$P_3 = P_4$$

$$Q_4 + A_2\dot{x}_3 = Q_3 - A_2\dot{z}_3$$

Low-Pressure Pump

$$Q_5 - A_3\dot{z}_4 = (Q_4 + A_2\dot{x}_4) + Q_{A1} - sC_{b1}P_4$$

$$P_5 = (m_1 + 1)P_4 - Z_{p1}Q_5 + R_{p1}A_3\dot{z}_4$$

97

LPOP Discharge Suppressor

$$Q_6 - A_3 \dot{z}_4 = Q_5 - A_3 \dot{z}_4 + Q_{A2}$$

$$P_5 = P_6$$

Interpump Line

$$P_6 - P_7 = Z_i Q_6 - A_3 R_i \dot{z}_7$$

$$Q_6 = Q_7$$

High-Pressure Pump

$$Q_8 - A_4 \dot{z}_7 = Q_7 - A_3 \dot{z}_7 + Q_{A3} - s C_{b2} P_7$$

$$P_8 = (m_2 + 1) P_7 - Z_{p2} Q_8 + R_{p2} A_4 \dot{z}_7$$

Discharge Line

$$P_8 - P_9 = Z_d Q_8 - R_d A_4 \dot{z}_7$$

$$Q_9 = Q_8$$

Injector and Chamber

$$P_9 - P_c = Z_j Q_9 - R_j A_4 \dot{z}_7$$

$$P_c = R_c (Q_9 - A_4 \dot{z}_7)$$

In the above equations, A_i, Q_i and P_i denote the flow areas, absolute volume flows, and pressure perturbations at various locations within the system. The Q_{Ai} denote the volume flows from the pogo suppression devices: $(m_1 + 1)$ and $(m_2 + 1)$ are the LPOP and HPOP gains; C_{b1} and C_{b2} denote the cavitation compliance at the inlets to the LPOP and HPOP, respectively, while s is the Laplace variable; the $\dot{x}_i, \dot{z}_i$ are the longitudinal and lateral velocities of the structure at various points of the system while $\dot{x}\ell_1$ and $\dot{z}\ell_2$ denote the average

translational velocities of the two feedline segments. It will be noted that the lateral velocity of the HPOP, thrust and injection chambers are taken to be the same. The individual impedances Z_i that appear in the above equations are as follows:

First Feedline Segment

$$Z_1 = L_1 s + R_1$$

Second Feedline Segment

$$Z_2 = L_2 s + R_2$$

Low-Pressure Pump

$$Z_{p1} = L_{p1} s + R_{p1}$$

High-Pressure Pump

$$Z_{p2} = L_{p2} s + R_{p2}$$

Interpump Line

$$Z_i = L_i s + R_i$$

Discharge Line

$$Z_d = L_d s + R_d$$

Injector

$$Z_j = L_j s + R_j$$

The engine impedance that appears in the equations of motion for the combined structural/propulsion system is defined as

$$Z_e = L_e s + R_e$$

where

$$L_e = L_j + L_d + L_{p2}$$

$$R_e = R_j + R_c + R_d + R_{p2}$$

The transmission coefficients for the first feedline segment are defined as follows:

$$\alpha_{11} = \alpha_{22} = \cosh \theta_1$$

$$\alpha_{12} = - Z_1 \frac{\sinh \theta_1}{\theta_1} \qquad\qquad \alpha_{13} = - A_1 R_1 \frac{\sinh \theta_1}{\theta_1}$$

$$\alpha_{21} = - \frac{1}{Z_1} \theta_1 \sinh \theta_1 \qquad\qquad \alpha_{23} = - \frac{A_1 R_1}{Z_1} (1 - \cosh \theta_1)$$

where θ_1 is defined by

$$\theta_1^2 = s^2 \tau_1^2 \left(1 + \frac{R_1}{s L_1}\right)$$

with $\tau_1 = \ell_1 / a$ where ℓ_1 is the length of the feedline segment and a is the speed of sound in the liquid oxygen. The coefficients, $\tilde{\alpha}_{ij}$, for the second feedline segment are similar with A_1, R_1, Z_1, θ_1 being replaced by A_2, R_2, Z_2, θ_2, respectively.

The volume flow, Q_{Ai}, from the pogo suppression devices are related to the propulsion system and specific suppressor parameters. The precise form of these relationships is given in Section A.3.

A.2 Equation of Motion for Structural Mode

The response of the vehicle structure is taken to be in the nth normal mode. The structural motion $\vec{x}$ at some point $\vec{r}$ is written

$$\vec{x} = q_n e^{st} \phi_n(\vec{r})$$

where q_n is the generalized coordinate and $\phi_n(\vec{r})$ is the associated mode shape. For the case that the structural system is defined with closed-bottom tanks, the equation of motion governing q_n is

$$M_n \left| s^2 + 2 \zeta_n \omega_n s + \omega_n^2 \right| q_n$$

$$= \mathscr{P}_n(tb)\dot{Q}_R + P_t A_1 \phi_n^{(x)}(tb) + \sum_i \vec{F}_i \cdot \vec{\phi}_{ni}$$

where $\mathscr{P}_n(tb)$ is the modal tank-bottom pressure and Q_R is the relative volume outflow from the propellant tank. The detailed development of the contribution of the outflow contribution is found in reference 3. From the results of reference 3, the tank-bottom pressure, P_t, is related to the vehicle motion by

$$P_t = \mathscr{P}_n s^2 q_n$$

The relative outflow Q_R is written

$$Q_R = Q_t + A_1 s \, q_n \phi_n^{(x)}(tb)$$

The $\vec{F}_i$ comprises the drag forces on the feedline segments, the interpump line and the discharge line, the forces at the two feedline corners, the forces on the LPOP and HPOP and the forces on the injector and thrust chamber. The precise form of these various forces is as follows:

Drag on Feedline Segments

$$F_1^{(x)} = \frac{-A_1 R_1}{Z_1} (P_t - P_2 + A_1 L_1 s \, \dot{x}_{\ell 1})$$

$$F_1^{(z)} = \frac{A_2 R_2}{Z_2} (P_2 - P_4 - A_2 L_2 s \, \dot{z}_{\ell 2})$$

Drag on Interpump Line

$$F_i^{(z)} = A_3 R (Q_7 - A_3 \dot{z}_7)$$

Drag on Discharge Line

$$F_d^{(z)} = A_4 R \left(Q_8 - A_4 \dot{z}_7 \right)$$

Forces at First Feedline Corner

$$F_{c1}^{(x)} = - P_2 A_1 - \overline{f} \left(2 \frac{Q_1}{A_1} + \dot{x}_1 \right)$$

$$F_{c1}^{(z)} = - P_2 A_2 - \overline{f} \left(2 \frac{Q_2}{A_2} - \dot{z}_1 \right)$$

Forces at Second Feedline Corner

$$F_{c2}^{(x)} = P_4 A_2 + \overline{f} \left(2 \frac{Q_4}{A_2} + \dot{x}_3 \right)$$

$$F_{c2}^{(z)} = P_4 A_2 + \overline{f} \left(2 \frac{Q_3}{A_2} - \dot{z}_3 \right)$$

Forces at LPOP

$$F_{p1}^{(x)} = - P_4 A_2 - \overline{f} \left(2 \frac{Q_4}{A_2} + \dot{x}_4 \right)$$

$$F_{p1}^{(z)} = - P_5 A_3 - \overline{f} \left(2 \frac{Q_5}{A_3} - \dot{z}_4 \right)$$

Forces at HPOP

$$F_{p2}^{(z)} = P_7 A_3 - P_8 A_4 + 2 \overline{f} \left(\frac{Q_7}{A_3} - \frac{Q_8}{A_4} \right)$$

Force at Injector

$$F_i^{(z)} = A_4 P_9$$

Force at Thrust Chamber

$$F_t^{(x)} = A_T P_c$$

In the above expressions $\overline{f}$ denotes the mean mass flow of the propellant

$$\overline{f} = \rho \overline{V} A$$

where ρ is the mass density of the propellant and $\overline{V}$ is the steady flow velocity. The items that involve $\overline{f}$ derive from the convective derivative in the fluid momentum equation.

A.3 Description of Accumulator

The volume flow, Q_A, from an accumulator in the system is written as

$$Q_A = -\sum_j K_j(s) h_j$$

where the h_j are the allowable feedback parameters (i.e., pressure, flow rate and motion at various points in the system) and where the $K_j(s)$ denote the associated feedback constants.

SHUTTLE LOX SYSTEM PARAMETERS

RESISTANCE,[*]   MN s/m^5 (sec/in.^{2})

R_1 = 0.4 (0.0236)

R_2 = 0.11 (0.0064)

R_{p1} = 8.8 (0.52)

R_{p2} = 44.7 (2.64)

R_i = 1.9 (0.11)

R_e = 156 (9.19)

R_c = 42.3 (2.50)

R_d = 8.3 (0.49)

R_j = 60.2 (3.56)

INERTANCE,[*]   MN s^2/m^5 (sec^2/in.^{2})

L_1 = 0.71 (0.0417)

L_2 = 0.19 (0.0113)

L_{p1} = 0.017 (0.001)

L_{p2} = 0.042 (0.0025)

L_i = 0.22 (0.013)

L_e = 0.38 (0.0225)

L_d = 0.25 (0.015)

L_j = 0.085 (0.005)

---

[*]Resistance in SI units is based upon pressure divided by volume flow; in engineering units, weight flow is employed. The flow difference also applies to inertance.

PRECEDING PAGE BLANK NOT FILMED

CAVITATION COMPLIANCE

$$C_{b1} =$$
$$C_{b2} =$$

See figure 2

PUMP GAIN

See figure 3

TIMES (sec)

$$\tau_1 = \quad 0.0656$$
$$\tau_2 = \quad 0.0178$$

Feedline Travel Time

AREAS (in.^{2})

$$A_1 = \quad 75.7$$
$$A_3 = \quad 31.2$$
$$A_4 = \quad 12.6$$
$$A_T = \quad 158$$

APPENDIX C

STRUCTURAL MODE DATA

The detailed modal data employed in the stability analyses are given in this Appendix. The data for the structural modes used at the orbiter end-burn event are given in the first table.

Mode \ Item	E1	E7	E30	E34	E35
$\phi_x(\ell_1)$	-0.156	0.054	0.022	0.222	0.022
$\phi_x(1)$	-0.33	-0.079	-0.752	0.37	0.0194
$\phi_x(3)$	-0.33	-0.079	-0.752	0.37	0.0134
$\phi_x(4)$	0.255	-0.556	-1.71	-2.13	2.63
$\phi_x(7)$	0.255	-0.556	-1.71	-2.13	2.63
$\phi_x(tb)$	-0.209	-0.259	-7.74	4.443	5.336
$\phi_z(\ell_2)$	0.037	0.431	-0.372	0.017	-0.09
$\phi_z(1)$	0.037	0.431	-0.372	0.017	-0.09
$\phi_z(3)$	0.037	0.431	-0.372	0.017	-0.09
$\phi_z(4)$	0.846	-1.95	-0.12	1.0	-1.56
$\phi_z(7)$	0.846	-1.95	-0.12	1.0	-1.56
$\mathscr{P}_n$	0	0	0	0	0
M_n	292	292	292	146	146
ζ_n	0.01	0.01	0.01	0.01	0.01

In the table the subscripts x and z denote motion in the longitudinal and lateral directions respectively; the quantities $\phi(1)$ and $\phi(3)$ are the modal amplitudes at the first and second corners of the feedline; $\phi_x(\ell_1)$ and $\phi_z(\ell_2)$ are the modal amplitudes of the longitudinal and lateral sections of the feedline; $\phi(4)$ and $\phi(tb)$ are the modal amplitudes at the LPOP and the Lox tank; $\phi(7)$ denotes the amplitude of both the HPOP and the thrust champer; $\mathscr{P}_n$ is the modal tank-bottom pressure (given in units of lb-sec^2/in.^{3}) and ζ_n is the structural damping ratio. The generalized mass is denoted by M_n and is given in units of lb-sec^2/in. It will be noted that the generalized mass values assigned to the E34 and E35 modes has been reduced by a factor of two. This reduction was introduced as a simple means of doubling the structural gain in these two modes. As discussed in the main text, see Section 2.1, the increase in structural gain was made to take account of possible destabilizing coupling between these two modes.

The corresponding data for the modes employed in the stability analyses at lift-off are given in the next table.

Item \ Mode	L1	L18	L26	L49	L51	L62
$\phi_x(\ell_1)$	-1.27	0.61	-2.57	-0.01	-0.205	-0.38
$\phi_x(1)$	-0.80	0.368	-2.14	-2.86	-1.0	-0.93
$\phi_x(3)$	-0.80	0.368	-2.14	-2.86	-1.0	-0.93
$\phi_x(4)$	-2.38	-1.71	-2.63	-6.66	-2.29	11.34
$\phi_x(7)$	-2.38	-1.71	-2.63	-6.66	-2.29	11.34
$\phi_x(tb)$	-0.137	-0.127	-0.035	-3.28	-6.42	-0.77
$\phi_z(\ell_2)$	-0.316	-0.271	0.754	0.59	-0.49	-1.40
$\phi_z(1)$	-0.316	-0.271	0.754	0.59	-0.49	-1.40
$\phi_z(3)$	-0.316	-0.271	0.754	0.59	-0.49	-1.40
$\phi_z(4)$	-2.68	-6.89	-0.40	0.29	0.155	-6.5
$\phi_z(7)$	-2.68	-6.89	-0.40	0.29	0.155	-6.5
$\mathscr{P}_n$	-1.0×10^{-3}	-3.65×10^{-5}	-2.92×10^{-5}	-1.93×10^{-2}	-6.3×10^{-2}	-3.9×10^{-5}
M_n	3592	3592	3592	3592	3592	3592
ζ_n	0.01	0.01	0.01	0.01	0.01	0.01

The data for the two modes employed at the after SRB separation event are given in the final table.

Mode \\ Item	A1	A46
$\phi_x(\ell_1)$	0.53	0.33
$\phi_x(1)$	0.208	0.74
$\phi_x(3)$	0.208	0.74
$\phi_x(4)$	1.28	-6.61
$\phi_x(7)$	1.28	-6.61
$\phi_x(tb)$	0.257	-0.065
$\phi_z(\ell_2)$	0.094	0.908
$\phi_z(1)$	0.094	0.908
$\phi_z(3)$	0.094	0.908
$\phi_z(4)$	1.68	3.7
$\phi_z(7)$	1.68	3.7
$\mathscr{P}_n$	-2.16×10^{-3}	3.3×10^{-7}
M_n	1282	1282
ζ_n	0.01	0.01

APPENDIX D

LIST OF SYMBOLS

Units: M (mass), F (force), L (length), T (time)

a	acoustic velocity $[LT^{-1}]$
A	area $[L^2]$
A_T	effective area of thrust chamber $[L^2]$
C	compliance $[F^{-1}L^5]$
$\bar{C}_{b2}$	coefficient in Aerospace suppressor design [eq. (2)] $[L^5F^{-1}]$
E	coefficient in NASA suppressor design [eq. (10)] $[L^5F^{-1}T^{-1}]$
$\bar{f}$	mean mass flow of propellant $[MT^{-1}]$
G_e	structural gain for engine motion, $\phi^2(e)/M_n$, $[M^{-1}]$
i	imaginary unit, $\sqrt{-1}$
K_x	coefficient in motion feedback design [eq. (5)] $[L^2]$
K_p	coefficient in pressure feedback design [eq. (8)] $[L^5F^{-1}T^{-1}]$
ℓ	line length $[L]$
L	inertance $[FL^{-5}T^2$ or $ML^{-4}]$
m+1	pump dynamic gain $[-]$
M	mass $[M]$
M_n	generalized mass of nth structural mode $[M]$
$\mathscr{P}_n$	modal tank-bottom pressure per unit acceleration of generalized coordinate $[FL^{-3}T^2]$
P	oscillatory pressure $[FL^{-2}]$
q_n	generalized displacement of nth structural mode
Q	volumetric flow $[L^3T^{-1}]$
R	resistance $[FL^{-5}T]$

s	Laplace variable used to denote the complex frequency, $\sigma + i\omega$, $[T^{-1}]$
t	time $[T]$
T	thrust $[F]$
x	structural displacement along longitudinal axis $[L]$
z	structural displacement along lateral axis $[L]$
$\overline{V}$	steady flow velocity of propellant $[LT^{-1}]$
Y	flow admittance $[F^{-1}L^5T^{-1}]$
Z	flow impedance $[FL^{-5}T]$
α	coefficient in NASA suppressor design [eq. (10)] [-]
α_{ij}	coefficients in feedline transmission function (Appendix A) [-]
ζ	ratio of critical damping for coupled system mode [-]
ζ_a	ratio of critical damping for accumulator [-]
ζ_n	ratio of critical damping for structural mode [-]
θ	complex propagation angle
γ	parameter in NASA suppressor design [eq. (10)] $[T^{-1}]$
ρ	propellant mass density $[ML^{-3}]$
τ	travel time in a hydraulic line, $\sqrt{LC}$ or ℓ/a, $[T]$
ϕ_n	modal displacement [-]
ω	angular frequency $[T^{-1}]$
ω_a	natural frequency of the accumulator $[T^{-1}]$
ω_n	natural frequency of structural mode $[T^{-1}]$

Subscripts

a	accumulator
b	bubble

112

c	chamber
d	discharge
e	engine
n	n^{th} structural-system mode
p	pump
R	real part; relative
t	tank

REFERENCES

1. Farrel, E.C. and Fenwick, J.R.: Pogo Instabilities Suppression Evaluation. NASA CR-134500, November 1973.

2. Lock, M.H. and Rubin, S.: Passive Suppression of Pogo on the Space Shuttle. NASA CR-132452, April 1974.

3. Rubin, S.; Wagner, R.G.; Payne, J.G.: Pogo Suppression on Space Shuttle - Early Studies. NASA CR-2210, March 1973.

4. Holt, J.F.: ACS Mule, General Root Finding Subroutine. Report No. TOR-0073(9320)-8, The Aerospace Corporation, El Segundo, California, March 1973.

5. SSME Model, Engine Dynamic Characteristics Related to Pogo. Report No. RSS-8549-2, Rocketdyne Division, Rockwell International, Canoga Park, California, September 1973.

6. Ghahremani, F.G.; Rubin, S.: Empirical Evaluation of Pump Inlet Compliance. Report No. ATR-73(7257)-1, The Aerospace Corporation, El Segundo, California, August 1972.

7. Rubin, S.: Longitudinal Instability of Liquid Rockets Due to Propulsion Feedback (POGO). J. Spacecraft Rockets, 3(8), August 1966, pp. 1188-1195.

8. Anon: Prevention of Coupled Structure - Propulsion Instability (Pogo), NASA Space Vehicle Design Criteria (Structures), SP-8055, 1970.

9. Pedersen, N.E.; Lynnworth, L.C.; and Carnevale, E.H.: Non-intrusive Dynamic Flowmeter. NASA CR-112313, June 1973.

PRECEDING PAGE BLANK NOT FILMED